FUNCTION AND REGULATION OF THE CLASP-DEPENDENT MICROTUBULE ARRAY AT THE GOLGI

By

Paul Myron Miller

Dissertation

Submitted to the Faculty of the

Graduate School of Vanderbilt University

In partial fulfillment of the requirements

for the degree of

DOCTOR OF PHILOSOPHY

in

Cell and Developmental Biology

August, 2010

Nashville, Tennessee

Approved:

Professor Steve Hanks, Chair

Assistant Professor Irina Kaverina

Assistant Professor Ryoma Ohi

Associate Professor Todd Graham

Professor David Bader

To my wonderful parents, Leola and Paul, who have provided infinite support and guidance as I have chosen my own path in life

ACKNOWLEDGEMENTS

My years of graduate school here at Vanderbilt have truly been a life-changing experience. Looking back at my first year, only now can I appreciate how much I have learned and developed during this time. I would never be where I am now without the support and guidance of my mentor, Irina Kaverina. From the very beginning, she taught me to strive for excellence and also opened many doors by putting me out there on the front lines speaking at conferences, even during my first year within the lab. For this, I am truly grateful. I would also like to thank my committee members for all of their help, suggestions, and encouragement: Steve Hanks, David Bader, Todd Graham, and Puck Ohi. Additionally I would like to thank Susan Wente and the Department of Cell and Developmental Biology for providing support and an excellent educational environment. Moreover, the work presented in this thesis was produced with the help of funding from NIH NIGMS grant 1R01GM078373-01 to I.K. and a pilot project to I.K. from NIH NCI GI SPORE grant P50CA095103 as well as an American Heart association Predoctoral Fellowship 09PRE2260729 to P.M.

I am very fortunate to have such great colleagues within as well as outside of the Kaverina Lab. To Andrey Efimov, thank you for your time and patience in mentoring me when I first came into the lab. To Nadia Efimova, I cannot imagine how I would have survived in the lab without your help, guidance, and friendship. To Ana Rita Maia, thank you for all of your help with experiments as well as

being a truly genuine friend. To Christopher Arnette, thank you for being a great friend and bringing much needed humor and laughter into the lab.

Outside the lab, I would like to give special thanks to Larisa Ryzhova. Thank you for allowing me to ask you every question possible about cloning, biochemistry, reagents, et cetera. I truly appreciate all of the help and advice you have given me. Andrew Folkmann, thanks for contributing critical experiments to my manuscript. Julie Merkle and Jeanne Jodoin, thanks for allowing me to vent and helping me through good times as well as bad. Ali Hanson, thank you for all of the musical entertainment.

Finally, I would like to thank my parents, Leola and Paul, for all your love and support. You have always been there to support whatever decisions I have made in life and have believed in me from the very beginning. I am very proud to be your son, and I dedicate all of this work and effort to you.

TABLE OF CONTENTS

LIST OF FIGURES

CHAPTER I

INTRODUCTION

Microtubule Network

Cell migration in higher organisms is essential for multiple physiological and pathophysiological processes including embryonic development, tissue regeneration, immune responses, and cancer cell metastasis and invasion. In order for cells to move, they must first polarize into the leading and the trailing edge. Microtubules (MTs) are indispensable for polarized cell migration and major tissue morphogenetic movements such as gastrulation in a majority of cell types. Formation of cell edge protrusions and retractions continues in the absence of MTs, but these are no longer distributed in a polarized fashion. MTs are therefore thought to support polarized distribution of regulatory motility signals within a cell.

MTs are major structural components of the cytoskeleton. Each MT is composed of α and β-tubulin monomers that dimerize and organize into a 13 member protofilament with a diameter of approximately 25nm. Crucial to the formation of the MT protofilament is the γ-tubulin ring complex (γ-TURC). γ-TURCs are concentrated in microtubule organizing centers (such as the centrosome) within the cell and serve as a structural scaffold upon which α/β-tubulin dimers organize and polymerize. γ-TURCs also cap the minus (-) end of

the MT and serve as anchoring points from which the plus (+) end of the MT grows away from.

MT growth is regulated by a unique property called dynamic instability. Dynamic instability is characterized by periods of MT growth in the presence of a GTP tubulin cap and MT depolymerization when hydrolysis of GTP tubulin to GDP tubulin catches up with the + tip of the MT (Kirschner and Mitchison 1986). The switch from MT growth to MT depolymerization is termed catastrophe and the switch from shrinking to growing is termed rescue. The period of time between growth/shrinking is termed pausing.

Dynamic instability allows the MT network to be rapidly remodeled in response to the ever-changing cellular environment. This is a crucial feature due to the fact that the MT network plays critical roles in cellular organization and dynamics in both mitotic and interphase cells. In mitotic cells, the MT network organizes into astral and kinetochore fiber subsets that are critical for proper chromosome alignment and segregation during cell division. In motile interphase cells the MT network organizes an asymmetric array that modulates regulated delivery of cargos to distinct cellular domains (Sheetz 1996; Small and Kaverina 2003; Noritake et al., 2005; Watanabe et al., 2005). This asymmetric network aids in the polarized remodeling of the actin cytoskeleton (Krendel et al., 2002; Rodriguez et al., 2003; Bretscher 2005; Siegrist and Doe 2007) as well as efficient focal adhesion turnover at the leading and trailing edges of the cell

(Chabin-Brion et al., 2001; Ezratty et al., 2005). The majority of our studies are focused in interphase cells, therefore I will elaborate mainly on the function of the interphase MT network.

The MT network is also utilized as an internal "highway system" in order to deliver cargos and organelles to distinct locations (Hirschberg et al., 1998; Musch 2004). The nature of this transport relies on molecular motors that allow cargo delivery along the MT network (Sheetz 1996; Hirokawa 1998). Specifically, kinesin-dependent transport is essential for post-Golgi cargos to be transported to the cell periphery, and dynein-dependent transport is required for ER-to-Golgi transport and proper Golgi organization (Burkhardt et al., 1997; Roghi and Allan 1999). If the MT network becomes perturbed, for instance by nocodazole treatment that depolymerizes MTs, the process of intracellular transport becomes chaotic (Hirschberg et al., 1998). Therefore, an intact MT network is required for efficient delivery of intercellular signals that regulate the process of cell motility.

CLASP Family Proteins

CLASPs are 170 kDa CLIP (cytoplasmic linker protein) associated proteins that exist as two similar isoforms in mammalian cells known as CLASP1 and CLASP2 (Akhmanova et al., 2001; Galjart 2005; Mimori-Kiyosue et al., 2005). For simplicity, both isoforms will be identified herein as CLASPs. CLASPs are well-known regulators of microtubule (MT) dynamics, primarily serving as MT stabilizing factors, and are known to play important roles in both

interphase and mitotic cells (Akhmanova et al., 2001; Hannak and Heald 2006; Lansbergen et al., 2006). In interphase cells, CLASPs predominately localize to the centrosome, MT tips, and the Golgi apparatus (Akhmanova et al., 2001; Maiato et al., 2003; Mimori-Kiyosue et al., 2005). During mitosis, CLASPs localize to the spindle pole body and the outer kinetochore and are essential for chromosome segregation (Inoue et al., 2000; Lemos et al., 2000; Maiato et al., 2002; Maiato et al., 2003; Hannak and Heald 2006).

Identification of mammalian CLASPs resulted from a yeast two-hybrid screen designed to reveal common binding partners of Cytoplasmic Linker Proteins (CLIP) -115 and 170 (Akhmanova et al., 2001). Since the function of CLIP proteins at the MT plus end was unclear at the time, a screen for common binding partners was performed in order to elucidate their function. Results of the screen identified CLASP1 and CLASP2 proteins (Akhmanova et al., 2001).

Initial characterization of mammalian CLASPs revealed that these proteins bind to microtubules and colocalize with CLIPs at the MT plus end where they serve as stabilizing factors. When subjected to a database search, it was found that CLASPs are similar to the microtubule-associated protein (MAP) Orbit/Mast that plays a role in regulating microtubule dynamics during mitosis in *D. melanogaster* (Inoue et al., 2000; Lemos et al., 2000; Akhmanova et al., 2001). Since their initial characterization in *D. melanogaster*, CLASPs have shown to be highly conserved; homologous proteins with similar functions have been

identified in organisms such as Peg1 in *S. pombe* (Grallert et al., 2006) and cls-2 in *C. elegans* (Gonczy et al., 2000).

Based upon sequence analysis, CLASP family proteins are predicted to contain three distinct domains. The N-terminus of the protein contains a dis1/TOG domain that is present in other known MT stabilizing proteins (Lemos et al., 2000). Although the presence of a dis/TOG domain suggests a role for MT stabilization, deletion of this domain from CLASP proteins did not affect MT stability. However, in CLASP proteins, this domain is thought to play a role in centrosomal MT nucleation in a manner similar to the role this domain plays in the localization of ZYG-9 and Mini Spindles to centrosomes and spindle poles (Matthews et al., 1998; Cullen et al., 1999). Further, variation within the N-terminal domain is also what lends to the slight differences in CLASP1 and CLASP2 isoforms. The second distinct domain of CLASP proteins resides in the central region of the protein. This region is known as the Serine/Arginine rich domain and has been shown by deletion analysis to be important for binding to MTs, End-binding protein 1 (EB1) and End-binding protein 3 (EB3). Phosphorylation of serine residues within this region by Glycogen Synthase 3 Beta (GSK3β) also directly regulates CLASP binding along the MT lattice as well as plus tips (Wittmann and Waterman-Storer 2005; Kumar et al., 2009). (In Chapter 5 of this thesis, I will go into further detail about the regulation of Golgi-associated CLASPs by GSK3β). The third distinct domain of CLASP proteins is the COOH-terminus. This domain of CLASP proteins is highly conserved and is

responsible CLIP protein and cell cortex interaction and also contains the Golgi binding domain (Akhmanova et al., 2001; Mimori-Kiyosue et al., 2005).

As most studies have studied the role of CLASPs at the MT tips, our lab has focused our efforts on characterizing the role of Golgi-associated CLASPs. Not only have we found that the Golgi apparatus is able to nucleate microtubules in a CLASP-dependent manner (Efimov et al., 2007), we have also determined the functional significance of the Golgi-derived MT array (Miller et al., 2009).

Golgi Apparatus

The Golgi is an asymmetric organelle with distinct *cis/trans* polarity (Griffiths and Simons 1986; Schweizer et al., 1988) that is in close proximity to the centrosome (Cole et al., 1996; Thyberg and Moskalewski 1999) and oriented toward the leading edge of motile cells. The Golgi exhibits a distinct "ribbon-like" morphology and is composed of individual interconnected Golgi stacks that each retains specific *cis/trans* polarity (Shorter and Warren 2002; Marra et al., 2007). The *cis*-Golgi face is concave and oriented toward the centrosome and nucleus. In contrast, the *trans*-Golgi exhibits convex morphology and is oriented toward the cell periphery.

Functionally, the Golgi is the major site of protein processing and sorting within the cell. In addition to this major function, our lab has found that the Golgi also serves as an alternative microtubule organizing center (MTOC) within the

cell (Efimov et al., 2007). The natural asymmetry of this organelle makes it a prime candidate for establishing an asymmetric MT array that is required for cell motility due to the fact that MTs are nucleated at the *trans*-Golgi network (Efimov et al., 2007), which is oriented toward the leading edge of motile cells. Since the work presented in this thesis focuses on the Golgi serving as an additional MTOC, I will not elaborate on the intricate process of protein processing and sorting performed by this organelle.

It has long been thought that there is an intimate relationship between the Golgi apparatus and the cellular MT network (Thyberg and Moskalewski 1985; Thyberg and Moskalewski 1999). In many mammalian cell types, the Golgi is in close proximity to the centrosome where MT minus ends are anchored. Not only is the Golgi in close proximity of the main MTOC within the cell, but the structural integrity of the Golgi itself is dependent upon MTs (Burkhardt 1998). If microtubules are depolymerized by nocodazole (Rogalski et al., 1984; Storrie and Yang 1998; Hong et al., 1999) or cold-treatment (Wallin and Stromberg 1995; Detrich 1997), the Golgi apparatus disperses into mini-stacks throughout the cytoplasm. Further, MT motors have been shown to associate with Golgi membranes and are implicated in maintaining Golgi organization (Thyberg and Moskalewski 1999; Short et al., 2005). Specifically, if the MT minus-end directed motor dynein in inhibited by either siRNA or over-expression of dynactin subunit p50, the Golgi ribbon disperses (Burkhardt et al., 1997; Roghi and Allan 1999; Thyberg and Moskalewski 1999; Caviston and Holzbaur 2006). Therefore an

intact MT array, including functional MT motors, is necessary for establishing and maintaining proper Golgi organization within the cell.

CLASP-Dependent Microtubule Nucleation at the Golgi

It is traditionally thought that all microtubules in mammalian cells originate solely at the centrosome (Luders and Stearns 2007), but recent studies, including a publication from our lab, have shown that MTs can be originated in a centrosome-independent manner (Chabin-Brion et al., 2001; Schmit 2002; Wiese and Zheng 2006; Efimov et al., 2007; Liu et al., 2007; Luders and Stearns 2007). The centrosome produces a radial MT array (Bergen et al., 1980; Salaycik et al., 2005), and it has long been unclear whether the interphase MT network can be organized asymmetrically from the nucleation step. Our lab has found that the Golgi apparatus is able to produce an asymmetric MT array (Efimov et al., 2007).

A method that includes labeling MT tips with a fluorescently labeled plus-tip marker (such as EB3) and monitoring new MT outgrowth by live cell imaging was used previously to analyze MT nucleation at the centrosome (Piehl et al., 2004). Our lab modified this method to allow tracing of non-centrosomal microtubules back to their point-of origin. Utilizing this method, we have determined that the Golgi apparatus is able to nucleate MTs in a CLASP-dependent manner (Efimov et al., 2007). Upon detailed analysis, we found that the Golgi produces approximately 50% of microtubules in Retinal Pigment Epithelial (RPE1) cells and that these MTs are primarily oriented toward the

leading edge of the cell. Further, utilizing centrosomal ablation experiments, we confirmed that the MTs nucleated at the Golgi apparatus are not captured upon centrosomal release. We also found that MTs growing from the Golgi apparatus are unique from centrosomal MTs due to the fact that they are specifically coated with CLASPs during their initial growth stage (Efimov et al., 2007).

The process of MT nucleation at the Golgi also requires gamma-tubulin and a Golgi-localized coiled-coil protein GCC185 (Fig. 1.1) (Efimov et al., 2007). Because gamma-tubulin is necessary for MT nucleation at both the centrosome and non-centrosomal sites within the cell (Moritz et al., 1995; Moritz et al., 2000; Efimov et al., 2007; Raynaud-Messina and Merdes 2007), it is not surprising that it is involved in the formation of the Golgi-associated MT array.

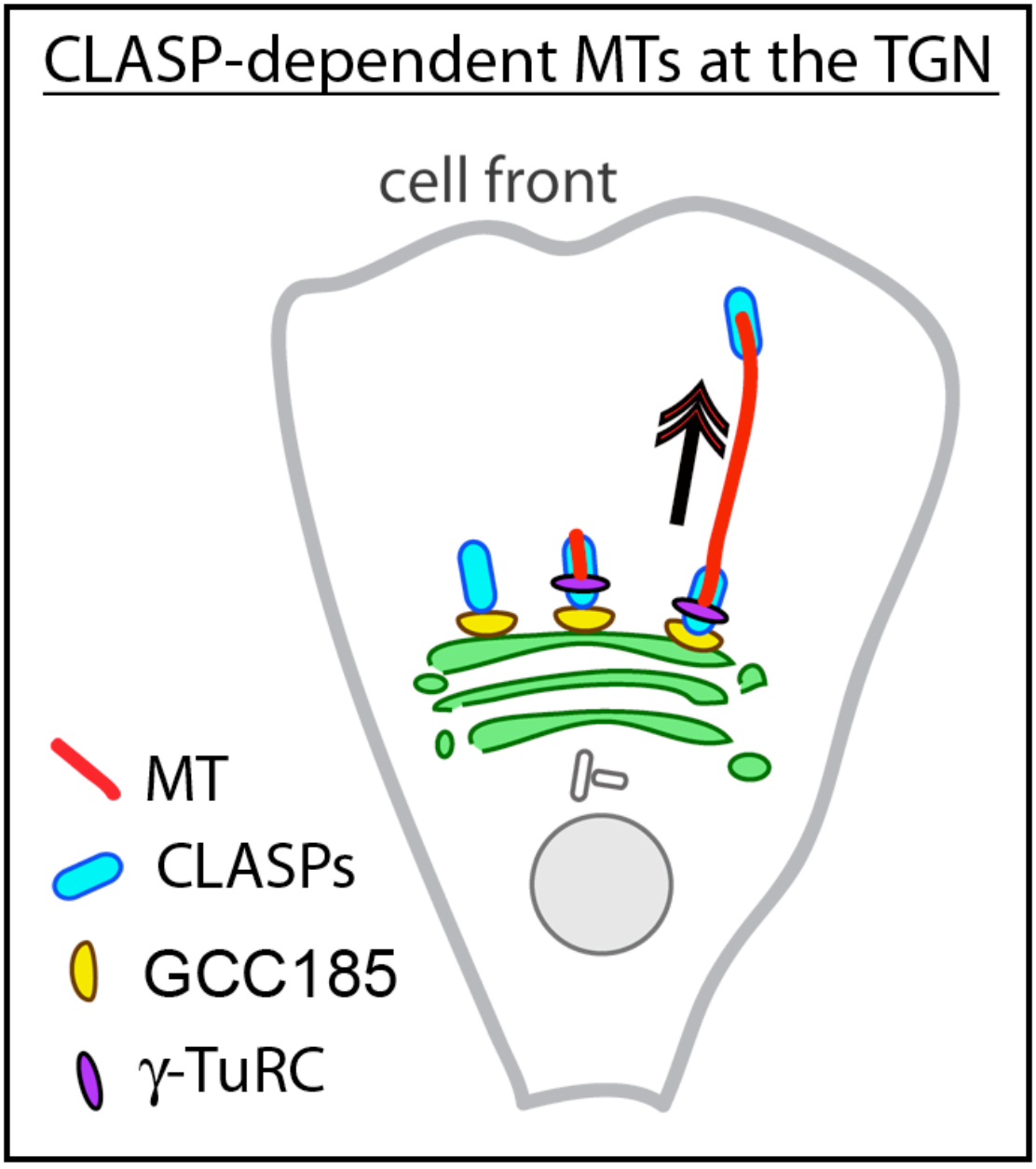

Figure 1.1. CLASP-dependent MTs at the TGN. Golgi-derived front-oriented MTs are nucleated by γ-TuRC, supported by CLASPs, and anchored to the TGN by GCC185.

Golgi localized Coiled-Coil protein 185 (GCC185)

The ability of microtubules to be nucleated at the Golgi is dependent upon CLASPs interaction with a *trans*-Golgi network golgin GCC185 (Efimov et al., 2007). Identification of GCC185 as a CLASP binding partner by mass spectrometry analysis (Efimov et al., 2007) provided a direct link between the CLASP-dependent microtubule array at the Golgi and the *trans*-Golgi network where these microtubules are nucleated. When GCC185 is removed from cells by siRNA, CLASPs no longer localize to the Golgi, and Golgi-derived MTs do not form (Efimov et al., 2007). Therefore the presence of GCC185 at the Golgi membrane serves as the limiting factor in MT formation at the Golgi.

GCC185 itself was identified in 2002 as a 185 kDa coiled-coil protein localized to the *trans*-Golgi network (Luke et al., 2003). The structure of GCC185 is unknown and very little is known about the regulation or function of this protein. Based upon sequence analysis GCC185 is predicted to contain five coiled-coil regions and a GRIP domain at the C-terminus. GRIP domains are ~42 amino acids and located at the C-terminus of protein and are responsible for protein targeting to the *trans*-Golgi network (Barr 1999; Kjer-Nielsen et al., 1999; Munro and Nichols 1999; Luke et al., 2003; Derby et al., 2007).

The regulation of GCC185 at the Golgi has been the center of great controversy. Most proteins containing GRIP-domains are regulated by the GTPase Arl1 (Arf-like protein) at the Golgi (Graham 2004; Short et al., 2005) however, it has been demonstrated that GCC185 is not regulated by this

particular Arl (Derby et al., 2004; Derby et al., 2007). The controversy about GCC185 localization to the Golgi seemed to be resolved in 2008 when a report by Burguete et al. stated that Rab6 and Arl1 cooperatively localize GCC185 to the Golgi (Burguete et al., 2008). However, this model was short-lived due to the fact that it was based predominantly on *in vitro* interactions. Shortly thereafter, a report by Houghton et al. in 2009 showed that this model did not hold true for endogenous proteins *in vivo* (Houghton et al., 2009). To date, the exact mechanism regulating the Golgi-localization of GCC185 remains unknown.

Functionally, it is known that GCC185 plays a role in maintaining proper Golgi structure and that this protein is essential for proper transport between recycling endosomes and the TGN (Derby et al., 2007). Our lab has identified another function of GCC185 as serving as a scaffolding protein for CLASPs in Golgi interaction (Efimov et al., 2007). The latter of these two functions is more pertinent to the studies presented herein.

Thesis Summary

The work presented in this thesis follows up on our initial finding that the Golgi apparatus serves as an additional MTOC within the cell (Efimov et al., 2007). Not only did this publication identify a new subset of cellular MTs; it also opened the door to many unanswered questions: What is the functional significance of Golgi-derived MTs? How is the CLASP-dependent MT array at the Golgi regulated?

In Chapter II, I highlight my efforts that contributed to the publication in *Developmental Cell* in 2007 (Efimov et al., 2007) that initially identified the Golgi apparatus as an additional MTOC. Chapters III and IV focus more on the function of the Golgi-derived MT array. Chapter III discusses how Golgi-derived micotubules contribute to the establishment of an asymmetric MT array that is required for directional cell migration and Chapter IV highlights the importance of this microtubule subset in Golgi assembly and organization, polarized post-Golgi trafficking, and directional cell migration. Switching gears, Chapter V focuses on the regulation of the Golgi-derived MT array via GSK3β regulation of Golgi-associated CLASPs. Overall, this thesis contributes to a better understanding of the functional significance and regulation of the CLASP-dependent MT array at the Golgi.

CHAPTER II

GCC185 ANTIBODY DEVELOPMENT AND CLASP-SPECIFIC COATING OF GOLGI-DERIVED MICROTUBULES

This chapter highlights my contribution as a co-author to a publication from our lab in *Developmental Cell,* June, 2008 (Efimov et al., 2008).

Development of Polyclonal antibody VU-140

The production of an antibody against GCC185 was necessary to complete the studies performed in Efimov et al (Efimov et al., 2007) as well as future studies in the lab. Our collaborator Paul Gleeson kindly provided us with a small amount of antibody for initial experiments, but larger quantities were needed to complete all necessary experiments (Luke et al., 2003). Further complicating matters was the fact that we could not immunostain for endogenous CLASP and GCC185 at the same time because both were rabbit polyclonal antibodies. Therefore, initial co-localization experiments were accomplished by transient expression of a Myc-tagged GCC185 construct and staining against endogenous CLASPs. However, the antibody supply was short and we wanted to look at endogenous proteins in order to minimize artifacts that can result from protein over-expression. The polyclonal rabbit GCC185 antibody also posed problems in siRNA knockdown experiments due to the fact that we needed to be able to examine the localization of endogenous CLASPs and concurrently verify knockdown of endogenous GCC185 protein.

In order to circumvent all of the problems listed above, one of my first tasks in the lab was to develop our own antibody against GCC185 (VU-140) with different species reactivity. Our new antibody was designed recognize the C-terminus of GCC185 (nucleotide positions 4816-5064 of the KIAA0336 cDNA) and produced in guinea pig by Covance Inc, (CA). Our new guinea pig polyclonal antibody VU-140 recognized endogenous as well as transiently expressed Myc-tagged versions of GCC185 in RPE1 cells by immunostainings and western blot (Fig. 2.1 A-C). This new antibody allows the ability to examine endogenous CLASP and GCC185 simultaneously by immunofluorescence.

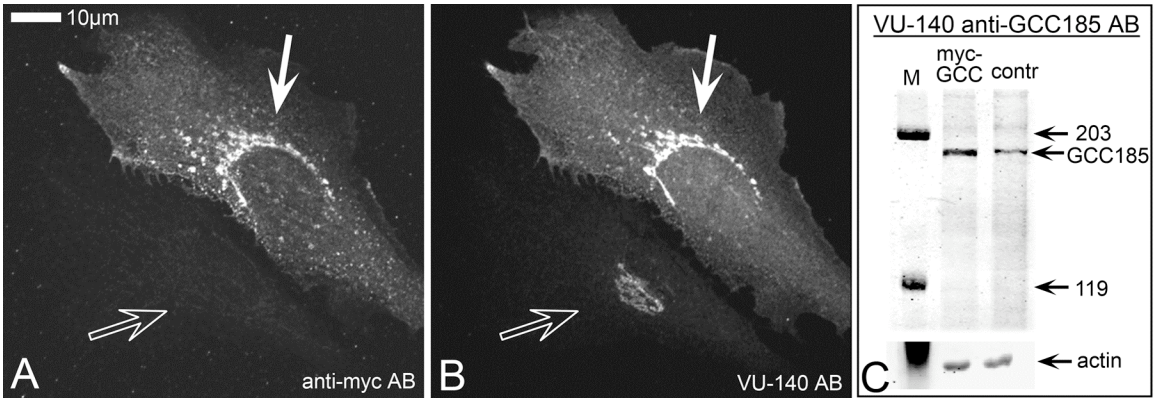

Figure 2.1. Characterization of guinea pig polyclonal antibody VU-140 against GCC185. (A-B) RPE1 cells transiently transfected with 3myc-GCC185 and immunostained with anti-myc (A) and VU-140 (B) antibodies. Note that VU-140 recognized over-expressed myc-GCC185 (white arrows) as well as endogenous GCC185 (hollow arrows). (C) VU-140 antibody staining specifically reveals GCC185 in Western blotting. Note the wide band in 3myc-GCC185 expressing cells (myc-GCC lane) as compared to non-transfected cells (contr). Actin, loading control. (Figure S9 from (Efimov et al., 2007)).

Golgi-derived Microtubules are Specifically Coated with CLASPs

Since siRNA targeting of CLASPs disrupts MT formation at the Golgi and does not alter centrosomal MT nucleation, CLASPs must play a specific role in formation of Golgi-derived MTs. Consistent with this idea, initial immunostaining experiments in RPE1 cells revealed that the amount of CLASPs associated with Golgi-derived MTs was significantly higher than those growing from the centrosome (Fig. 2.2 A-B). This result was confirmed by live-cell imaging in steady-state (Fig. 2.2 C-D). However, we needed to confirm that the same result holds true for newly formed MTs after nocodazole washout. Immunostaining showed after 45 seconds of nocodazole washout that CLASP intensity on non-centrosomal MTs was significantly higher than CLASP intensity on centrosomal MTs (Fig. 2.2 E-G). Ultimately confirming that these CLASP-coated MTs are indeed nucleated at the Golgi, I performed live-cell imaging with GFP-CLASP and mCherry GT (Golgi marker) upon nocodazole washout (Fig 2.2 H-K). These experiments confirmed that Golgi-derived MTs are specifically coated with CLASPs during their initial growth phase, whereas centrosomal MTs are not. To date, this is the only defining characteristic distinguishing centrosomal and Golgi-derived MT composition. No other post-translational tubulin modifications (such as acetylation, detyrosination, or polyglutamylation) have shown to be specifically enriched in either centrosomal or Golgi-derived MT subsets.

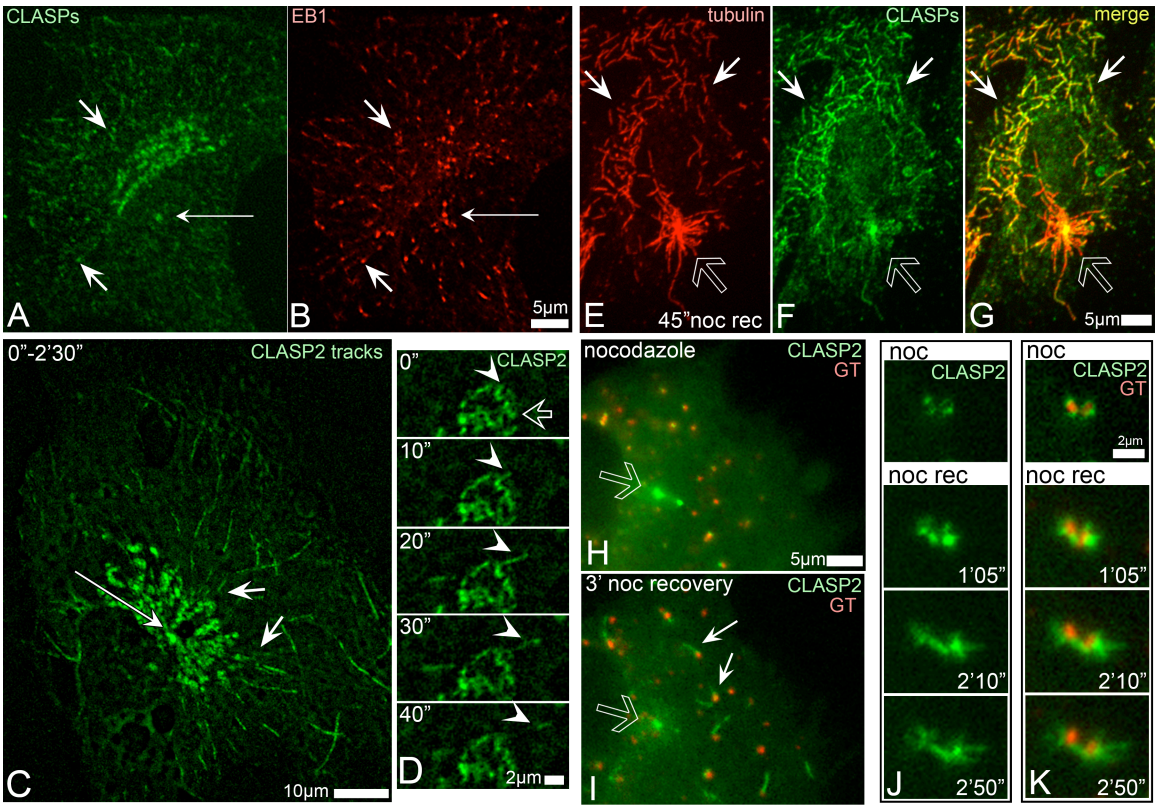

Figure 2.2. CLASPs preferentially bind to MTs originated at the Golgi.
(A) CLASPs (green) in RPE1 cells are associated with MT tips close to the Golgi (short arrows), but not around the centrosome (thin arrow). (B) EB1 (red) and the MT tips in the cell shown in (A). Immunostaining. (C) Overlaid live recording of GFP-CLASP2-expressing RPE1 cell within 2.5 min. CLASP2-associated MT tracks (short arrows) radiate from the TGN but not from the centrosome (thin arrow). (D) Live sequence illustrating formation of a GFP-CLASP2-decorated MT (arrowhead) at the CLASP-rich TGN (hollow arrow) in an untreated cell. CLASP2 coats whole newly formed MTs (10-20 s) but remains only at the tip at a later stage (30-40 s). (E-G) A cell fixed 45 s after nocodazole washout. (E) Tubulin (red). (F) CLASPs (green). (G) Merge. CLASPs localize to noncentrosomal (white arrows) but not to centrosomal (hollow arrow) MTs. (H and I) GFP-CLASP2 (green) localizations before and after nocodazole washout. In nocodazole (H), CLASP2 associated with Golgi stacks (mCherry-GT, red) and with the centrosome (hollow arrow). Three minutes after nocodazole removal (I), CLASP2 is detected at the Golgi-associated MTs (white arrows) but not around the centrosome (hollow arrow). (J and K) Video frames illustrating formation of GFP-CLASP2-coated MTs at GFP-CLASP2-enriched Golgi stacks in nocodazole washout. (J) GFP-CLASP2. (K) GFP-CLASP2, green; mCherry-GT, red. Time after nocodazole removal is shown. (Figure 6 from (Efimov et al., 2007)).

CHAPTER III

MICROTUBULE NETWORK ASYMMETRY IN MOTILE CELLS: ROLE OF GOLGI-DERIVED ARRAY

This chapter is published under the same title in *Cell Cycle*, July, 2009 (Vinogradova T, Miller P.M., and Kaverina I., 2009). I was second author on this review and contributed data for a figure and manuscript edits.

Abstract

Cell migration requires polarization of the cell into the leading edge and the trailing edge. Microtubules (MTs) are indispensable for polarized cell migration in the majority of cell types. To support cell polarity, MT network has to be functionally and structurally asymmetric. How is this asymmetry achieved? In interphase cells, MTs form a dynamic system radiating from a centrosome-based MT-organizing center (MTOC) to the cell edges. Symmetry of this radial array can be broken according to four general principles. Asymmetry occurs due to differential modulation of MT dynamics, relocation of existing MTs within a cell, adding an asymmetric nucleation site, and/or repositioning of a symmetric nucleation site to one side of a cell. Combinations of these asymmetry regulation principles result in a variety of asymmetric MT networks typical for diverse motile cell types. Importantly, an asymmetric MT array is formed at a non-conventional MT nucleation site, the Golgi. Here, we emphasize the contribution of this array to the asymmetry of MT network.

Importance of MT Asymmetry in Motile Cells

Cell migration in higher organisms is essential for multiple physiological and pathophysiological processes including embryonic development, tissue regeneration, immune responses, and cancer cell metastasis and invasion. The first requirement for directional cell movement is a polarization of the cell into the leading edge and the trailing edge. A highly regulated asymmetric remodeling of the actin cytoskeleton controlled by small GTPases of the Rho family drives polarized motility (for reviews see refs. (Raftopoulou and Hall 2004; Small and Resch 2005)). Motility also involves asymmetric formation and turnover of focal adhesions – the cell anchorage sites (for a review see ref. (Kaverina et al., 2002)) and directed post-Golgi trafficking to the protruding lamella (for a review see ref. (Mellor 2004)).

Microtubules (MTs) are indispensable for polarized cell migration in a variety of cell types, including fibroblasts, astrocytes and neurons (Vasiliev et al., 1970) (for reviews see refs. (Small et al., 2002; Etienne-Manneville 2004)) and for major tissue morphogenetic movements such as gastrulation (Kwan and Kirschner 2005). Formation of cell edge protrusions and retractions continues in the absence of MTs but is not distributed in a polarized fashion. MTs are therefore thought to support polarized distribution of regulatory motility signals within a cell.

Some specialized cells, like fish keratocytes or neutrophils, do not need the MT-driven intracellular management for migration, likely due to their small size and simplicity (Small et al., 2002; Etienne-Manneville 2004). But, although neutrophils are able to move in the absence of MTs, they exhibit impaired directionality of migration (Xu et al., 2005). The effect of MT disruption on neutrophil motility, though unusual, is likely due to depolarization of signaling events. Thus, in the majority of cell types MTs are needed for the spatial coordination of molecular events leading to efficient cell relocation. In Dictyostelium amoebae that exhibit similar minor MT dependence MTs directed toward the cell rear are responsible for trafficking of adenylyl cyclase-containing vesicles in that direction, which, in turn, coordinates migration of following cells (streaming) (Kriebel et al., 2008). In this case, asymmetric MT distribution is important for coordination of signals on the multicellular level rather than within each small cell. In many systems, an external signal triggers initial asymmetry of adhesive and actin systems that further need MTs for maintenance (Oliferenko et al., 2000; Condeelis et al., 2005). In some cases (e.g. in differentiating neurons (de Anda et al., 2005)), MTs appear to be involved in the initiation of polarity.

Many asymmetric processes essential for cell migration, such as Rac1-dependent actin polymerization (Waterman-Storer et al., 1999) and focal adhesion turnover, (Kaverina et al., 1999; Ezratty et al., 2005) are coordinated by MTs. MTs have been shown to deliver and control various functional molecules involved in motility, either as protein complexes or within vesicular membranes.

These include b-actin mRNA (Oleynikov and Singer 1998) and members of Rho GTPase pathways (Waterman-Storer et al., 1999; Krendel et al., 2002) to organize actin and adhesion rearrangements, integrins to initiate adhesion (Caswell and Norman 2006), membrane to provide building blocks for protrusion (for a review see ref. (Nabi 1999)) and many others. Some molecules (e.g. integrins) are simply transported to their functional sites by MTs; the functional activity of others, like Rho GEF H1, (Zenke et al., 2004) can be modulated by MT binding. Moreover, MT-binding properties of certain active molecules often depend on the dynamic status of MTs. For instance, certain kinesins preferentially bind de-tyrosinated stable MTs (Dunn et al., 2008; Konishi and Setou 2009; Zekert and Fischer 2009) and a number of diverse factors surf growing MT plus ends (for a review see ref. (Akhmanova and Hoogenraad 2005)). Accordingly, the presence of a reliable MT "track" is central for some pathways, while even subtle modulations in MT dynamics can be critical for others. In this regard, it is noteworthy that both MT distribution and dynamics are asymmetric in motile cells.

Variants and Principles of MT Asymmetry

In order to differentially control diverse domains in a polarized cell, the MT system must be functionally asymmetric. The most logical way to support spatial functional asymmetry is to use a structurally asymmetric regulatory system. How is this asymmetry achieved? In general, MTs form a dynamic system radiating from a perinuclear centrosome-based MT-organizing center (MTOC) to the cell edges. In fibroblasts and other cells with mesenchymal motile phenotype, the

distribution of MTs is asymmetric, with a substantial array extended in the direction of movement. This front-oriented array is likely essential for persistent directional motility of these cell types via facilitating actin polymerization, (Waterman-Storer et al., 1999) adhesion turnover (Kaverina et al., 1999; Rid et al., 2005) and vesicular trafficking (Prigozhina and Waterman-Storer 2004) toward the protrusion. On the contrary, in migrating neutrophils MTs are directed almost exclusively toward the trailing cell edge (Eddy et al., 2002). Upon MT depolymerization, these cells demonstrate defects in finding the shortest way to the chemo-attractant. Interestingly, directional motility of neutrophil disturbed by MT disruption can be restored by inhibiting Rho kinase at the cell rear where MTs are located (Xu et al., 2005). Similarly, MTs are predominantly directed toward the rear of migrating Dictyostelium amoebae where their major signal distribution function is associated with backward vesicular transport (Kriebel et al., 2008). Another example, neurons present an extreme example of MT asymmetry, with principally distinct MT organization in dendrites and axons, which corresponds to distinction in major vesicular transport functions (for reviews see refs. (Goldstein and Yang 2000; Arimura and Kaibuchi 2007)). In all three scenarios, despite obvious differences, asymmetric MT organization is well suited to provide uneven distribution of signals within a cell and can be achieved by a few variably combined mechanistic principles.

As mentioned above, MTs in interphase cells are nucleated at the centrosome in the cell center. However, MT arrays initially produced by the

centrosome are radially symmetric both *in vitro* (Bergen et al., 1980; Holy et al., 1997) and in polarized cells (Salaycik et al., 2005). Four general principles can be applied to breaking symmetry of the MT network (Fig. 3.1). First, centrosomal MT array can be modified by differential regulation of MT dynamics at distinct locations. As a result of site-specific modulation of MT dynamics, MTs can be stabilized at one cell side and/or destroyed at the other side. Second, MTs can be moved either within the array or after detachment from the array. Third, an alternative, non-centrosomal source of MTs can produce an additional, asymmetric MT array. Finally, relative positioning of MT nucleation sites within a cell can also modulate the MT asymmetry. For example, locating the centrosome to one cell side would be sufficient to apply a certain degree of asymmetry to the MT network.

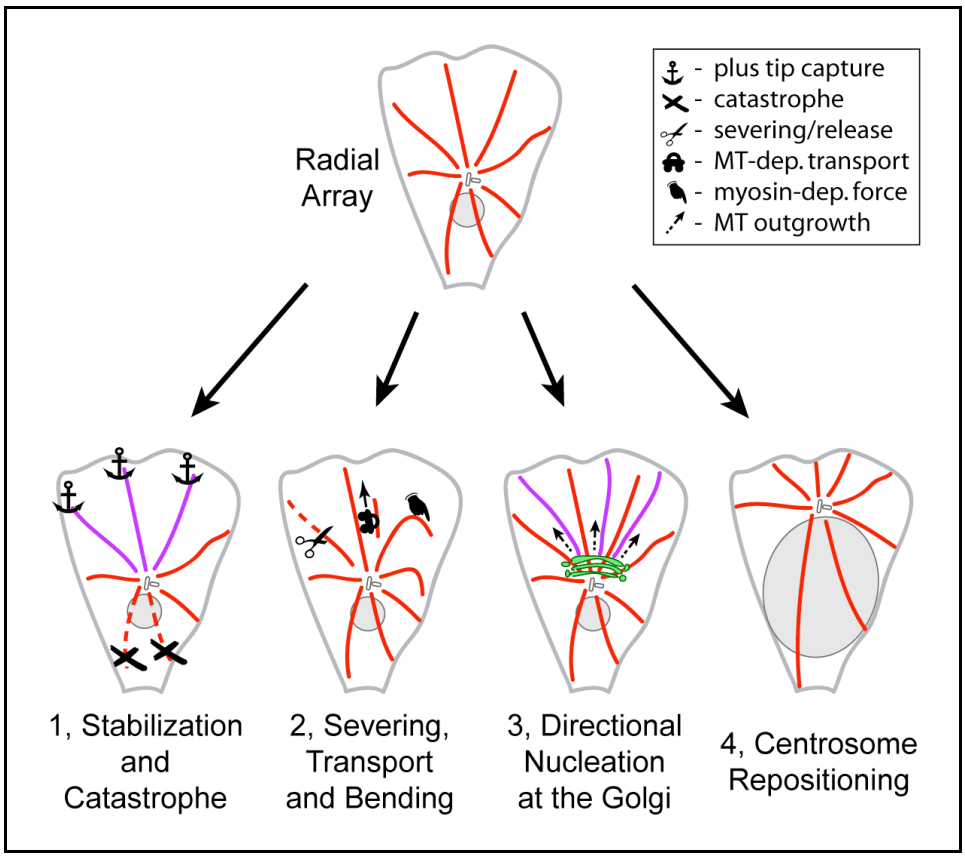

Figure 3.1. Principles of MT asymmetry.
Radial array (top) can be transformed into asymmetric network by 1) modulations of MT dynamics, 2) re-positioning of existing MTs, 3) directional MT formation at alternative MT nucleation sites (bottom, right) and/or 4) repositioning of MTOCs within a cell.

Regulation of MT Asymmetry via Modulation of Plus End Dynamics

Dynamic properties of individual MTs in cells are diverse. While many MTs undergo “dynamic instability” (Kirschner and Mitchison 1986), characterized by particular frequencies of catastrophes (switch to depolymerization) and rescues (switch to polymerization), certain “stable” MTs remain unchanged for hours (Gundersen and Bulinski 1988). A majority of MTs exhibit persistent growth through the cytoplasm and undergo diverse dynamic changes when they reach cell periphery (Komarova et al., 2002). In a motile cell, MT dynamic parameters are specific for certain cell regions. For example, a particularly long-lived subset of MTs extends from the cell center toward the leading edge in migrating fibroblasts (Gundersen et al., 1984). In addition, the time that otherwise dynamic MT ends spend in pauses as well as MT catastrophe frequency varies significantly in distinct PTK1 epithelial cell domains (Wadsworth 1999). Dynamic diversity of MTs can be regulated through general stabilization of MT lattice by MAP binding or through alteration of plus end MT dynamics as a function of the cell periphery (for a review see ref. (Amos and Schlieper 2005)). The latter is highly relevant for migrating cells where properties of peripheral cytoplasm are distributed asymmetrically. Mechanisms of plus end dynamics modulation have been intensively studied over the past decade.

Long MT lifetimes can be achieved by a few complementary mechanisms. A number of phenomena described in variable fibroblastic and epithelial cells, including MT capture, stimulated persistent growth and/or frequent rescues of

MTs close to the cell front, lead to longer MT existence. MT capture at the cortex involves association of MT plus-tips with a number of proteins specifically accumulated at the leading edge protrusions, including APC *(*Watanabe et al*.,* 2004; Wen et al., 2004) and LL5beta (Lansbergen et al., 2006) and is ruled by Rho family of small GTPases through Rac effector IQGAP (Fukata et al., 2002) and Rho effector mDia (Wen et al., 2004). One such local mechanism involves capture of MT plus ends specifically at lipid rafts at the protruding cell edge (Watanabe et al., 2004). MT lifetime is also increased by MT-associated proteins that preserve MT from depolymerization by promoting efficient rescues (Morrison et al., 1998; Komarova et al., 2002; Mimori-Kiyosue et al., 2005). Anchoring of MTs at cortical accumulations of LL5-Beta and ELKS proteins, which together with plus tip proteins CLASPs form cortical clusters in close focal adhesion proximity, (Lansbergen et al., 2006) may explain MT capture at focal adhesion phenomenon observed previously (Kaverina et al., 1998).

Additionally, persistent MT growth can be stimulated by excluding catastrophe activity from a certain cellular area. Small GTPase Rac1 that is locally active at the protruding edges inhibits MT depolymerization factor stathmin through Rac effector PAK1-driven stathmin phosphorylation (Wittmann et al., 2003; Wittmann et al., 2004). At the same time, an increasing gradient of stathmin activity extends backwards and may be at least partially responsible for significant increase in MT catastrophe frequency at the trailing edge as compared to the leading edge (Niethammer et al., 2004). However, mechanisms

that support catastrophes at the cell back are not completely understood. MT plus ends that interact with adhesion sites in the process of targeting in fish fibroblasts are subjected to local catastrophe-inducing activity of unknown origin, which specifically requires presence of a major adhesion protein paxillin (Efimov et al., 2008). Since adhesions are particularly large at the cell rear, and catastrophes at the back are dependent on Rho activity (Wadsworth 1999) that simulates adhesion growth through a mechanosensory mechanism (for a review see ref. (Geiger and Bershadsky 2002)), we speculate that Rho stimulates catastrophes via enlarging adhesions as sites of catastrophe factor accumulation at the cell rear.

Regulation of MT Asymmetry via MT Transport

Besides changes in dynamics that influence MT lifetimes, distribution of existing MTs can be changed by moving MTs within a cell. Such movements, driven by molecular motor activity, are often specific for distinct domains a of a motile cell (Yvon and Wadsworth 2000) (Waterman-Storer and Salmon 1997).

In many cases motors move MTs that are still attached with their minus ends to the MTOC. For example, in neutrophils, myosin II-driven MT bending results in complete re-directing of symmetrically nucleated MT array toward the cell rear (Eddy et al., 2002). Similarly, myosin II in neurons and epithelial cells can induce MT bending that results in excluding them from protruding lamella due to actin retrograde flow (Waterman-Storer and Salmon 1997; Schaefer et al.,

2002). Myosin contractility also facilitates MT re-organization and bundling behind the leading edge in axonal growth cones (Burnette et al., 2008).

Molecular motors can also relocate MTs that are no longer anchored at their nucleation sites. However, MT release from the centrosome in epithelial and fibroblastic cells – a source for both tubulin turnover and free MT fragments (Keating et al., 1997; Komarova et al., 2002) – has not been shown to exhibit any asymmetry. In neurons, on the contrary, MTs fragments produced by katanin and spastin-dependent severing are transported to distinct cell locations to build up highly asymmetric MT system within axons and dendrites (for reviews see refs. (Baas 1998; Baas et al., 2006)). Transport of MT fragments can be performed by acto-myosin dependent movements (Hasaka et al., 2004) or by MT motors (for reviews see refs. (Goldstein and Yang 2000; Baas et al., 2006)). Strikingly, asymmetric MT transport in neurons can be regulated by kinesin-5 (Myers and Baas 2007) which has been previously well studied as a major force that moves MTs along each other in the mitotic spindle.

Regulation of MT Asymmetry via Directed Non-centrosomal Nucleation

The MT pattern depends largely on the process of nucleation at the MTOC. In many motile cells, the centrosome is located in front of the nucleus, and it is thought to be an important stage of polarization of both the MT system and the whole cell (Etienne-Manneville and Hall 2003). Indeed, formation of asymmetric MT arrays in differentiating neurons shows a direct correlation with

centrosome positioning (de Anda et al., 2005). It is noteworthy in this regard that MT nucleation can also occur by centrosome-independent means (Bartolini and Gundersen 2006). A number of MT-organizing structures have been identified in certain specialized cell types. Among these are the nuclear envelope in myotubes (Bugnard et al., 2005) and melanosomes in pigment cells (Malikov et al., 2004). A more abundant alternative MT-nucleating site is the Golgi complex as it carries out MT nucleation in retinal pigment epithelial cells (Efimov et al., 2007; Rivero et al., 2009) and in multiple other epithelial cell lines (Efimov et al., 2007).

In interphase cells, the Golgi complex is asymmetric. It forms a “ribbon” that consists of membrane cisternae stacks with distinct *cis*-to-*trans* polarity (Ladinsky et al., 2002). MT depolymerization causes disruption of the Golgi ribbon into individual stacks but the polarity within each stack is preserved (Cole et al., 1996). In the presence of MTs, the Golgi complex accumulates close to the centrosome due to the function of dynein, a minus-end directed MT motor (Barr and Egerer 2005; Vaughan 2005). The generally accepted view is that the cis-compartment predominantly faces the centrosome, while the trans-compartment looks toward the cell periphery. Thus, the centrosome, being symmetric, maintains an asymmetric organelle in close proximity. MT array that is formed at the Golgi is also asymmetric: Golgi-derived MTs grow predominantly toward the front of motile cells (Efimov et al., 2007). Thus, the centrosome may influence MT asymmetry indirectly via positioning of the Golgi complex.

Mechanisms and Regulation of MT Nucleation at the Golgi

Golgi-associated MT nucleation appears to be a significant factor in establishing of MT asymmetry (Fig. 3.2). It is important to understand molecular machinery that underlies directional mode of MT outgrowth at the Golgi (Fig. 3.3). MT nucleation at the Golgi continues upon laser ablation of the centrosome indicating that the Golgi acts as a centrosome-independent MTOC (Mimori-Kiyosue et al., 2005). However, it requires presence of gamma-tubulin, the major component of the MT nucleating gamma-tubulin ring complexes (gamma-TuRCs) (Chabin-Brion et al., 2001; Efimov et al., 2007). Is initial enrichment of gamma-TuRC in proximity of CLASP accumulations important for organization of MT arrays? In most cases, levels of gamma-tubulin detected at the Golgi membrane do not exceed cytosolic gamma-tubulin concentrations. However, gamma-tubulin has been found associated with Golgi membranes in vitro (Chabin-Brion et al., 2001) and in vivo upon overexpression of a potential recruiter GMAP210, (Rios et al., 2004) a cis-Golgi associated protein though it has been a subject of debate (Barr and Egerer 2005). Recent evidence suggests that gamma-tubulin may be recruited to the Golgi membranes through interaction with AKAP450, a protein involved in MT regulation both at the centrosome and the Golgi (Larocca et al., 2006; Rivero et al., 2009). Notably, AKAP450 is required for Golgi-derived MT formation and can be found in close association with their minus ends (Rivero et al., 2009). It is possible that AKAP450 stimulates Golgi-derived MT formation by elevating concentration of gamma-tubulin at the Golgi membrane.

Importantly, nucleation *per se* appears to be insufficient for MT formation: gamma-TuRCs nucleated MT seeds cannot give rise to MTs unless they are associated with Orbit/MAST/CLASP, a well-studied regulator of MT dynamics (Mimori-Kiyosue et al., 2005). Depletion or misplacement of this protein from the Golgi membrane leads to elimination of Golgi-derived MT array and impairs MT asymmetry (Fig. 2). In mammalian cells CLASP (Cytoplasmic Linker Associated Protein) is present as two closely related isoforms, CLASP1 and CLASP2. Here, we will refer to both isoforms together as CLASPs. CLASPs are essential regulators of MT dynamics both in mitotic and interphase cells. During mitosis, CLASPs support incorporation of tubulin subunits into kinetochore fibers (Maiato et al., 2005; Hannak and Heald 2006) and thus assure correct chromosome segregation. In motile interphase cells, CLASPs laterally anchor MTs at peripheral cortical sites, increasing their stability and growth persistence (Lansbergen et al., 2006). In both cases, CLASP function is connected with lateral stabilization of MTs that favors polymerization at the plus ends. It is plausible to suggest that CLASP function at the Golgi is accomplished by a similar mechanism. Indeed, CLASPs coat Golgi-associated MTs to trigger their formation (Efimov et al., 2007). Such coating and subsequent stabilization of MT seeds may be regulated by changing CLASP affinity to MTs by phosphorylation (Akhmanova et al., 2001; Wittmann and Waterman-Storer 2005). Moreover, for MT coating to occur, CLASP molecules undergo fast exchange at the membrane (our unpublished data). Altogether, these data suggest that modulating CLASP association with the Golgi membranes can alter MT-organizing potential of the

Golgi. CLASPs are accumulated at the Golgi via TGN (Trans Golgi Network) protein GCC185 (Efimov et al., 2007). GCC185, in turn, is recruited to the TGN membranes by cooperative action of two small GTPases, Arl1 and Rab6 (Burguete et al., 2008). Thus, being important components of trafficking-organizing signaling (for reviews see refs. (Munro 2005; Short et al., 2005)), Arl1 and Rab6 may have an indirect impact on MT organization.

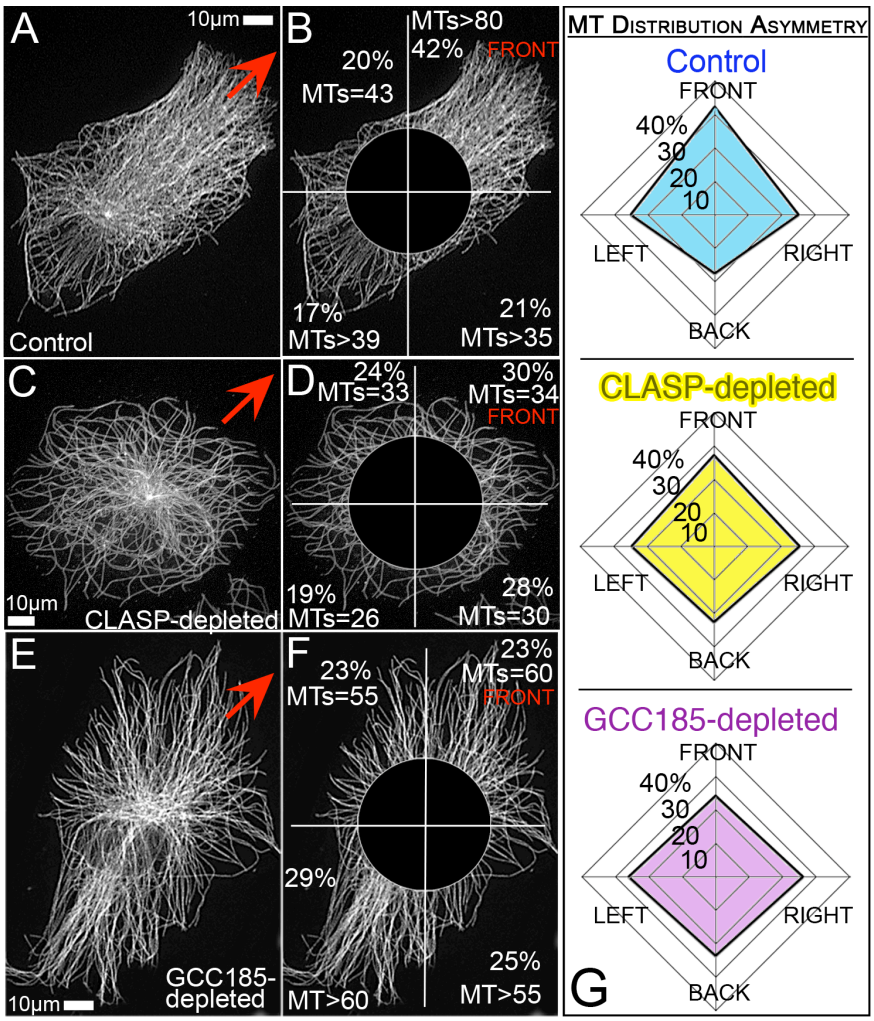

Figure 3.2. MT asymmetry requires Golgi-derived MTs.
Immunostained MTs in control (A,B), CLASP- (C,D) and GCC185-depleted (E,F) cells. CLASP depleted cells lack non-centrosomal MTs, while in GCC185 non-centrosomal MTs are not associated with the Golgi due to CLASP mis-localization (Efimov et al., 2007). Red arrows mark the front lamella direction. B,D,F, For analysis, central area is excluded and the rest of the cell divided in 4 sectors. For each sector, detectable MT numbers and average fluorescent intensity as percent of overall intensity are shown. G, Average percentage of edge MTs intensity distributed in 4 cell sectors. 20 cells for each set were analyzed. Note decreased asymmetry of diagrams for CLASP and GCC185-depleted cells. Standard deviations for front to back intensity proportion (not shown) do not overlap between control and knockdown cell populations.

Why is the Golgi-derived MT Array Asymmetric?

Protein machinery that triggers MT formation at the Golgi can function even in the absence of typical Golgi membrane, for example, upon brefeldin A treatment. Under these conditions MTs form throughout a cell (Efimov et al., 2007) and can be often found at ER exit sites (Rivero et al., 2009). Both CLASP coating (Efimov et al., 2007) and AKAP450 presence at MT minus ends (Rivero et al., 2009) were shown necessary to support non-centrosomal MTs under these conditions. However, mis-placement of MT nucleation from the Golgi (e.g. by GCC185 depletion, Fig. 3.2) leads to elimination of MT asymmetry in these cells. Thus, specific localization of this MT array to the Golgi is needed for its polarized geometry.

As we discussed above, the Golgi complex is intrinsically asymmetric. Distinct components of MT-initiating machinery are found at distinct compartments within the Golgi. While nucleation has been associated with cis-Golgi markers (e.g. AKAP450), MTs successfully grow from the Golgi membrane only after being stabilized by TGN-associated MT regulators (CLASPs). Thus, plausible scenarios of MT seed location within a polarized Golgi stack include: a) concentration of gamma-tubulin at the cis Golgi membrane provides a pool of MT seeds that later redistribute to TGN to serve as MT templates at this location, or b) MT seeds associated with the cis-Golgi give rise to multiple unstable MTs, a certain portion of which reaches out to TGN and is being stabilized by CLASPs (Fig. 3.3).

In either case, asymmetry of Golgi-derived MTs toward the cell front can be directly connected to the asymmetry of the Golgi ribbon itself because MTs grow from the outer face of the Golgi ribbon (Efimov et al., 2007). This model is valid only when the Golgi ribbon is indeed polarized as a whole. However, spatial asymmetry has been strictly shown at a level of a single Golgi stack. On the contrary, the asymmetry of the whole Golgi complex is not a given but requires a certain organization of stacks relative to each other. Our data suggest that both Golgi-derived and centrosomal MTs are necessary for establishment of a polarized Golgi ribbon (Miller et al., 2009). A large number of integral Golgi proteins are also required for the proper organization of the Golgi (for a review see ref. (Short et al., 2005)) as they support both cisternal membrane fusion (Puthenveedu et al., 2006) and stacking (Bisel et al., 2008). Additionally, proteins that regulate centrosome-nucleus attachment (Robinson et al., 1999; Malone et al., 2003; Tanaka et al., 2004; Collin et al., 2008) can influence organization and shape of the Golgi complex. In the case of tight centrosome-nucleus attachment, Golgi elements cannot penetrate between the centrosome and nuclear envelope. Such spatial restraint facilitates flat, asymmetric Golgi ribbon shape (our unpublished data).

Alternatively, it is possible that the shape of the Golgi complex is not critical for asymmetry of the MT array. Rather, this asymmetry could depend on differential affinity of CLASP binding to MTs if it is regulated in a polarized fashion across the Golgi complex. CLASP binding to MTS can be diminished by

GSK3beta-dependent phosphorylation. This regulation was shown to be spatially specific (Wittmann and Waterman-Storer 2005) because local inactivation of GSK3beta in protruding lamellae causes extensive CLASP binding to MT lattice. A similar mechanism involving local activation of GSK3beta at the centrosome (evident from GSK3beta localization at the centrosomes (Bobinnec et al., 2006) and phosphorylation of centrosomal proteins (Howng et al., 2004)) or at the nuclear envelope (Miller et al., 1999) could restrict CLASP binding to MT seeds at the TGN areas close to the centrosome/nucleus and result in predominantly front-directed MT outgrowth.

Besides a distinct CLASP-dependent formation mechanism, Golgi-derived MTs (and, possibly, also centrosomal MT in the Golgi proximity) possess specific properties that include post-translational modifications and MT-binding proteins. Golgi-associated MTs were described as excessively detyrosinated, acetylated (Thyberg and Moskalewski 1993) and/or polyglutamylated (Spiliotis et al., 2008), properties that can influence MT motors affinity and specificity of these MTs as trafficking routes (Reed et al., 2006; Dunn et al., 2008; Spiliotis et al., 2008). Certain Golgi-associated proteins may locally modulate MT stability (e.g. Golgi-associated CAP350 that has been implicated in MT stability and anchoring to the centrosome (Hoppeler-Lebel et al., 2007)). If distributed asymmetrically within the Golgi ribbon, such proteins could influence survival of MTs growing in a certain direction.

Role of the Organelle Positioning and Combination of Factors

All discussion provided above on the issue of transforming of a radial array into asymmetric one assumed that the centrosome is located in the center of a cell providing a symmetric array. Indeed, in many motile cells the centrosome localized to the cell centroid in dynein-dependent manner.(Burakov et al., 2003) However, asymmetry can be introduced by shifting the MTOC (or both MTOCs) to one side of a cell, for example by a large organelle. This can produce a concentrated MT density at the closest cell edge. Such shifting can occur in cells where the nucleus takes a large part of cell volume (e.g. lymphocytes (Hulspas et al., 1994)).

Relative positioning of MTOCs and the nucleus can introduce asymmetry as a result of relocation of the nucleus rearward even while the centrosome stays in the cell centroid (Gomes et al., 2005). In this case, due to the tight attachment of the centrosome to the nucleus, the Golgi ribbon can be shifted in front of the centrosome so the Golgi-derived array becomes front-oriented. According to this model, three factors including 1) maintenance of the centrosome in the cell centroid, 2) rearward nucleus movement and 3) TGN-derived MT array formation are sufficient to provide initial asymmetry to MT network, which can be further strengthened or modified by MT dynamics-driven and MT transport mechanisms.

Assorted combinations of MT network asymmetry principles described here allow highly variable and fine-tunable MT distribution in motile cells. Each of these mechanisms may contribute to microtubule asymmetries in multiple cell types, while some of the mechanisms could be more important in certain cells compared to others. Additionally, some of the mechanisms may be specific to distinct cell types. Here, we suggest a generalized systematic approach to MT asymmetry principles which allows to compare their contributions in particular cell types and address how tuning of MT regulations is handled throughout cell differentiation and morphogenesis.

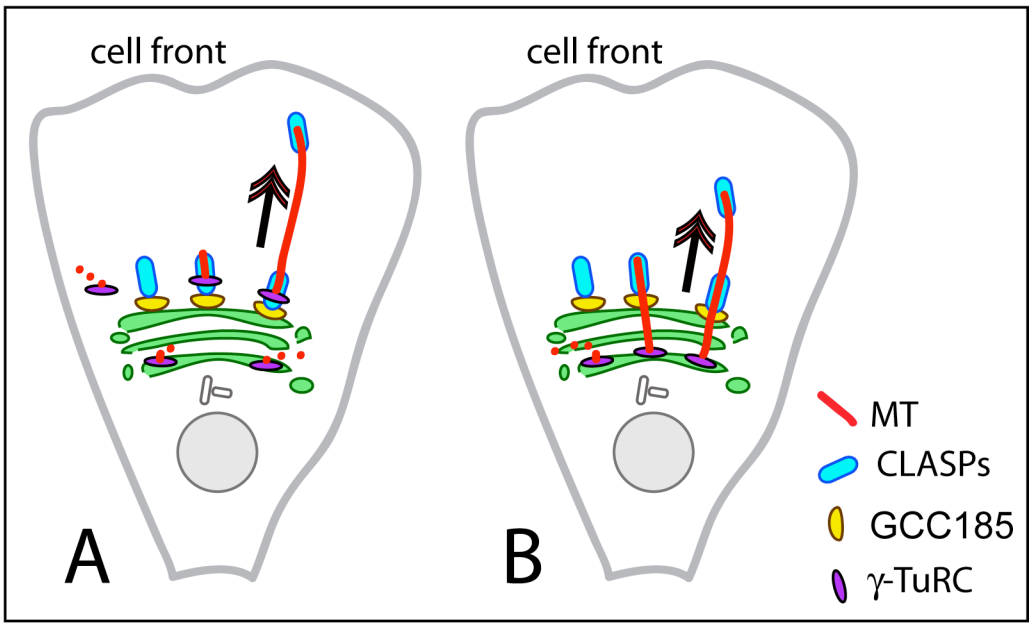

Figure 3.3. Non-centrosomal asymmetric MT array at the Golgi.
A. After MTs nucleation by γ-TuRC at cis-Golgi or in cytosol, those MT seeds, which redistribute to the TGN continue growing due to CLASP-dependent stabilization and anchoring to the TGN by GCC185. B, After MTs nucleation by γ-TuRC at cis-Golgi, those MTs, which extend to the TGN continue growing due to CLASP-dependent stabilization.

Acknowledgements

Work in the author's laboratory is supported by NIH NIGMS grant 1RO1GM078373-01A2 and pilot grant from NIH NCI SPORE in GI cancer # 5P50 CA095103-07.

CHAPTER IV

GOLGI-DERIVED CLASP-DEPENDENT MICROTUBULES CONTROL GOLGI ORGANIZATION AND POLARIZED TRAFFICKING IN MOTILE CELLS

This chapter is published under the same title in *Nature Cell Biology*, September, 2009 (Miller et al., 2009).

Abstract

Microtubules are indispensable for Golgi complex assembly and maintenance that is an integral part of cytoplasm organization in interphase mammalian cells. Here, we show that two discrete microtubule subsets drive two distinct, yet simultaneous, stages of Golgi assembly. In addition to the radial centrosomal microtubule array, which positions the Golgi in the cell center, we identify a role for microtubules that form at the Golgi membranes in a manner dependent on microtubule regulators CLASPs. These Golgi-derived microtubules draw Golgi mini-stacks together in tangential fashion and are critical for establishing continuity and proper morphology of the Golgi complex.

We propose that specialized functions of these two microtubule arrays arise from their specific geometries. Further, we demonstrate that directional post-Golgi trafficking and cell migration depend on Golgi-associated CLASPs suggesting that correct organization of the Golgi complex by microtubules is essential for cell polarization and motility.

Introduction

The microtubule (MT) cytoskeleton is to a large extent responsible for dynamic architecture of the cytoplasm, including global changes associated with cell cycle progression. In order to successfully adapt to dynamic conditions, cells often distribute the MT "work-load" to functional MTs subsets that are specific for interphase or mitosis (Karsenti et al., 1984; Zhai et al., 1996; Walczak and Heald 2008). MT subsets can be distinguished, for example, by their dynamic or motor binding properties. In particular, dynamic properties of mitotic MTs differ between kinetochore and astral MT subsets. Similarly, distinct front-oriented stable MT arrays establish polarity of motile interphase cells (Bulinski et al., 1988; Gundersen et al., 2004). Orientation and positioning of MTs within a cell, which are important for functional subset partition, to a large extent depend on the MT nucleation sites. For example, MTs originating at the centrosomes and kinetochores build a mitotic spindle in cooperative fashion due to their distinct geometry and growth directionality (O'Connell and Khodjakov 2007).

MT subsets of distinct origin also exist in motile interphase cells. In particular, we have recently discovered a novel MT subset that is nucleated at the Golgi apparatus (Efimov et al., 2007). In contrast to radial centrosomal MTs, Golgi-derived MTs form a wide array extending toward the cell edge. This array specifically depends on MT-stabilizing proteins CLASPs (CLIP-associated proteins), which coat Golgi-derived MTs and thus make them biochemically and dynamically dissimilar from the centrosomal array. Thus, the Golgi-derived MT

subset is characterized by specific origin, orientation, and protein composition. Do distinct properties of Golgi-derived MTs confer specific functional abilities to this MT subset?

Interphase mammalian cells typically have an integrated, centrally located Golgi complex that serves as the major center for protein sorting. Upon mitotic exit, Golgi mini-stacks are formed by tightly regulated fusion of small Golgi membrane vesicles into cisternae that undergo subsequent stacking. Formation of mini-stacks is MT-independent and can be reconstituted in a cell-free system (Tang et al., 2008) or in a MT-devoid cell at ER exit sites (Cole et al., 1996). Next, these mini-stacks utilize an evolving interphase MT network and the minus-end directed MT motor dynein (Burkhardt 1998; Thyberg and Moskalewski 1999; Allan et al., 2002; Bornens 2008) to form a continuous Golgi ribbon. However, it is not clear how correct organization of the Golgi ribbon is achieved by dynein transport. Given that CLASP-dependent MTs are closely associated with the Golgi membrane, their specific function may relate to the Golgi organization.

Here, we show that MTs growing from dispersed Golgi stacks exhibit a classical “search and capture” (Kirschner and Mitchison 1986) scenario whereby mini-stacks cluster in the cell periphery. Furthermore, Golgi-derived and centrosomal MTs act in concert to organize individual Golgi stacks into a continuous ribbon structure that, in turn, supports the polarity of post-Golgi vesicular trafficking in migrating cells. Centrosomal MTs alone appear to be

insufficient for proper Golgi ribbon formation though they actively support central Golgi positioning. Importantly, the distinction between centrosomal and Golgi-derived MT functions arises from their geometry and orientation within the cell. Our findings provide the first demonstration of the functional significance of Golgi-derived MTs and highlight the defining role of functionally distinct MT subpopulations in organization of cellular architecture.

Results

MTs assemble the Golgi ribbon in two stages

Individual Golgi mini-stack formation is MT-independent, while Golgi complex assembly requires MTs (Burkhardt 1998; Storrie and Yang 1998). To investigate in detail explicitly the MT-dependent assembly, we employed nocodazole washout assay. Full MT depolymerization in Human Retinal Pigment Epithelial (RPE1) cells by nocodazole treatment resulted in dispersal of Golgi mini-stacks (Fig. 4.1a,b). Live-cell imaging of Golgi re-assembly upon nocodazole washout (Fig. 4.1a) revealed that Golgi mini-stacks undergo initial clustering in the cell periphery (Fig. 4.1a). Quantitative analysis of both live imaging sequences and fixed immunostained samples revealed that Golgi particle size doubled at this time (Fig. 1d,e). Clusters then relocated to the cell center to complete Golgi ribbon assembly (Fig. 4.1a).

Thus, MTs assemble the Golgi by two distinct mechanisms: one that does not involve relocation toward the centrosome and another that occurs in vicinity of the centrosome. We refer to these processes as the “G-stage” (for Golgi) and the “C-stage” of the Golgi assembly (for centrosome), respectively.

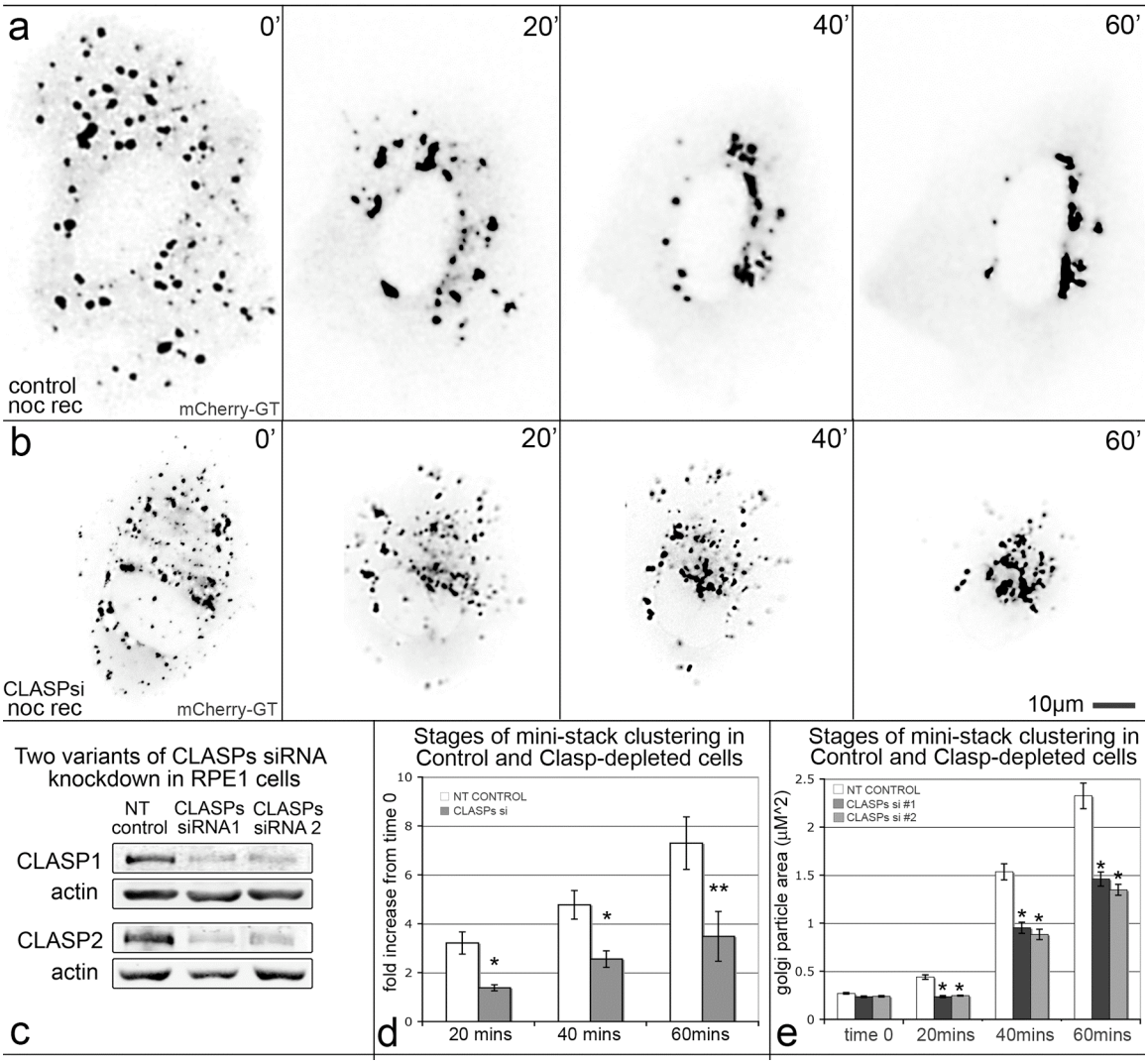

Figure 4.1. The two-stage process of Golgi assembly requires CLASPs.
(a-b) Video frames illustrating assembly of the Golgi marked by mCherry-tagged Galactosyltransferase (GT) in NT-control (a) and CLASP-depleted (siRNA combination #1, b) RPE1 cells recovering after nocodazole washout (noc rec). Time after nocodazole removal is shown. (c) Western blotting showing reduction of CLASP1 levels by ~75 % using siRNA combination #1 and by ~77 % using siRNA combination #2 and CLASP2 levels by ~88 % using siRNA combination #1 and by ~74 % using siRNA combination #2. Actin, loading control. (d) Golgi particle size upon nocodazole washout analysis based on live cell imaging experiments in NT-control (n=7, 6 independent experiments) and CLASP-depleted (n=7, 7 independent experiments) cells (as in a, b). Average fold size increase of Golgi particles relative to time 0 (nocodazole removal) is shown. Error bars, standard error. *P<0.01, **P<0.05, unpaired Student's t-test. (e) Average Golgi particle area (μm^2) upon nocodazole washout based on GM130 immunolabeled fixed samples for of NT-control, CLASP siRNA combination #1, and CLASP siRNA combination #2 cells (as in Fig.S1). n=50 for each condition, 3 independent experiments. Error bars, standard error. *P<0.001, unpaired Student's t-test.

CLASPs are required for initial Golgi clustering

We next addressed the roles of Golgi-derived versus centrosomal MTs in the two-stage process of Golgi assembly. Since CLASPs are essential for Golgi-associated MT nucleation, siRNA targeting of CLASPs (Fig. 4.1c) explicitly removes the Golgi-derived but not centrosomal MT subset (Efimov et al., 2007). Hence, we analyzed the process of Golgi assembly in CLASP-depleted cells (Fig 1b,d). Here and below, cells treated with two independent targeting sequences for CLASP1 and CLASP2 were compared to cells treated with non-targeting siRNA oligonucleotides (NT control). After nocodazole washout, Golgi mini-stacks did not form larger cytosolic clusters (G-stage) (Fig. 4.1b). Instead, unaltered mini-stacks relocated toward the cell center and gathered around the centrosome (C-stage), although they failed to form a well-organized Golgi ribbon (Fig. 4.1b).

Accordingly, Golgi particle size analysis based on both live imaging data and immunostainings revealed that Golgi particle area in CLASP-depleted cells remained constant by 20 minutes (Fig. 4.1e), and final average mini-stack area in CLASP-depleted cells was substantially lower than in control cells (Fig. 4.1d,e; Fig. 4.S1). These observations indicate that CLASPs are essential for the G-stage of Golgi assembly, and that the C-stage alone is not sufficient for the proper Golgi ribbon assembly.

Two-stage Golgi assembly occurs upon mitotic exit

Next we visualized Golgi assembly in untreated cells after mitotic exit (Fig. 4.2). In mCherryRab6- or GFP-GM130-expressing cells exiting mitosis, the average size of detected Golgi mini-stacks (0.34±0.01μm) did not differ from the size of mini-stacks in nocodazole-treated cells (0.35±0.02μm), indicating that these mini-stacks were likely assembled in MT-independent manner by fusion and stacking of membranes brought together by simple diffusion (Tang et al., 2008). During subsequent Golgi assembly, distinct G- and C- stages were easily distinguishable by analysis of the Golgi particle size increase (Fig. 4.2b). Mini-stack clustering in G-stage often occurred at the cell periphery away from the centrosome (Fig. 4.2c), suggestive of the role of Golgi-derived MTs that were detected at the periphery of cells exiting mitosis (Fig. 4.S2). The Golgi assembled faster, and temporal separation between G- and C-stages was less distinct than in nocodazole washout assay. Possibly, the efforts of centrosomal and Golgi-derived MTs were better coordinated in a rounded mitotic cell than in a spread cell. Because CLASPs are indispensable for mitosis, we did not directly test their role in post-mitotic assembly; our nocodazole washout results, however, suggest that G-stage Golgi clustering in this scenario is likely CLASP-dependent.

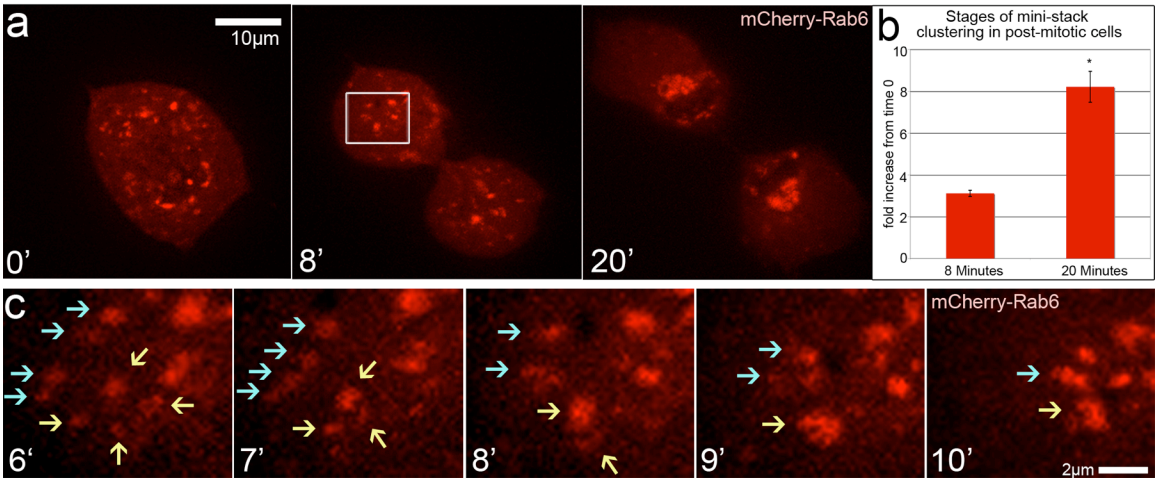

Figure 4.2. **Golgi assembly occurs in 2 stages upon mitotic exit.**
(a) Video frames illustrating post-mitotic Golgi assembly in mCherry-Rab6 expressing RPE1 cells. Time zero marks approximate onset of telophase. Boxed area is enlarged below. (b) Post-mitotic Golgi particle size based on live imaging experiments in NT-control (n=4, 4 independent experiments) cells. Average fold increase of Golgi particles relative to time zero is shown. Error bars, standard error. *P<0.001, unpaired Student's t-test. (c) Enlarged box from (a) showing Golgi mini-stack (red) clustering (6-9', blue and yellow arrows indicate two separate clusters) prior to re-location toward the centrosome (10').

Cooperation of Golgi-derived and centrosomal MTs drive two stages of Golgi assembly

To determine whether CLASPs support Golgi mini-stack clustering at the cell periphery via Golgi-derived MT formation, we directly followed MT involvement in this process. RPE1 cells were co-transfected with variable Golgi stack markers and 3GFP-EMTB to label MTs (Faire et al., 1999). As expected, nocodazole washout assay in NT-control cells revealed MT nucleation at individual Golgi mini-stacks as well as at the centrosome (Fig. 4.3a, c-d). To avoid overlap between G-stage and C-stage, we specifically followed G-stage clustering events at the cell periphery before centrosomal MTs extended into this area. As MTs formed at Golgi mini-stacks polymerized toward nearby mini-stacks, the latter ones were transported into close proximity of the former that allowed subsequent mini-stack linking. Transport of mini-stacks during the G-stage occurred in random directions, often tangential relative to radial centrosomal array.

In contrast, CLASP-depleted cells failed to show MT nucleation at Golgi mini-stacks (Efimov et al., 2007) while centrosomal MT nucleation remained functional (Fig. 4.3b). Early clustering of mini-stacks at the cell periphery was not detected. However, centrosomal MTs transported Golgi mini-stacks into close proximity of each other and supported their clustering in the central cell area (Fig. 4.3e-f). In these cells, mini-stack clustering occurred in a radial manner consistent with radial architecture of the centrosomal MT array. Thus, centrosomal MTs are responsible for the C-stage of Golgi assembly including

gathering mini-stacks at the cell center and their limited linking along the radial axis.

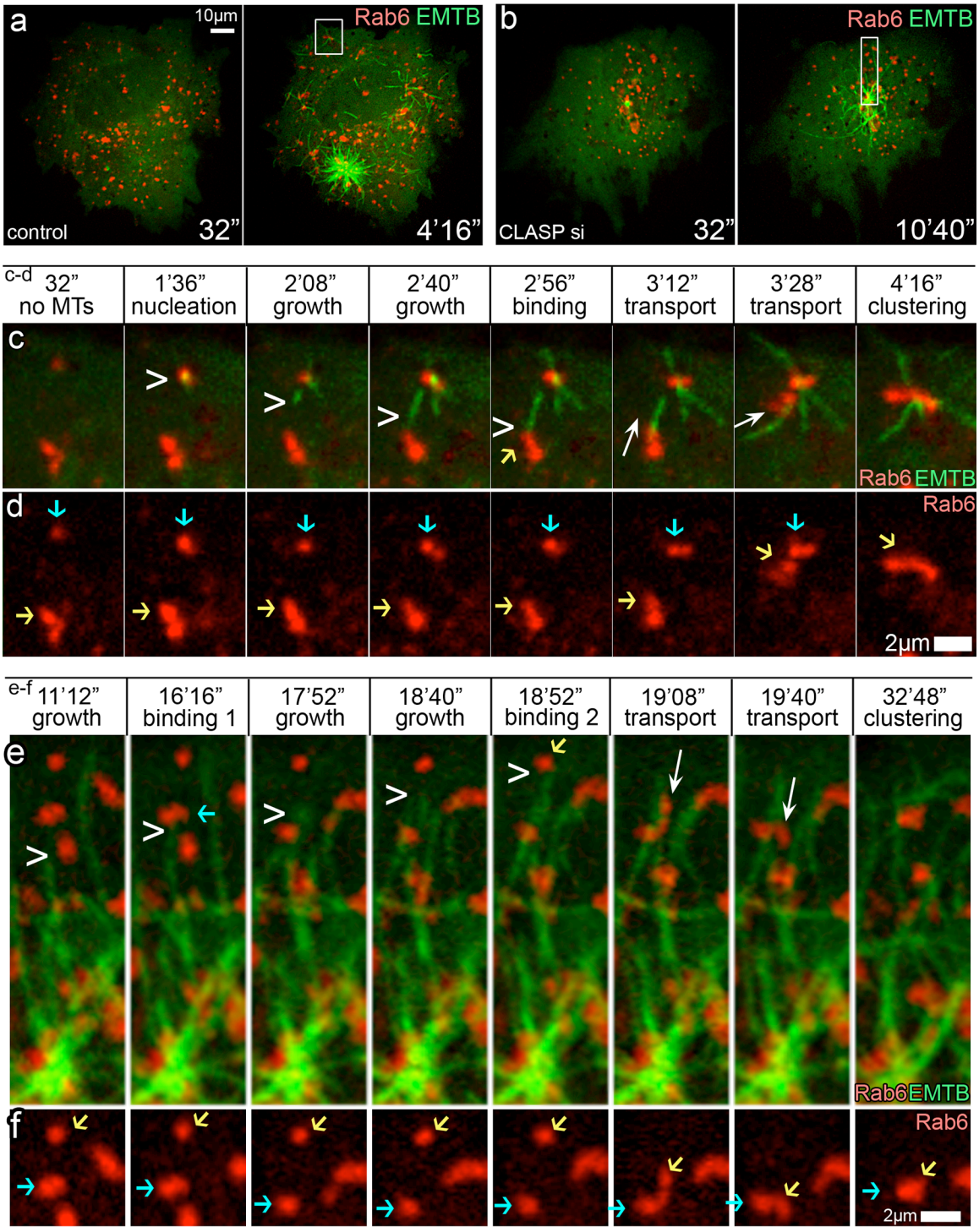

Figure 4.3. **Golgi mini-stacks clustering by Golgi-derived and centrosomal MTs.**

(a-b) Video frames illustrating MT formation in 3GFP-EMTB (green) and mCherry-Rab6 (red) expressing RPE1 cells upon nocodazole washout. Time after nocodazole removal is shown. (a) Control cell, MTs at Golgi mini-stacks and the centrosome. (b) CLASP-depleted cell (siRNA combination #1), MTs at the centrosome. Areas in boxes are enlarged below. (c) enlarged box from (a) showing MT nucleation (chevron) at Golgi mini-stacks (red), binding of mini-stacks to MT (yellow arrow), and transport along MT (white arrow) resulting in clustering along Golgi-nucleated MT. mCherry-Rab6 (red), GFP-EB3 (green). Note transport of a mini stack toward cell periphery and subsequent tangential linking. (d) Mini-stack clustering from (c), mCherry-Rab6 alone. Blue arrow, mini-stack where MT nucleates. Yellow arrow, transported mini-stack. (e) Enlarged box from (b) showing centrosomal MTs growing (chevron), binding to 2 mini-stacks subsequently (blue and yellow arrows), and transport (white arrow) of the second mini-stack resulting in radial clustering in peri-centrosomal area. mCherry-Rab6 (red), GFP-EB3 (green). (f) Mini-stack clustering from (e), mCherry-Rab6 alone. Blue arrow, mini-stack proximal to the centrosome. Yellow arrow, transported mini-stack.

MT orientation within arrays regulates Golgi organization

Because MT orientation appeared important for Golgi stack clustering in nocodazole washout assays, we further addressed the role of MT orientation in Golgi organization. MT directionality was detected as described in Efimov *et al* (Efimov et al., 2007). In brief, RPE1 cells were transfected with GFP-EB3 to mark MT plus-tips and mCherry-GT to label the Golgi, and time-lapse video sequences were recorded. Distinct centrosomal MT and Golgi-derived MT arrays were detected in NT-control cells (Fig. 4.4a,a''). Interestingly, while centrosomal MTs showed clear radial geometry, MTs formed at the Golgi were predominantly tangential. Golgi ribbons (Fig. 4.4a') were aligned along Golgi-derived MT tracks suggesting that they were primarily formed via tangential mini-stack linking and fusion (Fig. 4.4a).

In contrast, CLASP-depleted cells contained only radial MT tracks emanating from the centrosome (Fig. 4.4b,b''), while the Golgi (Fig. 4.4b') formed a poorly organized assembly distributed around the centrosome. Apparently, a radial MT array does not allow for tangential linking and fusion of Golgi mini-stacks in these cells. These data indicate that CLASP-dependent Golgi-derived MTs are required for tangential Golgi stack linking within the Golgi ribbon.

Dynein is required for both G-stage and C-stage of Golgi assembly

Since dynein is required to maintain an organized Golgi complex (Burkhardt 1998), we addressed whether it is involved in G-stage and/or C-stages of Golgi assembly. Nocodazole washout assays in RPE1 cells co-expressing Golgi markers and GFP-EB3 revealed that mini-stacks during G-stage moved in a minus-end directed manner (Fig. 4.4c). To test whether this movement is driven by dynein, dynein activity was inhibited by either p50 dynamitin (Burkhardt et al., 1997; Roghi and Allan 1999) or the CC1 domain of p150Glued (Quintyne and Schroer 2002) over-expression (Fig. 4.4d,f). Golgi particle size was analyzed in live cell imaging sequences (Fig. 4e) and in fixed immunostained cells (Fig. 4.4f). Golgi particle size did not change throughout nocodazole washout indicating that neither G-stage nor C-stage of stack clustering occurs in the absence of dynein-dependent transport (Fig. 4.4d). At the same time, plus-end motors remained functional and MTs were available for trafficking as evident from the transport of Golgi mini-stacks toward the cell periphery (Fig. 4.4d).

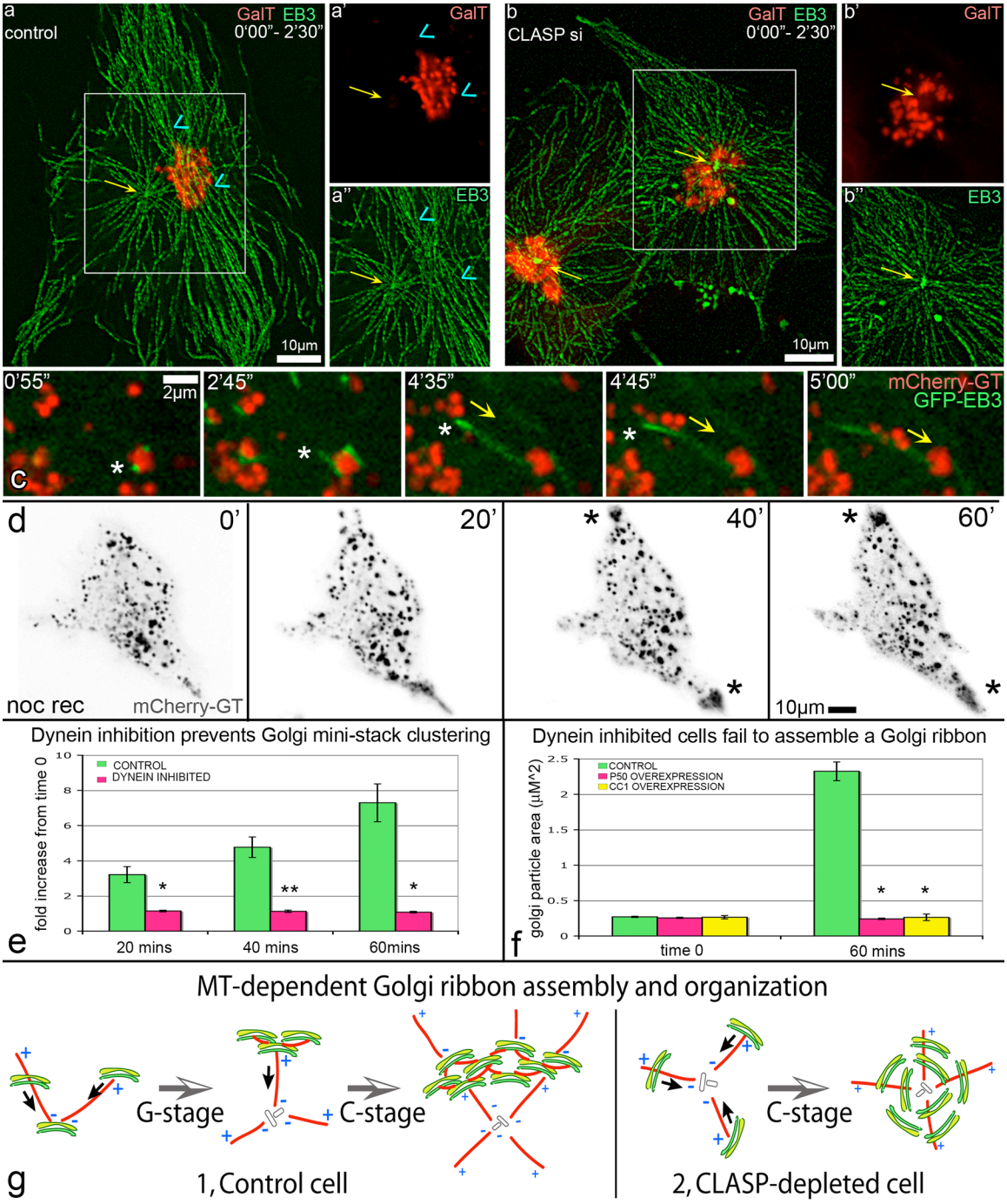
a
control
GalT EB3
0'00"- 2'30"
a'
GalT
a"
EB3
10μm
b
CLASP si
GalT EB3
0'00"- 2'30"
b'
GalT
b"
EB3
10μm
0'55"
2μm
2'45"
4'35"
4'45"
5'00"
mCherry-GT
GFP-EB3
c
d
0'
20'
40'
60'
noc rec
mCherry-GT
10μm
Dynein inhibition prevents Golgi mini-stack clustering
CONTROL
DYNEIN INHIBITED
fold increase from time 0
20 mins
40 mins
60mins
e
Dynein inhibited cells fail to assemble a Golgi ribbon
CONTROL
P50 OVEREXPRESSION
CC1 OVEREXPRESSION
golgi particle area (μM^2)
time 0
60 mins
f
MT-dependent Golgi ribbon assembly and organization
G-stage
C-stage
C-stage
g
1, Control cell
2, CLASP-depleted cell

Figure 4.4. **Golgi assembly depends on directionality of two MT subsets and on dynein activity.**
(a-b) Overlaid GFP-EB3 (green) and mCherry-GT (red) video frames within 2.5 min. (a) EB3 tracks in a control cell illustrate radial centrosomal (yellow arrow) and tangential Golgi-associated (blue arrowhead) MT arrays. Box is enlarged in (a') for mCherry-GT and in (a'') for GFP-EB3. (b) Radial centrosomal (yellow arrow) EB3 tracks in CLASP-depleted cell (siRNA combination #1). Box is enlarged in (b') for mCherry-GT and in (b'') for GFP-EB3. (c) Video frames illustrating minus-end directed mini-stack movement (yellow arrow) along Golgi-nucleated MTs upon nocodazole washout in mCherry-GT (red) and GFP-EB3 (green) expressing NT control cells. MT plus end, asterisk. Time after nocodazole removal is shown. (d) Video frames illustrating nocodazole washout in cell over-expressing GFP-P50 (not shown) and mCherry-GT (black). Mini-stacks move toward the cell periphery along forming MTs due to kinesin activity (asterisks). Time after nocodazole removal is shown. (e) Fold increase of Golgi particle size upon nocodazole washout based on live cell imaging of control (n=7, 6 independent experiments) and GFP-P50 over-expressing (n=8, 7 independent experiments) cells. Error bars, standard error. *P<0.001, unpaired Student's t-test. (f) Average Golgi particle area (μm^2) in nocodazole (time 0) and upon 60 min washout in fixed samples of control, GFP-P50 over-expressing, and RFP-CC1 over-expressing cells. n=50 for each condition, 4 independent experiments. Error bars, standard error. *P<0.001, **P<0.01 unpaired Student's t-test. (g) Role of Golgi-associated MTs in Golgi ribbon assembly (model).

CLASP-dependent MTs control Golgi-ribbon morphology

Our data support a model wherein Golgi-derived MTs play a distinct and essential role in Golgi organization (Fig. 4.4g). Indeed, while in NT-control cells a classic Golgi ribbon associated with Golgi-derived MT array was observed (Fig. 4.5a,e), in CLASP-depleted cells (Fig. 4.5b,c,f) MTs formed a radial array and the Golgi showed circular morphology (Fig. 4.5f). The Golgi shape was reverted back to a ribbon by expression of a non-silenceable GFP-CLASP2α rescue construct in CLASP-depleted cells (Fig. 4.5d). Dependence of the circular Golgi phenotype on the Golgi-associated CLASP fraction was confirmed by over-expressing GFP-tagged C-terminus of CLASP2 that competes full-length CLASPs off the Golgi (Fig. 4.S3). Similar to CLASP-knockdown, cells over-expressing GFP-CLASP2C had circular Golgi complex (Fig. 4.5g).

To quantify this phenomenon, Golgi circularity index was calculated in relation to CLASP intensity at the Golgi. In order to directly correlate CLASPs presence with observed phenotypes, cells transfected with CLASP siRNA and NT control siRNA were co-plated in a proportion of 1:1. In this mixed cell population, the Golgi outlines were identified by GM130 immunostaining. Golgi outline circularity indexes showed striking negative dependence on intensities of the immunostained CLASPs within this area (Fig. 5h). Accordingly, the Golgi circularity enhanced as full length CLASP2 was removed from the Golgi by GFP-CLASP2C expression (Fig. 4.5i) whereas GFP-only expression had no effect (Fig. 4.S4). These results indicate that Golgi-localized CLASPs maintain

polarized functional Golgi organization (Mellman and Simons 1992), probably through Golgi-derived MT nucleation.

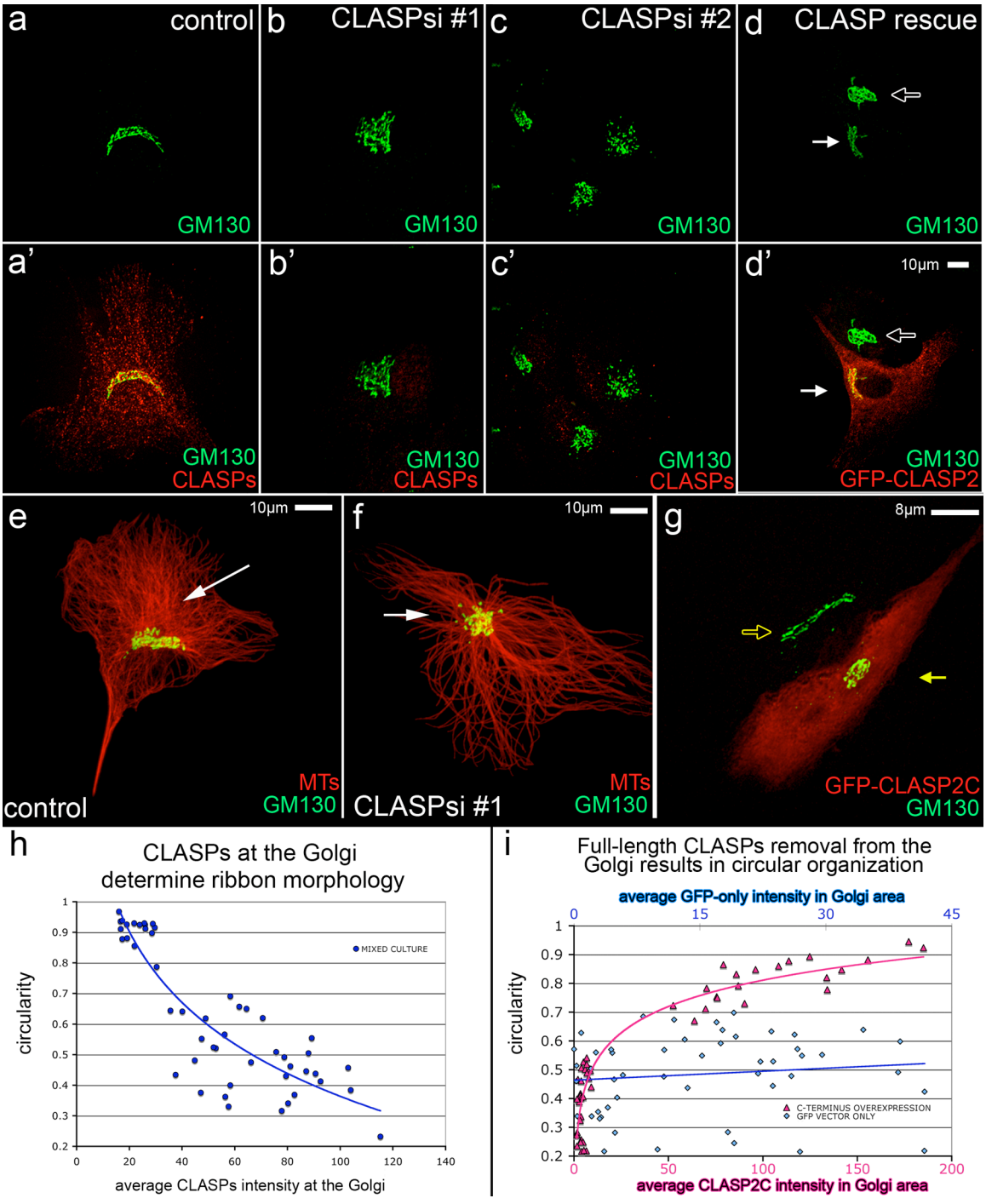

Figure 4.5. CLASPs at the Golgi determine ribbon morphology.
(a) Control cells have a ribbon-like Golgi (GM130, green) when CLASPs (red, a') are present. (b-c) Golgi (green) morphology is circular when CLASPs (red, b', c') are depleted from cells. (d) Ribbon-like Golgi morphology (white arrow) is restored in CLASP-depleted cells expressing a nonsilenceable GFP-CLASP2C construct (d', false-colored red). The Golgi (GM-130, false-colored green) remains circular in non-expressing cells (hollow arrow). (e-f) Immunostainings of Golgi (GM130, green) and MTs (red). (e) Control cell showing ribbon-like Golgi in the presence of Golgi-associated MTs (white arrow). (f) CLASP-depleted cell (siRNA combination #2) showing circular Golgi morphology and radial centrosomal MT array (white arrow). (g) Ribbon-like Golgi (GM130, false-colored green, hollow yellow arrow) turns circular (yellow arrow) in cells over-expressing GFP-CLASP2C (false-colored red). (h) Golgi circularity depends on CLASPs intensity at the Golgi. Average CLASP intensity at the Golgi in mixed-culture cell plotted against circularity index (n=50, 4 independent experiments). (i) Removal of full-length CLASP results in circular morphology. Average GFP-CLASP2C intensity (pink, lower x-axis) and GFP vector only intensity (blue, top x-axis) in the Golgi area plotted against circularity index (n=50, 3 independent experiments for each condition). Cells with similar overall expression levels are compared, in which GFP-CLASP2c intensity in the Golgi region is 4 to 5 times higher than GFP due to specific accumulation of GFP-CLASP2C in the Golgi area (~1/5 of the cell area). GFP-CLASP2C but not GFP expression leads to circular Golgi morphology.

CLASP-dependent MTs control Golgi ribbon continuity

If without Golgi-derived MTs Golgi mini-stack linking is incomplete, membrane fusion required for functional Golgi complex continuity would likely be defective. We performed 3-dimensional Golgi fragmentation analysis on cells immunostained for TGN-46 (data not shown) and GM130 (Fig. 4.S5). CLASP-knockdown cells contained significantly higher number of fragments as compared to NT-control (Fig. 4.6a,e). Rescue experiments returned Golgi fragment number back to control levels (Fig. 4.6a,e). Golgi continuity was further examined by FRAP (Fluorescence Recovery After Photobleaching) to assess GT flow within the Golgi network. As expected, fast recovery in control cells (Fig. 4.6b,f) was typical for a continuous Golgi ribbon where Golgi enzymes freely re-distributed throughout the structure (Lippincott-Schwartz et al., 1998; Puthenveedu et al., 2006; Feinstein and Linstedt 2008). Incomplete fluorescence recovery of CLASP-knockdown cells (Fig. 4.6c-d,f) indicated that Golgi enzyme mobility between stacks was significantly restricted.

Together, these data reveal that the Golgi is highly fragmented in CLASP-knockdown cells indicative of impaired membrane fusion, which is likely a result of missing tangential linking by Golgi-derived MTs.

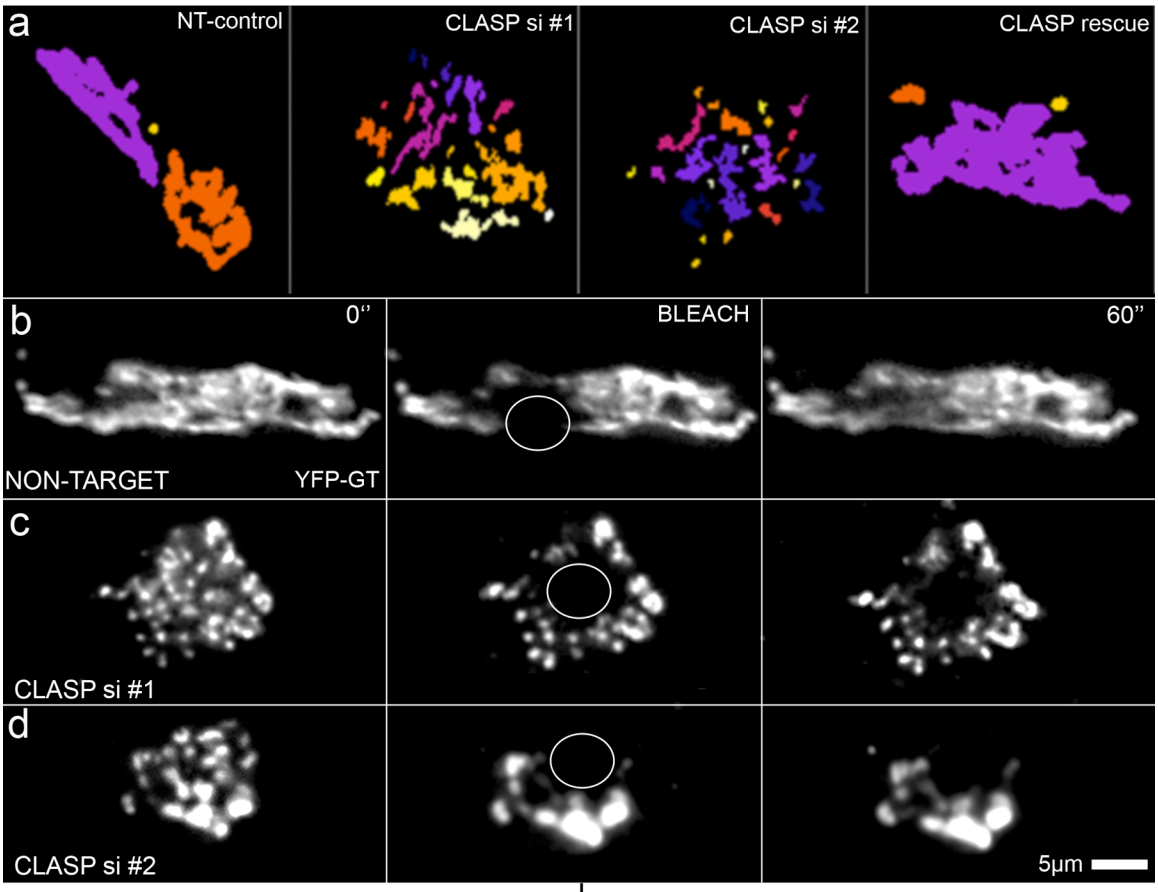
a
NT-control
CLASP si #1
CLASP si #2
CLASP rescue
b
0''
BLEACH
60''
NON-TARGET
YFP-GT
c
CLASP si #1
d
CLASP si #2
5µm

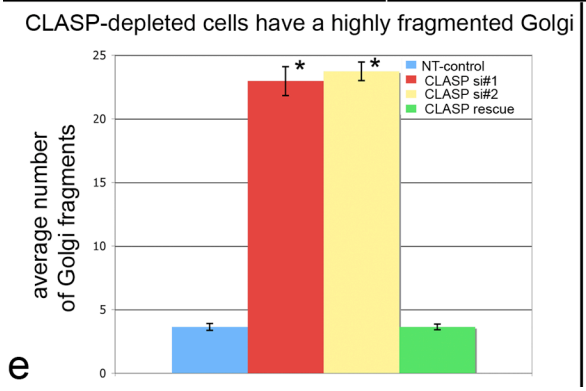
CLASP-depleted cells have a highly fragmented Golgi
average number of Golgi fragments
25
20
15
10
5
0
*
*
NT-control
CLASP si#1
CLASP si#2
CLASP rescue
e

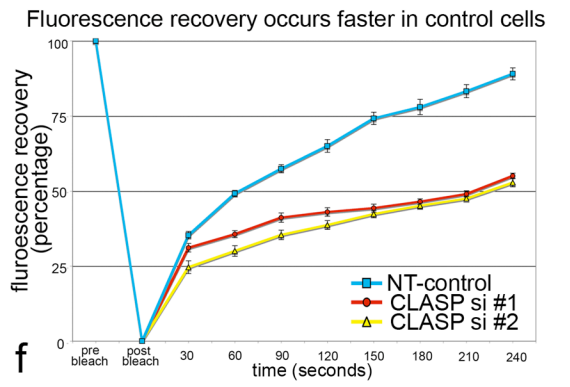
Fluorescence recovery occurs faster in control cells
fluorescence recovery (percentage)
100
75
50
25
0
pre bleach
post bleach
30
60
90
120
150
180
210
240
time (seconds)
NT-control
CLASP si #1
CLASP si #2
f

Figure 4.6. Golgi fragmentation in CLASP-depleted cells results in diminished enzyme mobility within the Golgi complex

(a) Representative data from 3-dimensional objects counter analysis based of GM130 immunostaining. Colored segments represent interconnected Golgi fragments. (b-d) Video frames illustrating fluorescence recovery after photobleaching in YFP-GT expressing cells. Time points shown are pre-bleach (0"), bleach, and 60 seconds post-bleach. Bleached regions are indicated by white circles. (b) NT-control. (c) CLASP depletion siRNA combination #1. (d) CLASP depletion siRNA combination #2. (e) Numbers of Golgi fragments in NT-ctl (blue), CLASPs-depletion #1 (red), CLASPs-depletion #2 (yellow), and CLASP rescue (green) cells. n=30, 5 independent experiments for each condition. Error bars, standard error. *P<0.001, unpaired Student's t-test. (f) Graph showing fluorescence recovery rates for NT-control (blue), CLASP siRNA combination #1 (red), and CLASP siRNA combination #2 (yellow). n=20 for each condition. NT-control = 4 independent experiments, CLASP si #1 and CLASP si #2 = 5 independent experiments.

Directional trafficking defects in cells lacking Golgi-derived MTs

One logical function of a properly organized Golgi ribbon is support of directional post-Golgi trafficking. Because CLASP-dependent MTs organize the Golgi ribbon, we examined their role in the process of polarized post-Golgi trafficking by monitoring secreted fluorescently tagged Neuropeptide-Y (NPY) (Bruun et al., 1986; Taraska et al., 2003). Individual NPY-containing vesicles (Fig. 4.7a,b) were tracked from the Golgi to the plasma membrane, vesicle tracks were created (Fig. 4.7a',b') and their directionality was quantified in four cell quadrants (Fig. 4.S6). While NT-control cells exhibited polarized trafficking toward the leading edge (Fig. 4.7a',c,d), cells after CLASP depletion (Fig. 4.7b',c, d) or removal from the Golgi by GFP-CLASP2C over-expression (Fig.4.7c, d) exhibited randomized symmetric trafficking patterns. VSVG trafficking assays (data not shown) show no differences in overall trafficking to the plasma membrane upon CLASP knockdown indicating that directionality but not efficiency of post-Golgi trafficking depends on Golgi-associated MTs. At the same time, overall MT network also becomes symmetric upon CLASP depletion (Fig. 4.S7), correlating with the fact that directional Golgi-originated MT array is missing in CLASP depleted cells (Efimov et al., 2007) (Fig. 4.4b).

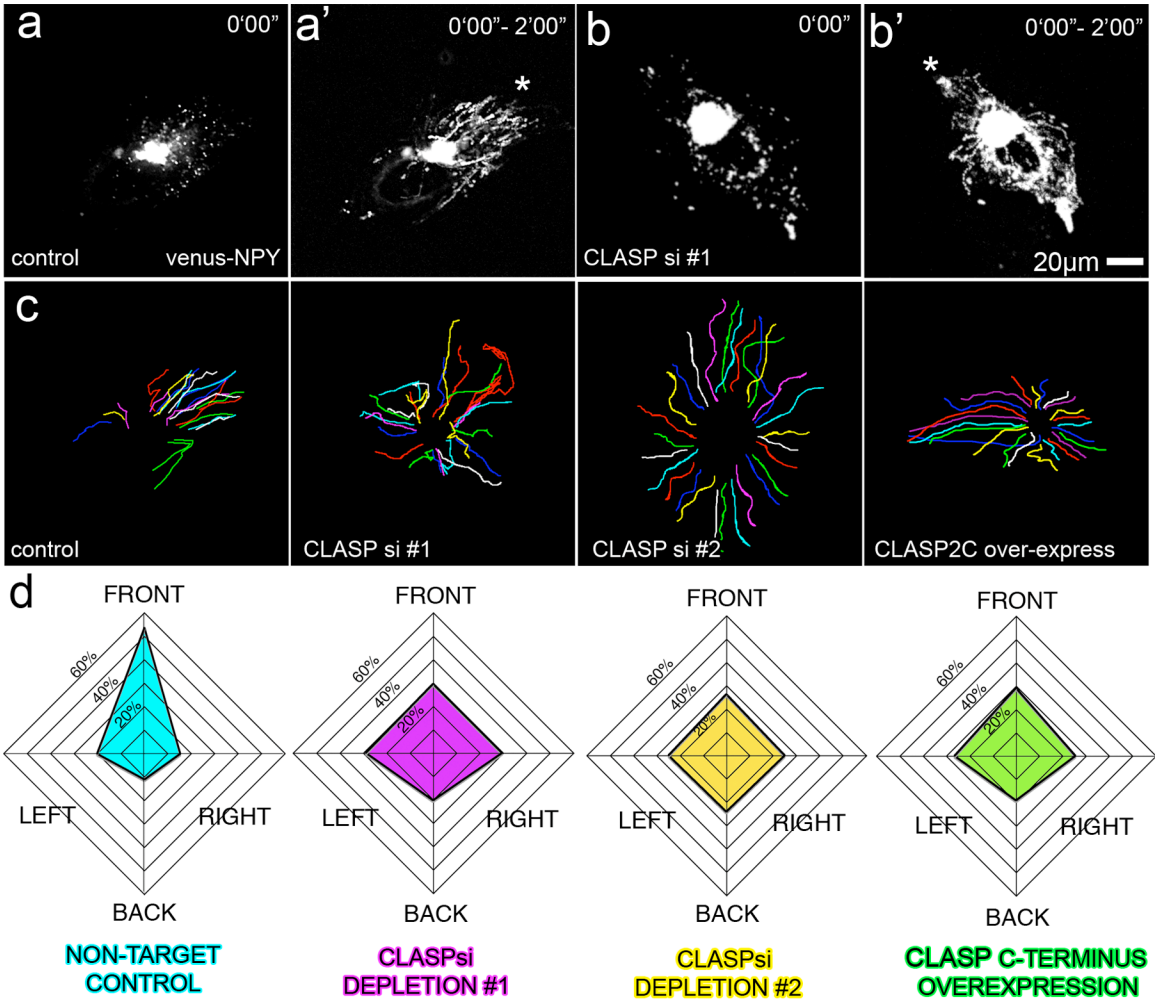

Figure 4.7. CLASP-dependent MTs polarize trafficking to the cell front
(a-b) Video frames showing post-Golgi trafficking in Venus-NPY expressing RPE1 cells. (a) NT-control. (b) CLASP-depleted cell. (a, b) Snapshot of NPY vesicles (a', b'). Overlaid Venus-NPY images within 2 minutes show directional trafficking toward the cell front (asterisks) in control cells (a') and symmetric trafficking (b') in CLASP-depleted cells. (c) Examples of particle tracking analysis. Particle movement tracks within 2 mins for NT-control, CLASP siRNA combination #1, CLASP siRNA combination #2, and GFP-CLASP2C over-expressing cells. (d) Graphs showing trafficking directionality in NT-control (blue), CLASP siRNA combination #1 (purple), CLASP siRNA combination #2 (yellow), and GFP-CLASP2C over-expressing (green) cells. Data represents average percentage of tracks corresponding to the cell front, right, rear, and left. n=30 for each condition, NT-control = 4 independent experiments, CLASP si #1 and CLASP si #2 = 6 independent experiments, CLASP C-term = 3 independent experiments.

Migration defects in cells lacking Golgi-derived MTs

Golgi ribbon integrity (Yadav et al., 2009) and asymmetry of post-Golgi transport (Prigozhina and Waterman-Storer 2004) are thought to play an important role in polarized cell motility along with other potential functions of front-oriented MT arrays (Small and Kaverina 2003; Noritake et al., 2005). To test for potential migration defects, single NT-control, CLASP-depleted, and GFP-CLASP2C over-expressing cells were monitored by DIC microscopy. CLASP-depleted cells were analyzed only if post-recording immunostaining confirmed non-detectable CLASP levels. NT-control cells migrated in directionally persistent fashion (Fig 4.8a,e). CLASP-depleted (Fig. 4.8b-d) cells exhibited random migration, consistent with previous findings (Drabek et al., 2006). Similar random migration of GFP-CLASP2C over-expressing cells (Fig. 4.8d,e) suggested that specifically Golgi-associated CLASPs were involved in migratory persistence.

Thus, random migration pattern was observed under the same conditions as the random trafficking (Fig. 4.7). In order to observe the trafficking pattern and cell edge protrusions in the same cell, we co-expressed NPY as a trafficking marker and RFP-cortactin (Daly 2004) as a marker of protrusion activity (Fig. 4.8i,j). Cell migration and cortactin distribution were followed within 1 hour of migration (Fig. 4.8k,l). One minute NPY tracks were recorded at the beginning and at the end of the cortactin recording. NPY track distribution was compared to the relative length of cortactin-rich cell edge within the same quadrants (Fig. 4.S6) throughout the recording. Persistence of cortactin accumulation over time

at one cell side directly correlated with the load of vesicular trafficking to that side (Fig. 4.8f-h) in both NT control and CLASP-depleted cells, suggesting that vesicular trafficking is likely involved in protrusion site stabilization and may serve a mechanism whereby Golgi-associated CLASPs supports directionally persistent migration.

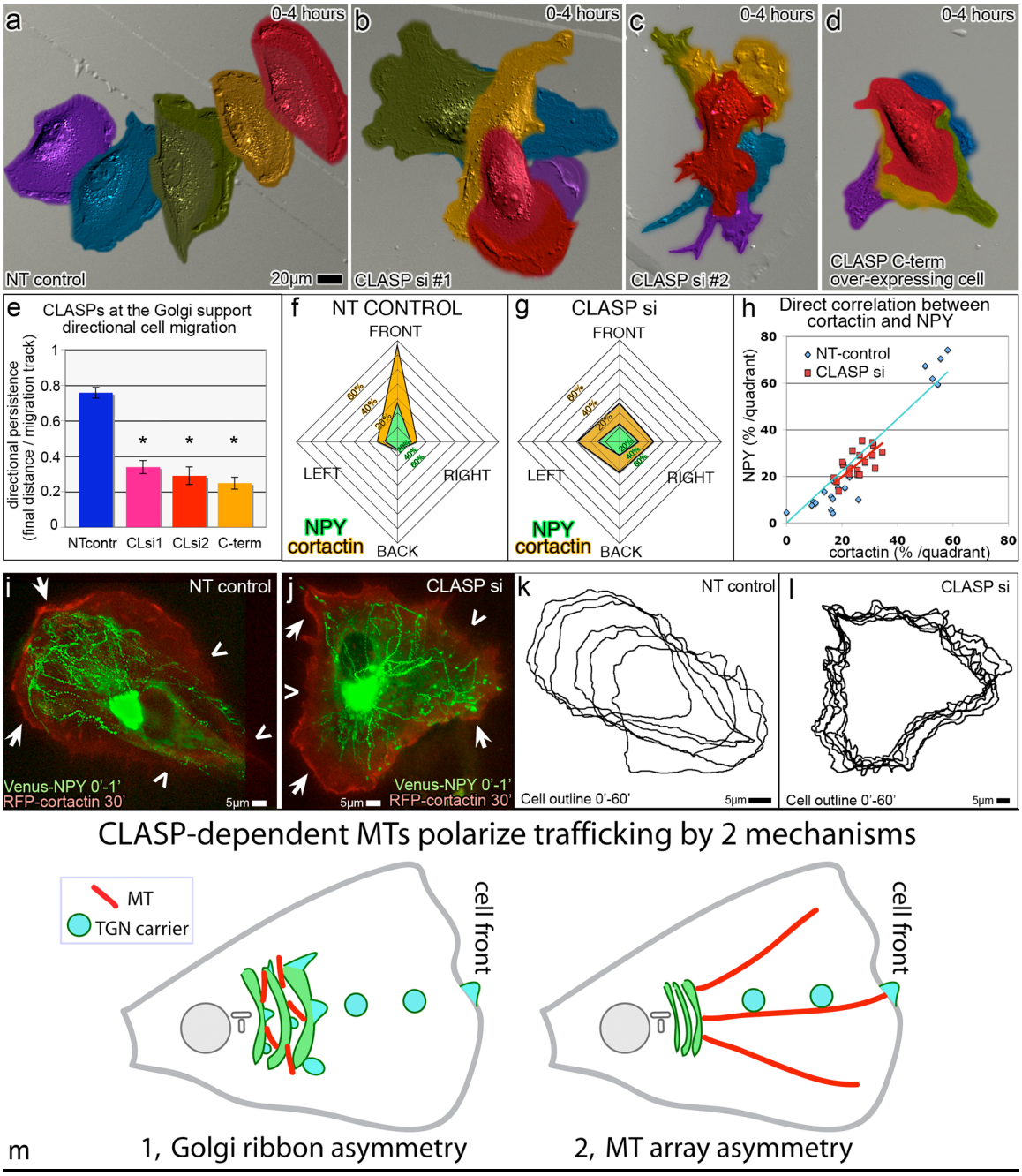

CLASP-dependent MTs polarize trafficking by 2 mechanisms

Figure 4.8. CLASP-dependent MTs regulate directional cell migration
(a-d) False-colored DIC video frames showing single RPE1 cell migration over a time period of 4 hours. Purple indicates time 0, blue = 1hr, green = 2hrs, yellow =3hrs, and red =4hrs. (a) Control cells exhibit directionally persistent migration. CLASP-depleted cells (b-c) and CLASP2C (d) over-expressing cells show random migration patterns. (e) Average directional persistence for NT-control (n=13, blue), CLASP siRNA combination #1 (n=12, pink) and #2 (n=17, red), and CLASP2C over-expressing (n=15, orange) cells each from 4 independent experiments. Error bars, standard error. *P<0.001, unpaired Student's t-test. (f-g) NPY trafficking (green) directionality and cortactin cell edge distribution (orange) in migrating NT-control (f) and CLASP-depleted (g) cells. Data represent average percentage per quadrant (Fig. S6) of track number within 1 min and cortactin-associated cell edge length over 30 min thereafter. n=5 from 4 independent experiments for each condition. (h) Direct correlation between NPY track number and cortactin-rich cell edge in NT-control (blue) and CLASP-depleted (red) cells. Each point represents correlation within one quadrant of an individual cell. (i-j) NPY tracks within 1 minute (green) overlaid with RFP-cortactin (red (see "Image processing")) at 30 minutes after track recording in NT-control (i) and CLASP-depleted (j) cells. Arrows, cortactin enrichment. Chevrons, regions lacking cortactin. (k-l) Cell outlines showing cell relocation and edge dynamics over 1 hour with 10 minute interval. (k) NT-control, same as (i). (l) CLASP-depleted cell, same as (j). (m) Proposed mechanisms by which CLASP-dependent MTs polarize trafficking (model).

Discussion

The major MT function is spatial organization of the cytoplasm at particular time points. MT network properties, including specific nucleation sites, orientation, dynamics and molecular motor affinity establish a fine-tunable machine for organelle positioning. The best-studied MT-driven positioning machine is the mitotic spindle. Chromosome location by a “search and capture” mechanism (Kirschner and Mitchison 1986) involves variability of all above-listed parameters. Assembly of the Golgi complex described herein is driven by a similar arrangement though this machinery is not understood as clearly as mitosis. Yet, Golgi assembly by G- and C-stage mechanisms provides a strong analogy to modern understanding of the mitotic spindle, which is cooperatively built by centrosomal and kinetochore-derived MTs (O'Connell and Khodjakov 2007). In both cases, correct organelle positioning is achieved by cooperation of two MT subsets bearing their own functions due to distinct sites of origin.

Upon nocodazole washout, Golgi undergoes two distinct, yet simultaneous, rearrangements. In G-stage, Golgi-derived MTs organize peripheral Golgi mini-stacks into larger clusters similar to melanosomes in pigment cells (Cytrynbaum et al., 2004). Simultaneously, the C-stage drives re-localizing stacks toward the cell center thought it appeared insufficient for correct Golgi assembly. Why is the unconventional, Golgi-based, nucleation mechanism so important for the Golgi assembly by MTs?

This question can be addressed from a purely geometric as well as from a biochemical point of view. One of the reasons for efficient mini-stack gathering by Golgi-derived MTs could be that the their anchoring sites are distributed evenly throughout the cytosol producing fusion templates of variable orientations. This geometry helps to overcome limitations of diffusion-based mini-stack association and leads to a rapid increase in Golgi particle size. As a result, the probability that centrosomal MTs will easily find and transport mini-stacks toward the cell center is significantly enhanced. This phenomenon likely enhances Golgi assembly rate and may be important for efficient cell cycle progression upon mitotic exit. In the assembled Golgi complex, tangential Golgi-derived MTs likely serve for lateral cross-linking of mini-stacks. Such cross-linking is essential for cisternal fusion and functional continuity of the Golgi complex as evident from Golgi fragmentation and low enzyme mobility in CLASP-depleted cells (Fig. 4.6).

Besides geometric clues, it is possible that Golgi-derived MTs possess distinct biochemical properties, such as altered balance between plus-end directed and minus-end-directed motor affinity or regulation of proteins involved in membrane fusion. It is known that Golgi membrane fusion requires highly regulated molecular machinery (Linstedt 2004; Rios et al., 2004). While our study does not address the biochemistry of fusion, it emphasizes that MT-driven mutual localization of membranes (Thyberg and Moskalewski 1999) is critical for this machinery to work. Multiple structural biology studies have proven the importance of proper mutual positioning of two entities for a chemically correct

interaction to occur. Such correct positioning is as important on the level of organelles as on the level of single molecules and their domains. Golgi mini-stacks in the absence of MTs fragment throughout the cytosol though their membranes carry all molecules required for efficient fusion. Therefore, Golgi mini-stacks need to be brought into close proximity for fusion machinery to proceed. Practically, MTs can be compared to surface catalysts, which hold membranes together. Since the membrane fusion machinery is compartment-specific (Shorter and Warren 2002; Puthenveedu and Linstedt 2005), MTs may promote connection of homotypic cisternae (e.g. *cis* with *cis*, or *trans* with *trans)*. To date, Golgi-derived MTs were suggested to bind either *cis*-Golgi through AKAP450 (Rivero et al., 2009) or the TGN (*trans*-Golgi Network) through CLASPs (Efimov et al., 2007). The latter possibility is supported by the recent finding that a CLASP-binding TGN protein (GCC185) is involved in lateral mini-stack cross-linking (Hayes et al., 2009). Nevertheless, whether Golgi-derived MTs catalyze homotypic fusion remains to be investigated.

Altogether, we propose that a properly organized Golgi ribbon arises from a concerted effort of G-stage tangential cross-linking and C-stage radial gathering of stacks (Fig. 4.4g). According to this model, the distinct geometry of Golgi-derived and centrosomal MTs underlies requirement of both MT subpopulations for Golgi ribbon organization.

Another important function of Golgi-derived MTs is support of directional trafficking in motile cells, which may be utilized by two mechanisms (Fig. 4.8m). First, MT-dependent Golgi morphology may contribute to trafficking directionality if post-Golgi carriers predominantly bud off one side of the polarized Golgi. Second, vesicular transport may be polarized due to direction bias of these MTs toward the cell front (Efimov et al., 2007). Either way, the observed correlation between the CLASP effects on trafficking and protrusion stability (Fig. 4.7) suggests that trafficking contributes to CLASP-dependent regulation of migration. Importance of polarized Golgi organization for directional cell motility has been recently supported by data arising from the Golgi ribbon disruption by a number of alternative protein depletions (Yadav et al., 2009). Additionally, CLASPs function in MT capture at cortical sites (Lansbergen et al., 2006) may be involved in regulation of migration. Notably, our results involving removal of CLASPs from the membrane (that may involve both Golgi and cortical site association (Lansbergen et al., 2006)) indicate that CLASP functioning at the membrane and not CLASP MT-binding is important for directional migration. It is yet unclear how CLASP activities at the Golgi and at cortical sites are coordinated. One possibility is that Golgi-derived MTs that possess high CLASP affinity as they form (Efimov et al., 2007) represent the same population of microtubules that are later associated with CLASP at the cell periphery (Wittmann and Waterman-Storer 2005) and anchored at the cortical sites (Lansbergen et al., 2006). Thus, we propose that Golgi-derived MTs facilitate directional persistence of cell migration, on one hand, through Golgi-ribbon organization and polarized trafficking, and, on

the other hand, by establishment of a directional array of CLASP-rich MTs extending toward the cell front.

Supplementary Materials

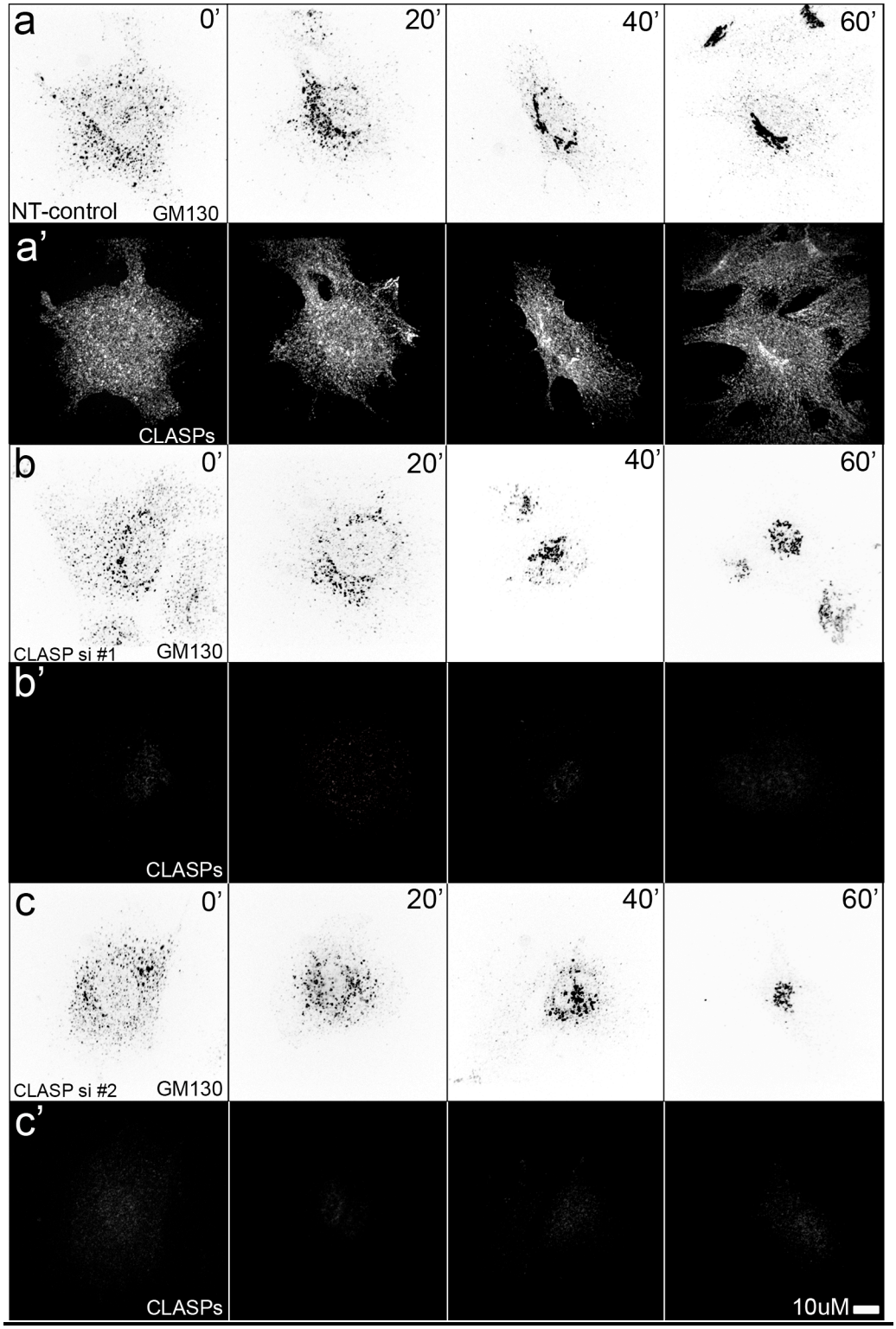

Fig. 4.S1. CLASPs are required for proper Golgi ribbon assembly
(a-c) Immunostainings showing Golgi (GM130, inverted image) assembly in the presence or absence of CLASPs (a'-c') upon nocodazole washout in representative images from fixed samples. Times shown are after nocodazole removal. (a, a') NT-ctl. (b, b') CLASPs siRNA combination #1. (c, c') CLASPs siRNA combination #2.

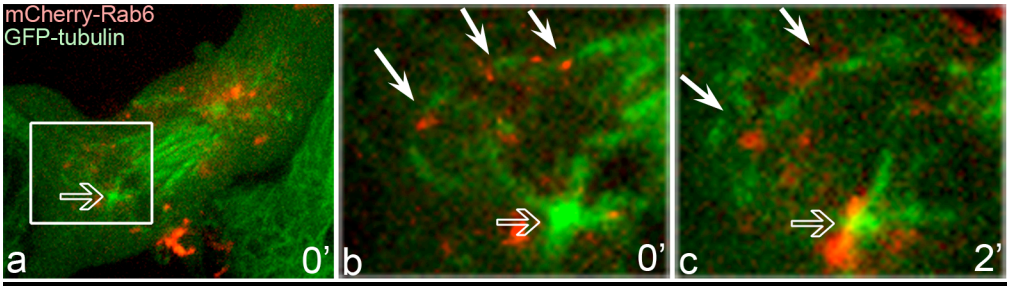

Fig. 4.S2. Golgi stacks cluster along non-centrosomal MTs in cells exiting mitosis.
(a) Snapshot from time-lapse movie showing MTs (green) and Golgi (red) in a mitotic LLC-PK1 cell (early telophase). Boxed area enlarged in b, c. (b-c) Video frames showing Golgi–associated non-centrosomal MTs and Golgi stack clustering (white arrows). Hollow arrow indicates centrosome.

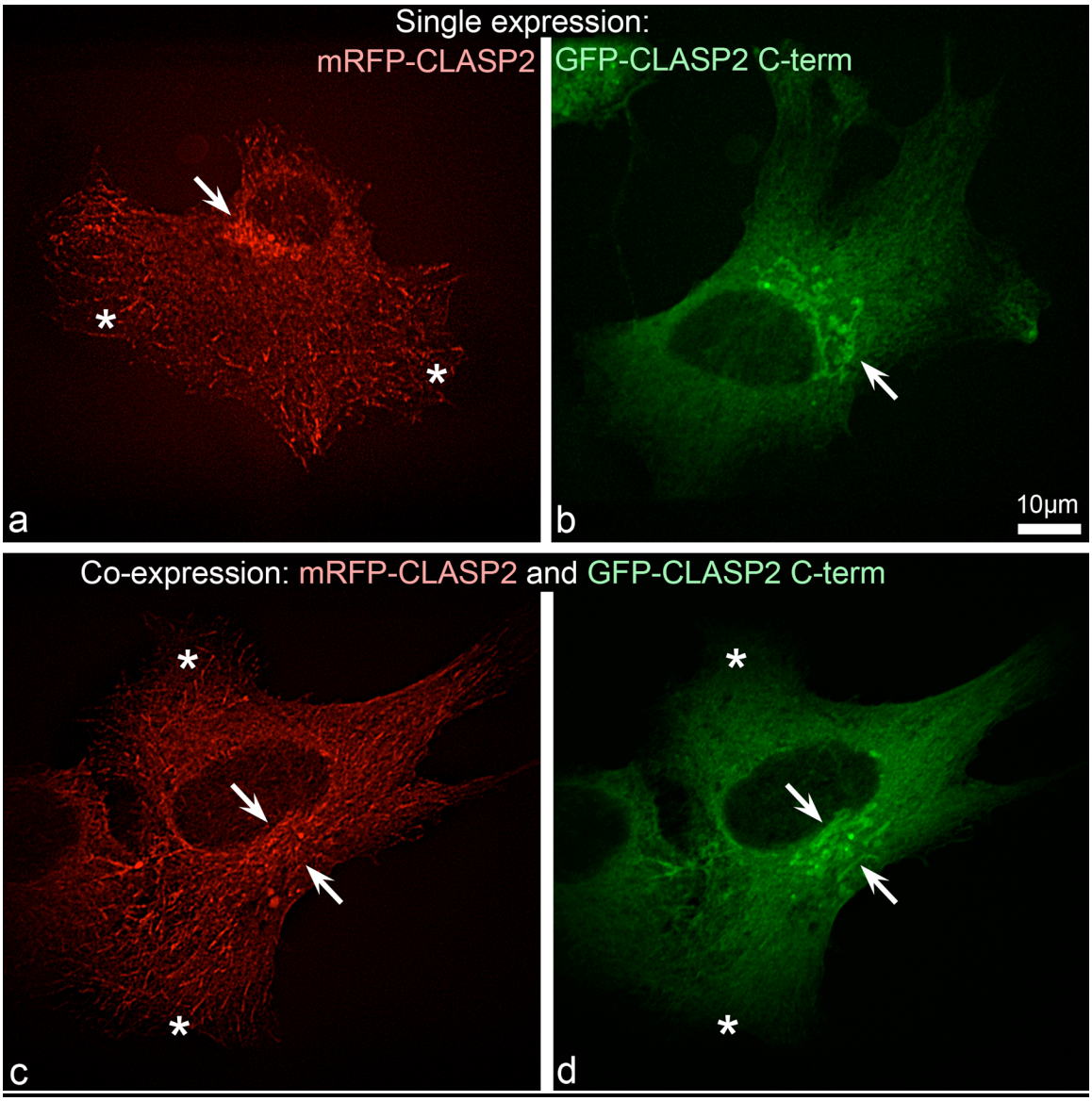

Fig. 4.S3. CLASP2C removes full-length CLASP2 from the Golgi.
(a) RFP-CLASP2 expressing RPE1 cell showing Golgi (white arrow) and MT tip (asterisks) localization. (b) GFP-CLASP2C expressing RPE1 cell showing Golgi localization (white arrow). (c-d) Co-expression of RFP-CLASP2 (red) and GFP-CLASP2C (green) in RPE1 cell. GFP-CLASP2C expression (d, white arrow) removes RFP-CLASP2 Golgi localization (c, white arrow). Peripheral CLASPs pattern and MT tip localization of RFP-CLASP2 (c, asterisks) are not affected by GFP-CLASP2C expression (d, asterisks).

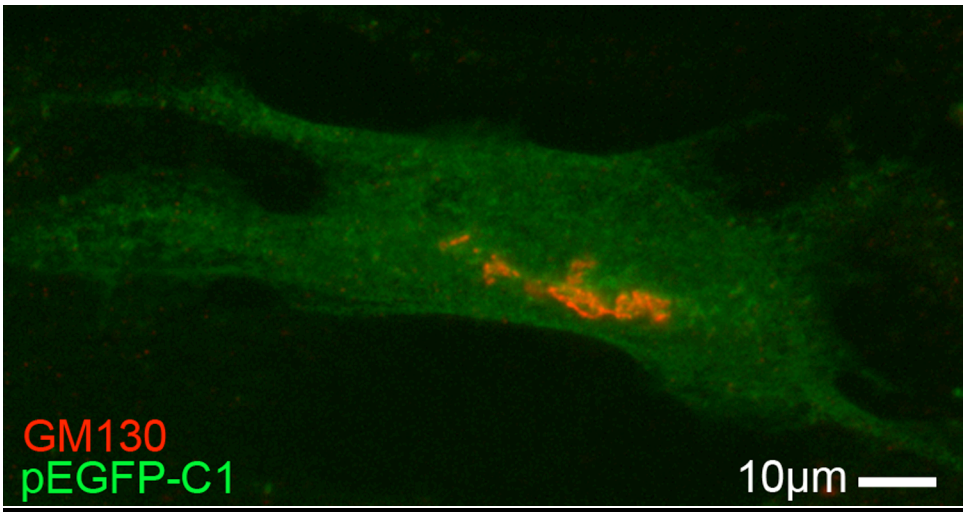

Fig. 4.S4. GFP only expression does not alter Golgi ribbon morphology. NT-control RPE1 cell expressing empty pEGFP-C1 vector (green) has a normal Golgi (red) ribbon morphology.

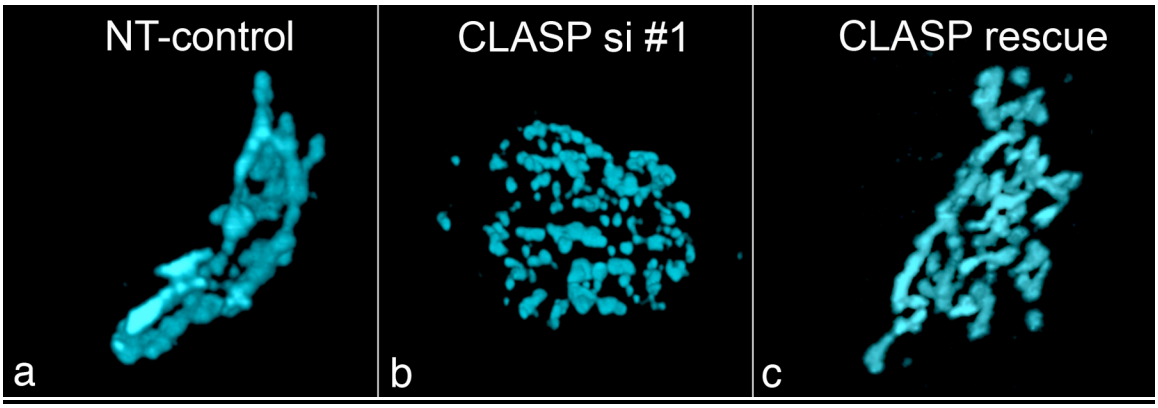

Fig. 4.S5. CLASP-depletion causes Golgi fragmentation.
(a-c) Snapshots of 3-D Golgi reconstruction showing Golgi fragmentation in CLASP-depleted cells (b) as compared to NT-control (a). Expression of CLASP2 rescue construct restores Golgi ribbon morphology (c). GM130 immunostaining, false-colored.

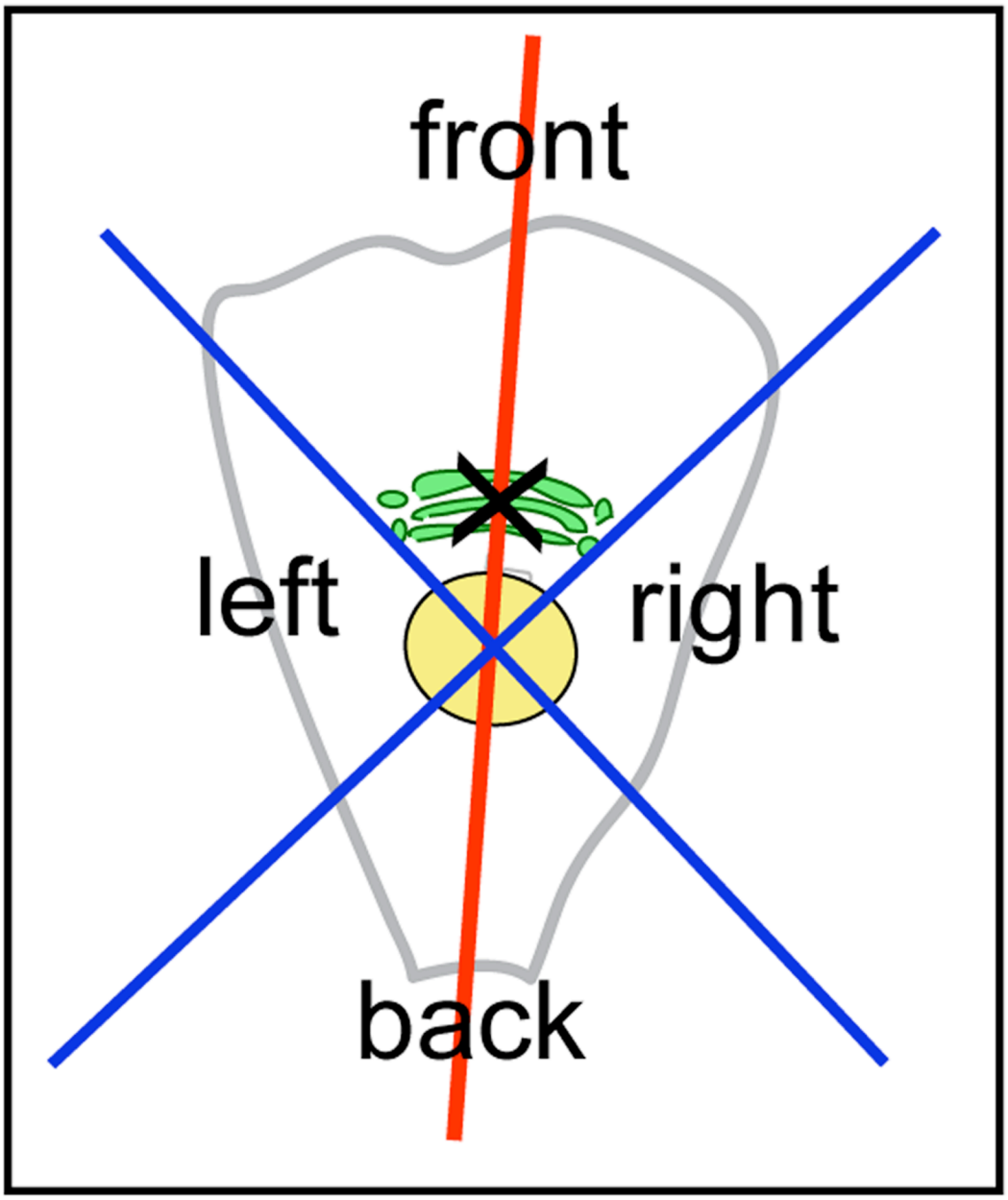

Fig. 4.S6. Schematic used for partitioning cells. Perpendicular lines crossing the center of the nucleus (blue) are aligned (red line) with the center of the Golgi (green, black cross) to divide the cell into four 90° quadrants. The cell front is always determined by the Golgi-containing quadrant.

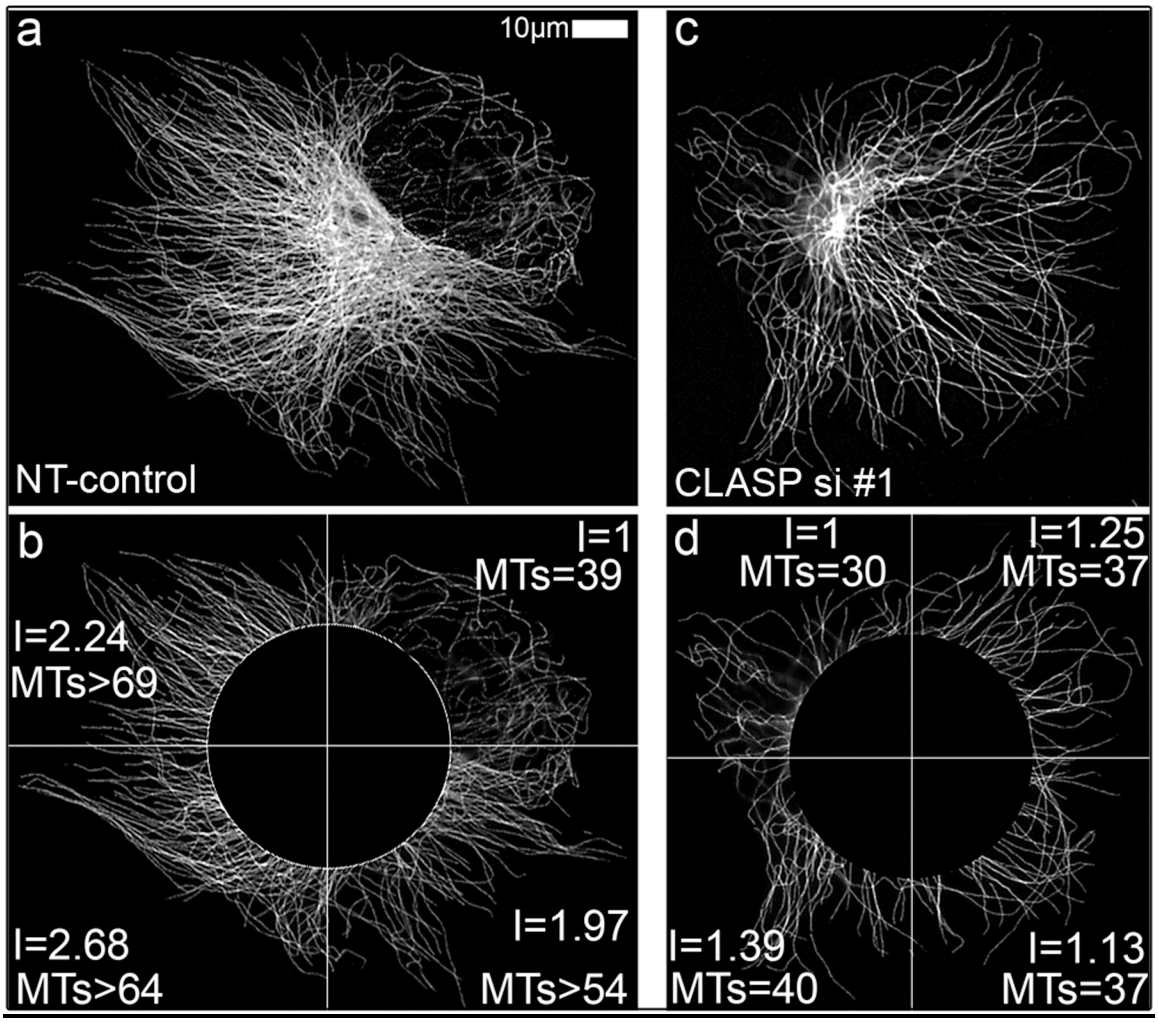

Fig. 4.S7. **Analysis of MT distribution**. Immunostained MTs in NT-control (a, b) and CLASP-depleted (c, d) RPE1 cells. In (b) and (d) the central area is excluded and the rest of the cell divided in 4 quadrants. Detectable MT numbers and relative average fluorescence intensity within each quadrant is shown. Note that edge MT numbers and intensities differ in control cell but not in CLASP-depleted cell.

Methods

Cells

Immortalized human retinal pigment epithelial cells hTert-RPE1 (Clontech) were maintained in DMEM/F12 with 10% fetal bovine serum (FBS). GFP-tubulin expressing LLC-PK1 stable line (renal epithelial cell line derived from porcine kidney, gift of P. Wadsworth, Amherst, MA) were cultured in a mixture of Opti-MEM and F10 (1:1) supplemented with 10% of fetal bovine serum. Cells were grown in 5% CO_2 at 37ºC. Cells were plated on fibronectin-coated glass coverslips 24 hours before experiments.

Treatments

For MT depolymerization and Golgi dispersal, nocodazole (2.5µg/ml) was added to culture media for 2 hours. For Golgi reassembly experiments, cells were rinsed five times with ice-cold medium to remove nocodazole and then moved to a dish with warm (37°C) medium (time 0 for Golgi reassembly). For live imaging of Golgi reassembly, cells were washed with cold medium directly at the microscope stage after initial recording of cells in nocodazole. Temperature was slowly raised to 37°C by the heated stage. For dynein inhibition cells were transfected with 1.5µg of GFP-p50 or RFP-RCC1 (gift from T.A. Schroer, Baltimore, MD).

siRNA and Expression Constructs

Two alternative combinations of mixed siRNA oligos against CLASP1 and CLASP2 (Mimori-Kiyosue et al., 2005) were transfected using HiPerFect (Qiagen) according to the manufacturer's protocol. Combination 1: CLASP1 siRNA targeted sequence 5'-GGATGATTTACAAGACTGG-3'; CLASP2 siRNA targeted sequence 5'-GACATACATGGGTCTTAGA-3'. Combination 2: CLASP1 siRNA targeted sequence 5'-GCCATTATGCCAACTATCT-3'; CLASP2 siRNA targeted sequence 5'-GTTCAGAAAGCCCTTGATG-3'. Experiments were conducted 72 hours post-transfection as at this time minimal protein levels were detected. Nontargeting siRNA (Dharmacon) was used for controls. Empty pEGFP-C1 vector (Clontech) served as a control for circularity quantifications. mCherry plasmid was provided by Dr. R. Tsien (San Diego, CA). YFP-GT (YFP-Galactosyltransferase; Clontech), mCherry-GT (modified from Clontech), GFP-GM130 (gift from C. Sütterling, Irving, CA), and Cherry-Rab6 (gift from A. Akhmanova, Rotterdam, The Netherlands) were used for Golgi visualization. EGFP-EB3 (gift from A. Akhmanova, Rotterdam, The Netherlands), mCherry-EB3 (gift from J.V. Small, Vienna, Austria), 3xGFP-EMTB (gift from J.C. Bulinski, New York, NY) were used for MT plus tip and MT visualization. GFP-CLASP1α, GFP-CLASP2α, RFP-CLASP2, GFP-CLASP2-C, and the nonsilenceable rescue construct GFP-CLASP2α are described in Mimori-Kiyosue et al (2005). GFP-Centrin (gift from M. Bornens, Paris, France) was used to mark the centrosome. RFP- and Venus-NPY constructs were provided by Atsushi Miyawaki (Saitama, Japan). Cell polarity marker RFP-cortactin was provided by Marko Kaksonen,

UC Berkeley. RPE1 cells were transfected with Fugene6 (Roche), and LLC-PK1 cells with Effectene (Qiagen) according to manufacturer's protocols.

Antibodies and Immunofluorescence Details

Rabbit polyclonal antibodies against CLASP2 VU-83 are described in Efimov et al. (Efimov et al., 2007). Rabbit polyclonal antibodies against CLASP1 were provided by Dr. F. Severin (Dresden). A mouse polyclonal antibody against Actin (NeoMarkers) was used. For Golgi compartment identification, a mouse monoclonal antibody against GM130 (Transduction Laboratories) and a sheep polyclonal antibody against TGN46 (Serotec) were used. MTs were stained with a rat monoclonal YL1/2 antibody (Abcam). Cells were fixed in cold methanol (10' at -20°C) for CLASPs stainings. For MT staining and Golgi reconstruction cells were fixed (15' at room temp.) in 2% paraformaldehyde, 0.1% Glutaraldehyde, 0.5% Saponin in cytoskeleton buffer (10 mM MES, 150 mM NaCL, 5 mM EGTA, 5 mM glucose, and 5 mM $MgCL_2$, pH 6.1). Alexa488 and Alexa568-conjugated highly cross-absorbed goat anti-mouse IgG antibodies, Alexa568-conjugated goat anti-rat IgG antibodies, and Alexa568 donkey anti-sheep IgG (Molecular Probes) were used as secondary antibodies.

Fluorescence Recovery after Photobleaching

RPE1 cells treated with non-targeting or CLASPs siRNA were transfected with YFP-GT or mCherry-GT and photobleached for 7 seconds with a 10mW DPSS laser 85YCA010 (Melles Griot) by focusing the laser light on the selected

Golgi area with a custom-made lens (Nikon) placed in position of the filter cube. Single-channel movies were recorded using wide-field microscopy for 5 minutes (3 seconds/frame) after bleaching.

Quantitative Analysis

Golgi assembly

Images from time points (nocodazole washout: 0, 20, 40, and 60 minutes; mitotic exit: 0, 8, and 20 minutes) were obtained from time-lapse movies of cells expressing either YFP-GT, mCherry-GT, or mCherry-Rab6 to label the Golgi. Images were processed by background subtraction and standardized entropy thresholding, then particle area was quantified using ImageJ analyze particles function.

MT plus end and NPY vesicle tracking analyses

For plus end and vesicle tracking, time-lapse recordings of RPE1 cells expressing fluorescently labeled MT tip marker EB3 (5 sec/frame) or NPY (Venus or RFP) to mark post-Golgi carriers (1 sec/frame) were processed by rolling-ball background correction. Then, a custom script in IPLab software created tracks by rolling average sequences over 4 frames to precisely follow MT tips and vesicles. The manual tracking plugin of ImageJ software was used to follow tracks.

Circularity

To apply circularity measurements to the Golgi, a freehand selection option in ImageJ software was used to outline the Golgi based on GM130

staining. Circularity index values were assigned to Golgi outlines by ImageJ circularity plugin where Circularity = 4pi(area/perimeter^2). A circularity value of 1 corresponds to a perfect circle. Circularity index was previously used by Patel *et al*. (Patel et al., 2008) to analyze overall cell shape and by Thomas and Wieschaus (Thomas and Wieschaus 2004) to measure microfilament ring circularity during cellularization.

3D Golgi analysis

Confocal z-slices (0.2μm) were analyzed for 3D continuity by ImageJ 3D objects counter plugin and ImageJ Volume Viewer plugin was used for 3D Golgi reconstruction.

Fluorescence recovery after photobleaching

Fluorescence intensity in bleached and non-bleached regions of the Golgi was measured using ImageJ software. Bleached areas were normalized to non-bleached areas both pre- and post-bleach in order to obtain fluorescence recovery values. Data represents percentage of fluorescence recovery in the bleached region.

NPY quantification

Cells were divided into four quadrants (Fig. S6). A line was drawn down the cell connecting the center of the Golgi and the center of the nucleus. This line was then rotated both +/- 45° in order to create four 90° quadrants

corresponding to the cell front (containing the Golgi), right, left, and rear. Tracking of post-Golgi cargos were assigned to each of these categories based upon which quadrant the track fused with the plasma membrane at the cell periphery.

Directional persistence of cell migration

Cell migration tracks were quantified by “Manual tracking” plugin of ImageJ using nuclei positions in DIC recordings of migrating single cells as reference points. Directional persistence was quantified as final distance of cell relocation divided by total migration track.

Cortactin quantification

Cells were divided into quadrants (Fig. S6). Cell outlines were generated by tracing around the entire cell to obtain a total perimeter measurement. A line was drawn to highlight cortactin rich regions of cell border and the total length of this line was quantified as a percentage of the total cell perimeter and assigned to the appropriate cell quadrant (same as for NPY quantification). Images from selected time points (0, 15, and 30 minutes) were calculated for each cell and combined to obtain a total average cortactin percentage per cell quadrant for each cell.

Image Acquisition and Processing

Fig.4.1a-b: Wide-field fluorescent video frames, 15 seconds between frames, 200ms exposure, inverted images. Fig. 4.2a, c: Maximum intensity projection of time-lapse confocal slices (10, 1 micron slices), 1 minute between frames, 100ms exposure time. Fig. 4.3a-f: Maximum intensity projection of time-lapse confocal slices (10, 0.20 micron slices), 16 seconds between frames, 200ms exposure time for red and green channels. Fig. 4.4a-c: Wide-field fluorescent video frames, 5 seconds between frames, 200ms exposure time red and green channels (a-c); 15 seconds between frames, 200ms exposure time (d) inverted image. Fig. 4.5: Maximum intensity projection of confocal stacks (10, 0.20 micron spacing (a-d); 20, 0.20 micron spacing (e-f); 10, 0.20 micron spacing (g)). Fig. 4.6b-d: Wide-field fluorescent video frames, 3 seconds between frames, 200ms exposure (b), 300ms exposure time (c-d). Fig. 4.7a-b: Wide-field fluorescent video frames, 1 second between frames, 40 ms exposure time. Fig. 4.8: False-colored DIC video frames (a-d), 1 minute between frames, 100ms exposure time; wide-field fluorescent video frames (i-j), 5 minutes between frames (cortactin), 200ms exposure time; 1 second between frames (NPY), 300ms exposure time. For images depicting cortactin (Fig. 4.8i-j) the image intensity in the cell center was artificially decreased for clarity with overlaid NPY tracks. This modification did not affect cell periphery intensity within 5μm from the cell edge (region of interest). The cell cortex, which is the area of interest used for quantification purposes, was not artificially altered. Fig. 4.S1: Wide-field fluorescent images inverted. Fig. 4.S2: Maximum intensity projection of time-

lapse confocal slices (10, 1 micron slices), 1 minute between frames, 200ms exposure (red), 100ms exposure time (green). Fig. 4.S3: False-colored snapshots of 3-Dimensional reconstructions from confocal z-sections (control= 8 slices, CLASP si= 15 slices, CLASP rescue= 8 slices; all 0.20 micron slices). Fig. 4.S6: Wide-field fluorescent image. Fig. 4.S7a,c: Maximum intensity projection of confocal stacks (16, 0.20 micron slices). Brightness and contrast were adjusted individually for each fluorescent channel. For images showing Golgi particles and MTs, gamma settings were adjusted to make small structures visible. Images showing MT tip and NPY tracks are shown as maximum intensity projections for background-subtracted time-lapse stacks (Figs.4.4a-b, 4.7a-b, 4.8i-j).

Quantifying MT asymmetry

Central cell area (30% total area centered at the cell centroid) is excluded from analysis because the brightness of central MTs often overrides otherwise significant differences in the rest of the cell and interferes with MT distribution analysis. Each cell was divided into radial quadrants and the average intensity (I) in each quadrant was quantified. This parameter correlates with the number of MTs in each quadrant. Degree of asymmetry is quantified as the ratio of the highest to lowest intensity.

Statistical Analysis

Statistical significance was determined by Student's t-test (two-tailed unpaired). P-values < 0.05 are shown.

Acknowledgements

We thank Drs James Goldenring, Matthew Tyska, and Ryoma Ohi for helpful discussions and Drs Anna Akhmanova, Laura A. Lee and Steven K. Hanks for critical reading of the manuscript.

This study was funded by NIH NIGMS grant 1R01GM078373-01 to I.K. and a pilot project to I.K. from NIH NCI GI SPORE grant P50CA095103.

A.R.R.M. was supported by Fundação para a Ciência e Tecnologia fellowship SFRH/BD/32976/2006 and by grant PTDC/SAU-OBD/66113/2006 from Fundacao para a Ciencia e a Tecnologia of Portugal.

CHAPTER V

CLASP TURNOVER REGULATED BY GSK3β INFLUENCES MICROTUBULE FORMATION AT THE GOLGI

Introduction

The binding of CLASPs to MTs is known to be spatially and temporally regulated by phosphorylation via Glycogen Synthase Kinase 3β (GSK3β) (Akhmanova et al., 2001; Wittmann and Waterman-Storer 2005; Kumar et al., 2009; Watanabe et al., 2009). This phosphorylation has been confirmed both *in vitro* and *in vivo* by downshift of CLASPs on immunoblots of cell extracts (Wittmann and Waterman-Storer 2005). Further, inhibition of GSK3β activity by lithium chloride treatment (a selective inhibitor of GSK3β activity (Klein and Melton 1996)) significantly increases the amount of CLASP bound to MTs. Conversely, over-expression of a constitutively active form of GSK3β (GSK-3β-S9A) abolishes CLASP localization to MTs (Akhmanova et al., 2001; Wittmann and Waterman-Storer 2005; Kumar et al., 2009).

In migrating cells, GSK3β spatially regulates CLASPs at the leading edge (Wittmann and Waterman-Storer 2005). Although these cells contain a natural gradient of GSK3β (high near the nucleus and low near the cell periphery), GSK3β is specifically inactivated in cell protrusions (Akhmanova et al., 2001; Etienne-Manneville and Hall 2003). This allows CLASPs to bind to and stabilize

microtubules at the cell edge, which contributes to directionally persistent protrusions.

Since the initial finding that CLASPs phosphorylation is regulated by GSK3β, researchers have identified at least eleven phosphorylation sites (Kumar et al., 2009; Watanabe et al., 2009). Nine of the phosphorylation sites reside within the conserved MT binding domain of CLASP (residues 568-614 of CLASP2). Phosphorylation of these residues regulates CLASP binding along the MT lattice as well as plus-tip binding (Kumar et al., 2009). Two additional sites (Ser 533 and Ser 537 of CLASP2) have been implicated in regulating CLASP interaction with actin-binding protein IQGAP1 (Watanabe et al., 2009). The phosphorylation of CLASP at these residues results in dissociation from IQGAP1. These data suggest that GSK3β regulates CLASPs in order to modulate the link between the actin and microtubule cytoskeletons at the leading edge of motile cells (Watanabe et al., 2009).

To date, the majority of the studies concerning the regulation of CLASPs by GSK3β have primarily been focused on CLASPs at the leading edge of motile cells. However, it is unclear if GSK3β plays a role in MT formation at the Golgi. Recently, a report by Fumoto et al. (Fumoto et al., 2006) showed that siRNA knockdown of GSK3β significantly reduced the amount of MTs in the cell center around the MTOC. Although these studies focused on the centrosome as the MTOC, we have identified that the Golgi apparatus serves as an additional

MTOC that is in close proximity to the centrosome (Efimov et al., 2007). Could this reduction in MT density be attributed to a decrease in the amount of Golgi-derived MTs?

Further, Fumoto et al. noted that in nocodazole washout assays, control cells contained more cytoplasmic MTs than GSK3β knockdown cells in the initial phase of MT re-growth (Fumoto et al., 2006). Based upon our studies (Efimov et al., 2007), we now know that a majority of cytoplasmic MTs formed upon nocodazole washout are nucleated at Golgi mini-stacks. Since we know that Golgi-derived MTs are specifically coated with CLASPs and that CLASP/MT binding is regulated by GSK3β, it is likely that GSK3β plays a role in CLASP-dependent MT formation at the Golgi.

Thus far, we have found that the amount of GCC185 at the Golgi membrane directly corresponds to the amount of CLASPs present and that GSK3β affects MT formation at the Golgi by regulating the turnover rate of CLASPs at GCC185 anchoring sites. We propose a model by which fast exchange of CLASPs at the Golgi allows coating and stabilization of MT seeds resulting in formation of Golgi-derived MTs.

Importantly, since all previous studies addressing GSK3β phosphorylation of CLASPs focused on the CLASP2 isoform (Kumar et al., 2009; Watanabe et al., 2009), and the fact that the residues phosphorylated by GSK3β are

conserved between CLASP1 and CLASP2; we focused our efforts CLASP2 as well. However, taking this into consideration, we confirmed that CLASP1 responds to lithium chloride treatment in the same manner as CLASP2 and performed siRNA rescue experiments with GFP-CLASP2 constructs in a CLASP2 and CLASP1 depleted background to make sure that CLASP1 is not compensating for CLASP2 activity.

Results

CLASPs distribute from the Golgi along newly formed Golgi-derived MTs

A defining feature of Golgi-derived MTs is the fact that they are specifically coated with CLASPs whereas centrosomal MTs are not. We have shown that this holds true for MTs formed in steady state as well as newly formed MTs in nocodazole washout experiments (Chapter II of this thesis) (Efimov et al., 2007). However, based upon these initial observations we could only speculate that this coating was achieved by CLASPs redistribution from the Golgi. Here utilizing 3-dimensional reconstruction and line scans to perform pixel intensity analysis, we have found that CLASPs indeed redistribute from the Golgi to coat newly growing MTs upon nocodazole washout (Fig. 5.1).

RPE1 cells transiently expressing GFP-CLASP2 were treated with nocodazole for 2 hours to depolymerize all MTs. Nocodazole was then removed and MTs were allowed to polymerize for 45 seconds before fixation. Upon fixation, cells were immunostained for GCC185 (Fig. 5.1 A-B, blue) to mark the Golgi and EB1 (Fig. 5.1 A-B, red) to highlight MTs. Confocal z-sections were

then taken at 0.2um intervals and utilized for analysis. A sum projection of 3 confocal slices (Fig. 5.1 A) shows an overview of the entire cell upon nocodazole washout. The inset from (Fig. 5.1 A) was used to create a 3-dimensional reconstruction (Fig, 5.1 B) and also used for pixel intensity analysis (Fig. 5.1 C). Snapshots from the 3-dimensional reconstruction (Fig. 5.1 B) clearly illustrate CLASP2 (green) redistributing from the Golgi (blue) toward the plus end of the newly formed MT marked by EB1 (red). Pixel intensity analysis of line scans along the MT (from the minus end toward the plus end) (Fig. 5.1 C, representative graph) confirms that CLASP (green) intensity is high at the Golgi (blue) and decays toward the plus end of the MT where EB1 (red) intensity increases. Therefore, CLASPs redistribute from the Golgi to coat and stabilize newly formed Golgi-derived MTs.

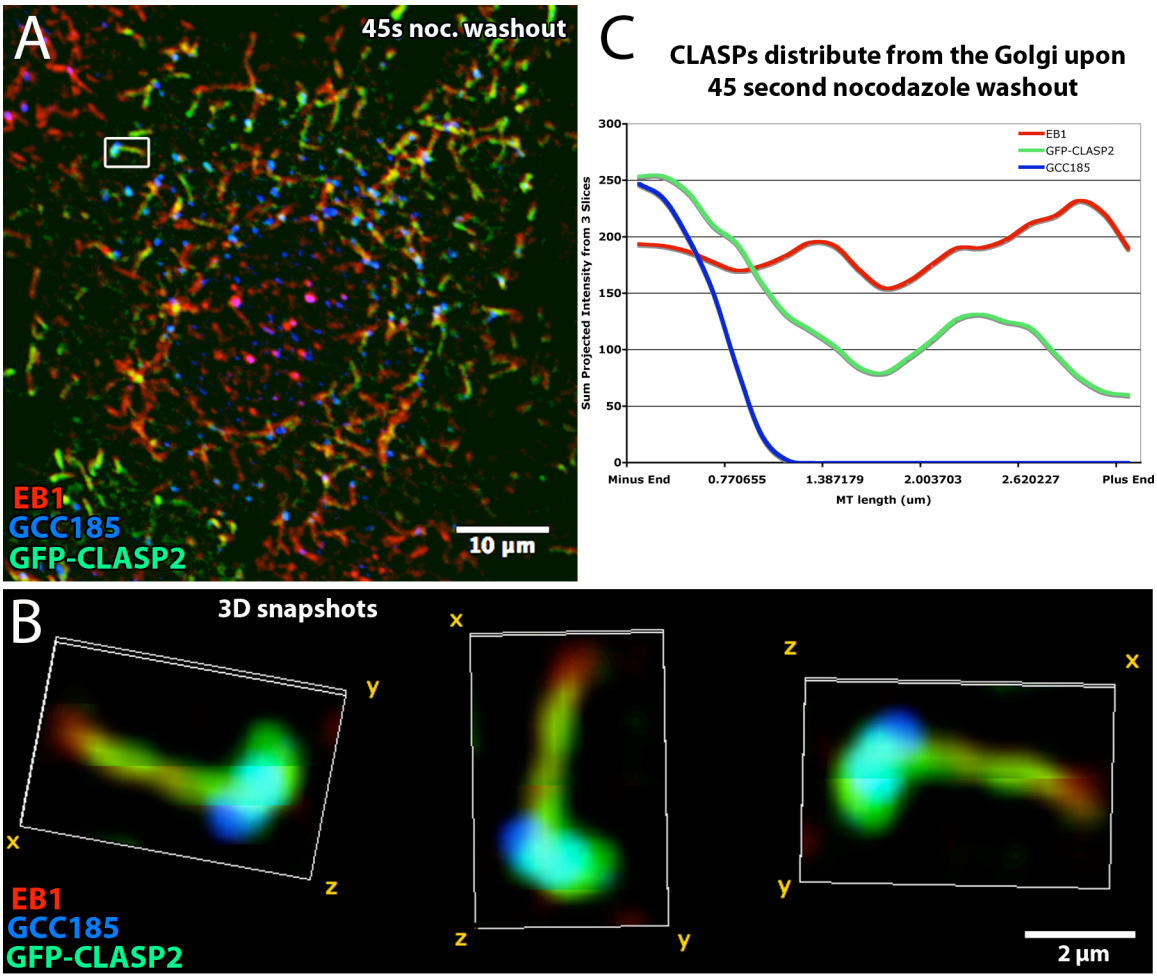

Figure 5.1. CLASP distribution from the Golgi along newly formed Golgi-derived MTs. **A,** Immunostaining of GCC185 (blue) and EB1 (red) in a GFP-CLASP2 expressing RPE1 cell fixed at 45 seconds of nocodazole washout. **B,** Angled snapshots from 3 dimensional reconstruction of a single Golgi-derived MT (white box from **A**) showing CLASP (green) distributing from the Golgi (blue) toward the plus end of the microtubule marked by EB1 (red). **C,** Representative intensity plots (32 MTs from 8 individual cells) from line scans of GCC185 (blue), GFP-CLASP2 (green), and EB1 (red) from the minus end of the MT toward the plus end.

Amount of CLASPs at the Golgi directly depends on GCC185 concentration

Since CLASPs play a key role in the formation of Golgi-derived MTs, it is important to understand what regulates the amount of CLASPs at the Golgi membrane. We have previously shown that GCC185 serves as a scaffold for CLASPs at the *trans*-Golgi network (TGN) (Fig 5.2 D) and is also required for MT formation at the Golgi (Efimov et al., 2007). Immunostaining a mixed culture of NT CTL and GCC185 depleted RPE1 cells confirm that in the absence of GCC185 (Fig 5.2 A, green, purple arrow) CLASPs (Fig. 5.2 A, red) are no longer localized to the Golgi (blue). In control cells (Fig 5.2 A, yellow arrow), CLASPs (red) and GCC185 (green) are both present at the Golgi (blue). Utilizing pixel intensity analysis we found that in control cells (Fig. 5.2 B) there is a direct correlation between the amount of CLASPs and GCC185 at the Golgi. Further, in GCC185 depleted cells (Fig. 5.2 C) we found that CLASP dissociation from the Golgi is directly dependent on the efficiency of GCC185 knockdown.

Together these data reveal that the actual amount of GCC185 present at the Golgi determines the amount of CLASP present at the membrane. Could GSK3β be regulating CLASP-dependent MT formation at the Golgi by altering the amounts of either CLASP or GCC185 present at the Golgi membrane? Immunostaining and pixel intensity analysis of endogenous CLASP and GCC185 at the Golgi in NT CTL, lithium chloride treated, and GSK3β knockdown cells showed no significant difference in the amount of either protein present at the Golgi. Although no significant changes in protein levels were observed, it was

still unclear if GSK3β regulated the turnover rate of CLASPs at the Golgi. To examine this further we utilized Fluorescence Recovery After Photobleaching (FRAP) analysis. We have shown that CLASPs redistribute from the Golgi to coat newly formed Golgi-derived MTs (Fig 5.1) and any perturbations of this process could affect the ability of MTs to be formed at the Golgi.

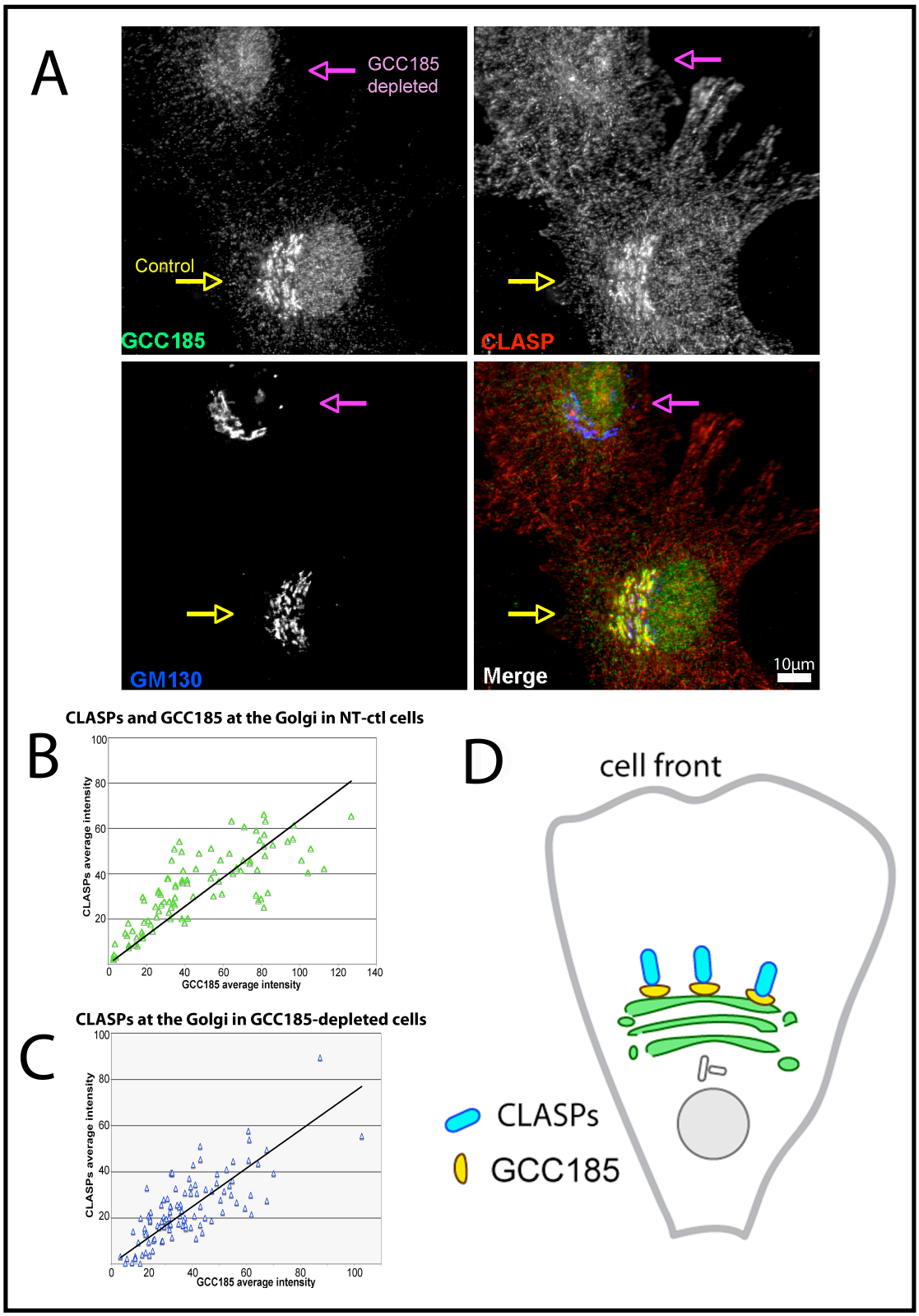
A
GCC185 depleted
Control
GCC185
CLASP
GM130
Merge
10µm
B
CLASPs and GCC185 at the Golgi in NT-ctl cells
CLASPs average intensity
GCC185 average intensity
C
CLASPs at the Golgi in GCC185-depleted cells
CLASPs average intensity
GCC185 average intensity
D
cell front
CLASPs
GCC185

Figure 5.2. Amount of GCC185 at the TGN directly correlates with the amount of CLASPs present at the Golgi. A, Immunostaining of GCC185, CLASPs, and GM130 in NT control (yellow arrow) and GCC185-depleted (purple arrow) RPE1 cells. CLASPs are absent from the Golgi in GCC185-depleted cells (purple arrows). **B,** In control RPE1 cells, CLASPs and GCC185 localization at the Golgi is coordinated. **C,** In GCC185-depleted cells, CLASPs show Golgi dissociation directly dependent upon the efficiency of GCC185 depletion. **D,** Model of GCC185 (yellow) anchoring CLASPs (blue) at the Golgi (green).

CLASPs rapidly exchange at GCC185 anchoring sites

FRAP was used to analyze and compare the exchange rates of CLASP and GCC185 at the Golgi. RPE1 cells were transiently transfected with td-Tomato GCC185 (Fig. 5.3 A, red) and GFP-CLASP2 (Fig. 5.3 A, green) and subjected to photobleaching experiments (Fig 5.3). Our data indicate that GFP-CLASP2 turns over at a t ½ of 2.55 seconds whereas td-Tomato GCC185 turns over at a t ½ of 12.62 seconds (Fig 5.3 B,C). Since GCC185 serves as a scaffolding protein for CLASPs at the TGN membrane (Efimov et al., 2007), this FRAP analysis indicates that CLASP can rapidly exchange at the GCC185-based anchoring sites.

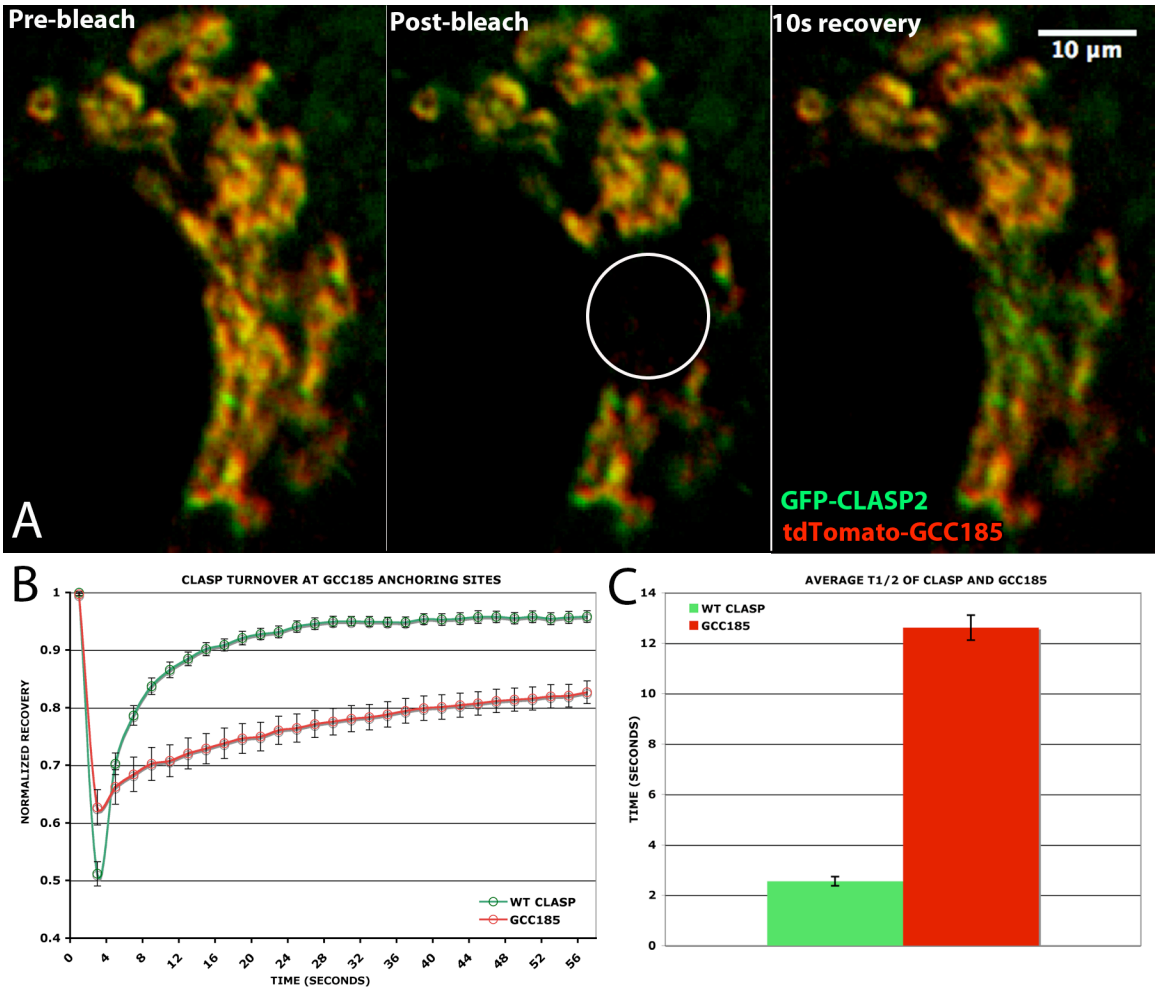

Figure 5.3. FRAP reveals that CLASP2 rapidly exchanges at GCC185 anchoring sites. A, Time-lapse images of td-Tomato GCC185 (red) and GFP-CLASP2 (green) expressing RPE1 cell. Pre-bleach (left), post-bleach (middle), and 10 seconds post-bleach (right). White circle indicates bleached region. **B,** Representative (N=20) recovery curves for CLASP2 (green) and GCC185 (red). **C,** Graph comparing average half-life recovery for CLASP (green, 2.55 seconds SEM +/- 0.18) and GCC185 (red, 12.62 seconds SEM +/- 0.49).

GSK3β inhibition significantly slows CLASP turnover rates at the Golgi

To test the effect of GSK3β on CLASP turnover at the Golgi we employed a multi-faceted approach. First, we performed FRAP analysis on a non-phosphoralatable form of CLASP (CLASP 9S/A) (Fig. 5.4). When expressed in cells, CLASP 9S/A is not affected by endogenous GSK3β activity (Kumar et al., 2009). Second, we inhibited GSK3β phosphorylation of CLASP by lithium chloride treatment (Klein and Melton 1996). We tested various conditions and determined by gel-shift assays that a concentration of 100mM LiCl treatment for at least 4 hours in RPE1 cells was most effective in dephosphorylating endogenous CLASP (Fig 5.5 A, downshift of band on gel is indicative of protein dephosphorylation). Third, we utilized siRNA to effectively remove approximately 80% of endogenous GSK3β from RPE1 cells. We also tested two small molecule inhibitors of GSK3β, BIO and SB216763, however both inhibitors showed off-target effects (drastic reduction of GCC185 from the Golgi) that were not observed with either lithium treatment or removal of GSK3β by siRNA.

FRAP analysis of GFP-CLASP 9S/A (Fig 5.6 A,C) reveals that non-phosphorylatable CLASP2 turns over approximately 1.7 times slower (4.3 seconds SEM +/- 0.24) than WT CLASP2 (2.5 seconds SEM +/-0.18. However, in this experiment, GFP-CLASP 9S/A was expressed on top of endogenous CLASP, which could alter turnover rates due to the fact that endogenous CLASP dissociates from the Golgi rapidly and makes more GCC185 docking sites accessible. When we inhibit phosphorylation of endogenous CLASP by LiCl

treatment and then express GFP-CLASP 9S/A, the turnover rate slows to 11.37 seconds SEM +/- 0.62 (Fig. 5.6 C, pink curve). These results are consistent with turnover rates of WT CLASP in cells treated with LiCl (10.44 seconds SEM +/- 0.55) indicating that when CLASPs are completely dephosphorylated, they turnover approximately 5 times slower than WT CLASP in the presence of endogenous GSK3β.

Rescue experiments have also been performed in a CLASP depleted background (Fig 5.7). In these experiments endogenous CLASP1 and CLASP2 were removed by siRNA targeting the 3'UTR of the protein. Although we are looking primarily at the CLASP2 isoform, we decided to deplete both CLASP1 and CLASP2 to make sure that CLASP1 is not compensating for CLASP2 function. Upon depletion, WT and 9S/A CLASPs (Fig. 5.4) were re-expressed. As expected, results of rescue experiments matched previous turnover rates; WT-CLASP turned over at 2.65 seconds SEM +/-0.64 and CLASP 9S/A turned over at a rate of 4.58 seconds SEM +/-0.24. Interestingly, CLASP 9S/A in the CLASP-depleted background did not turnover as slowly as CLASP 9S/A expressed in WT cells treated with LiCl (turnover rate 11.37 seconds SEM +/- 0.62). This rate may be faster due to the fact that CLASP-depletion was not 100% or due to the fact that there may be other phoshporylation sites within CLASP that have yet to be identified.

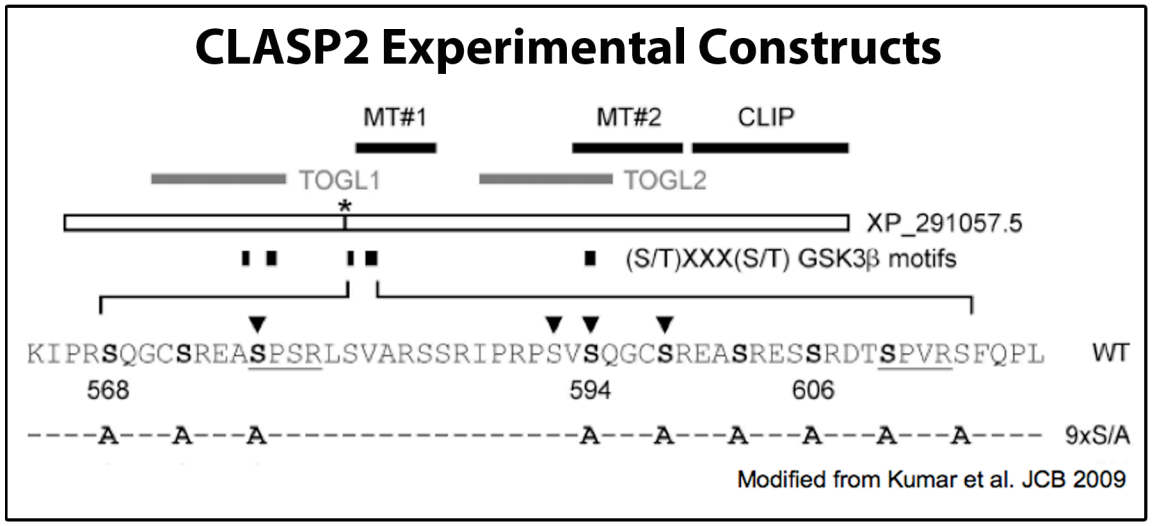

Figure 5.4. CLASP2 experimental constructs. WT CLASP contains all GSK3β phosphorylation sites. In CLASP 9 S/A, all GSK3β phosphorylation sites have been mutated from serine to alanine.

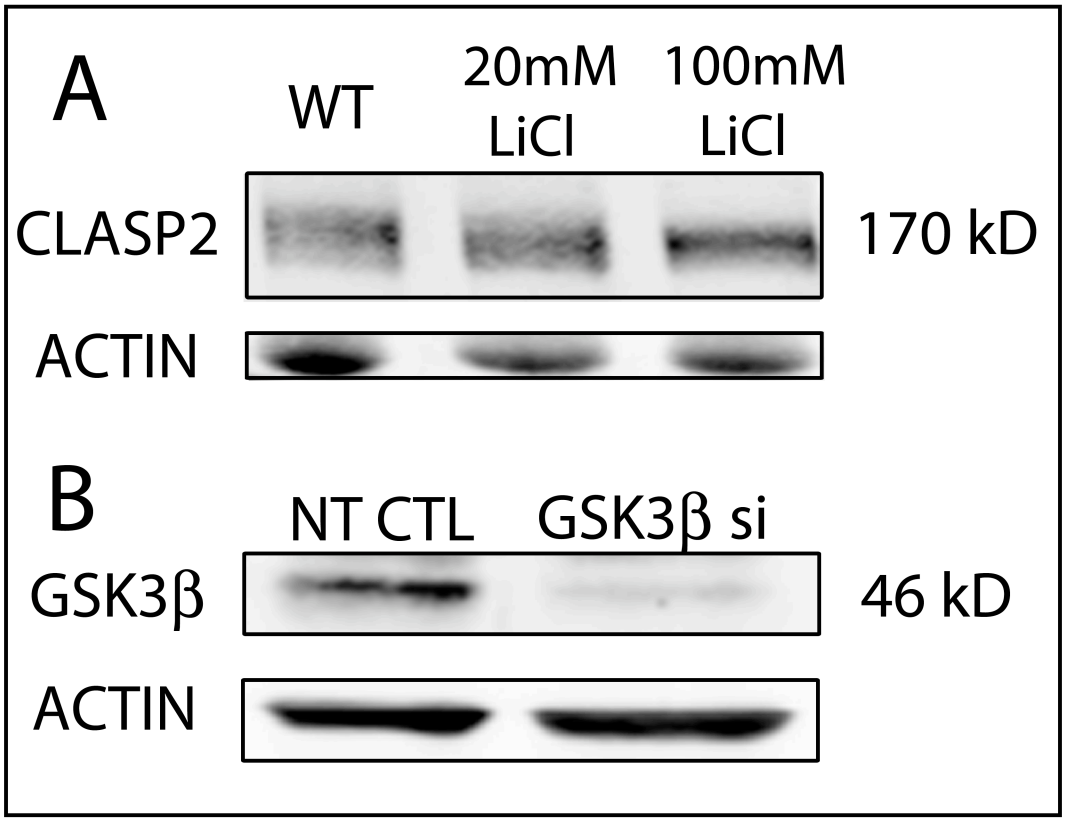

Figure 5.5. Inhibition of CLASP phosphorylation by lithium chloride and GSK3β knockdown. A, Immunoblot (7% gel) of WT and lithium chloride treated RPE1 lysates. Lithium chloride treatment (maximal effect at 100mM) resulted in a downshift of CLASP2, which is indicative of protein dephosphorylation. **B,** Immunoblot (10% gel) showing approximately 80% reduction of GSK3β in siRNA treated cells as compared to NT CTL cells.

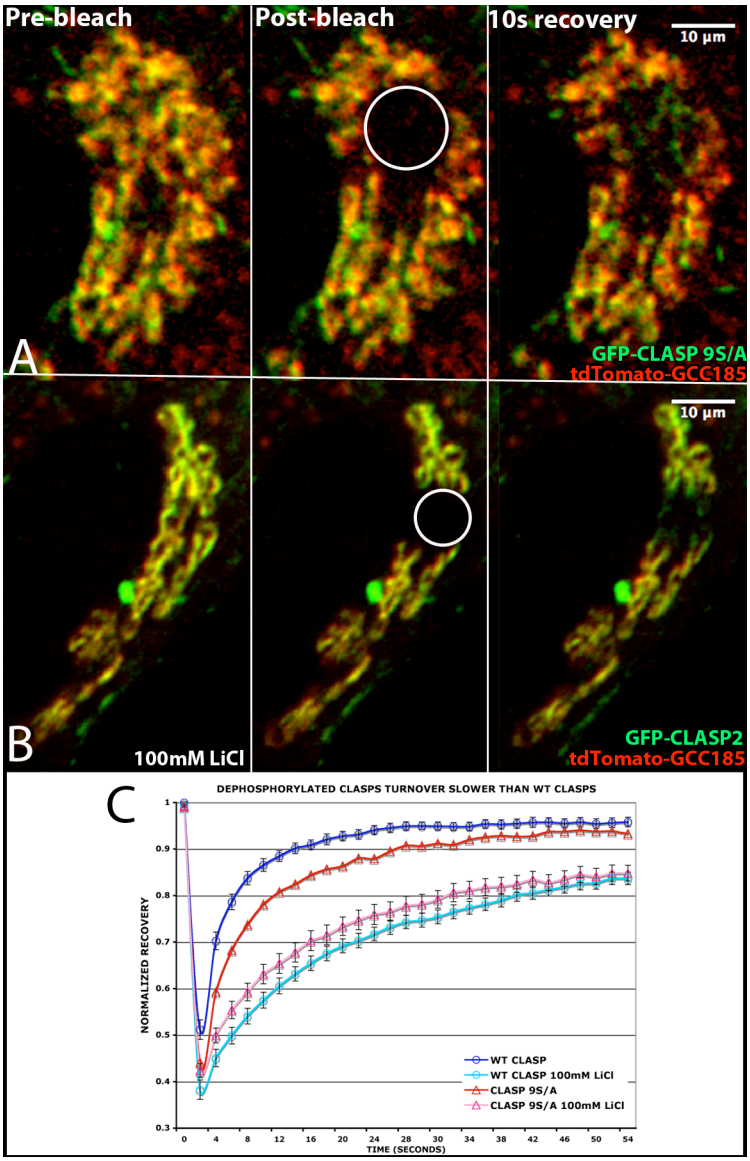

Figure 5.6. Dephosphorylated CLASP2 turns over slower at the Golgi. **A,** Time-lapse images of td-Tomato GCC185 (red) and GFP-CLASP 9S/A (green) expressing RPE1 cell. Pre-bleach (left), post-bleach (middle), and 10 seconds post-bleach (right). White circle indicates bleached region. **B,** Time-lapse images of td-Tomato GCC185 (red) and GFP-CLASP2 (green) expressing RPE1 cell treated with 100mM LiCl. Pre-bleach (left), post-bleach (middle), and 10 seconds post-bleach (right). White circle indicates bleached region. **C,** Representative (N=20) recovery curves for WT CLASP2 (blue), CLASP 9S/A (red), WT CLASP 100mM LiCl (light blue), and CLASP 9S/A in 100mM LiCl (pink). CLASP 9S/A curve is further shifted to the right when endogenous GSK3β activity is inhibited by LiCl.

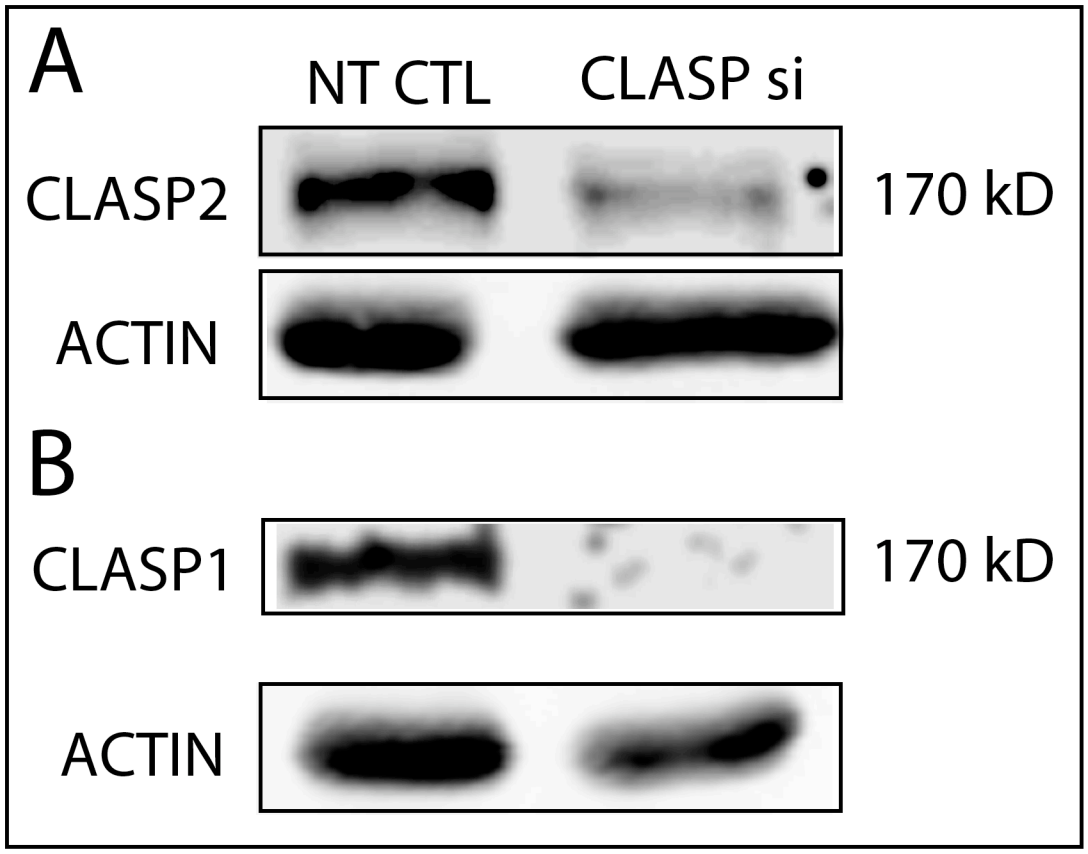

Figure 5.7. CLASP1 and CLASP2 depletion in RPE1 cells.
Immunoblot (10% gel) showing approximately 73 percent reduction of CLASP2 (**A**) and 95 percent reduction in CLASP1 (**B**) as compared to NT CTL RPE1 cell lysates. Actin, loading control.

The Golgi-derived MT array is absent in GSK3β inhibited cells

To examine MT nucleation sites in steady state, we performed EB3 tracking experiments in WT and lithium chloride treated cells. (For a complete description of this method refer to (Efimov et al., 2007; Miller et al., 2009)). In brief, RPE1 cells were transfected with td-Tomato GCC185 to mark the Golgi and GFP-EB3 to track growing MT tips. Cells were imaged by confocal microscopy at 5 second intervals over a period of two minutes. Overlaid EB3 tracks in WT CTL RPE1 cells (Fig, 5.8 A) reveal centrosomal (green arrow) and Golgi-derived (red arrow) MT arrays. In lithium chloride treated cells (Fig 5.8 B) the centrosomal MT array (green arrow) is prominent, however the Golgi-derived MT array (yellow arrow) is absent. This data confirms that in the absence of GSK3β activity, the Golgi-derived MT array is not formed in steady state.

We further confirmed that the Golgi-derived MT array is absent in GSK3β knockdown/inhibited cells by immunostainings (Fig. 5.9). Stainings of the entire MT cytoskeleton correspond to results from EB3 tracking experiments above. NT CTL cells exhibit centrosomal (red arrow) and Golgi-derived (green arrow) MT arrays (Fig. 5.9 A). In GSK3β knockdown (Fig. 5.9 B) and lithium chloride treated cells (Fig. 5.9 C), a radial centrosomal MT array is observed whereas Golgi-derived MTs are absent. These results are consistent with our previous findings that cells lacking Golgi-derived MTs predominately have radial MT arrays (Efimov et al., 2007; Miller et al., 2009). The Golgi-derived MT array is

tangential in nature (Fig, 5.8 A, red arrow; Fig. 5.9 A, green arrow) (Miller et al., 2009) and is clearly absent in lithium treated and GSK3β knockdown cells.

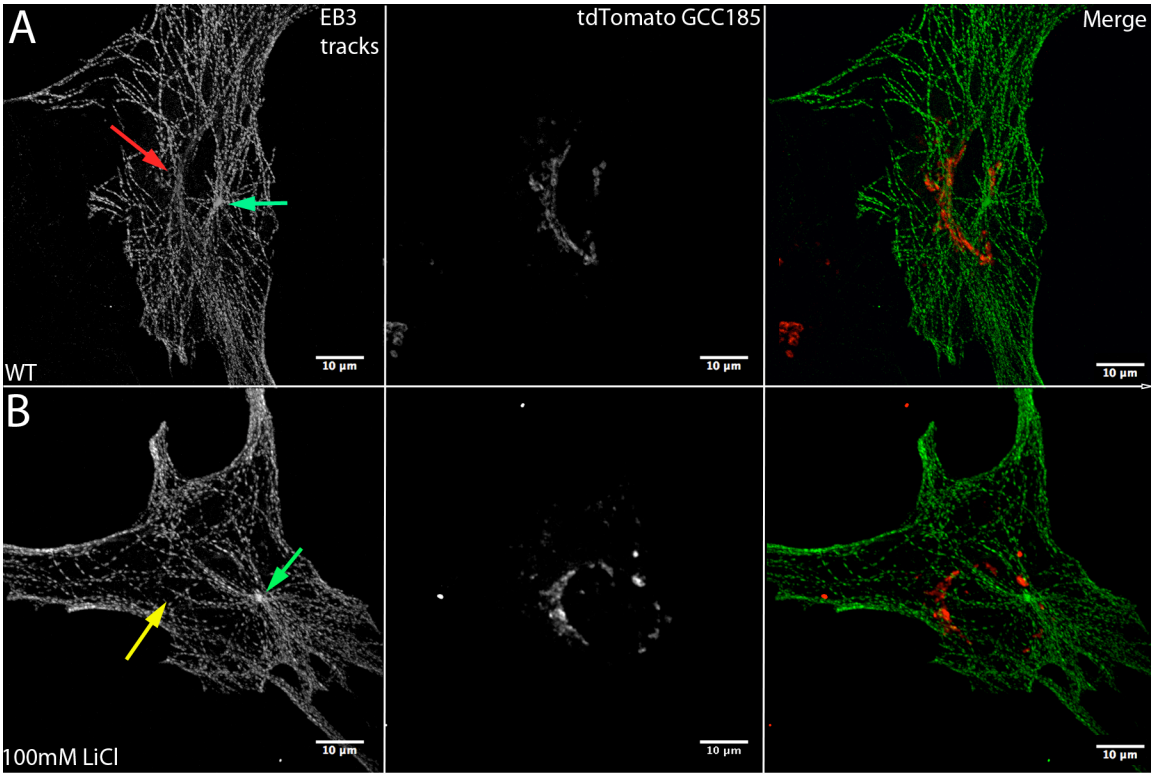

Fig. 5.8. Golgi-associated MT tracks are absent in GSK3β inhibited cells. WT (A) and LiCl treated (B) RPE1 cell expressing GFP-EB3 (left, green in merge) and td-Tomato GCC185 (middle, red in merge)**. A,** Overlaid EB3 tracks (0-2 minutes) shows centrosomal (green arrow) and Golgi-derived (red arrow) MT subsets. **B,** In GSK3β inhibited cel (100mM LiCl treatment), the centrosomal MT array remains intact (green arrow), however the Golgi-derived MT array is absent (yellow arrow).

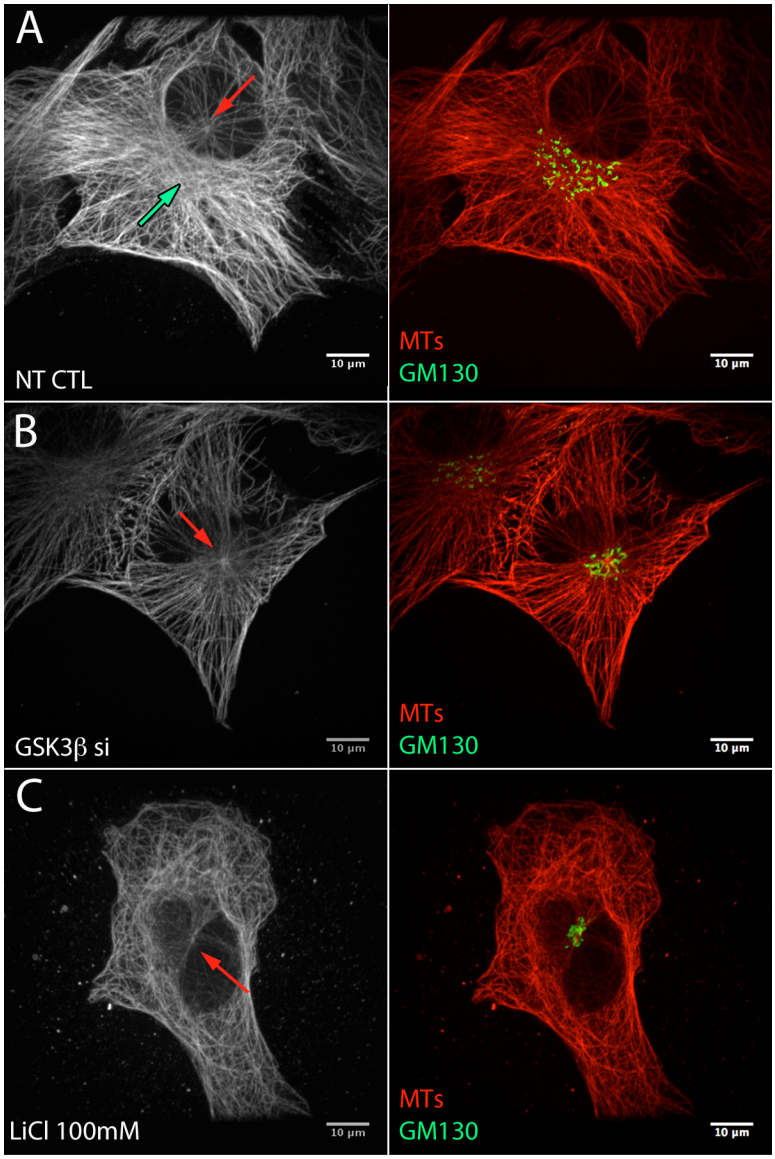

Fig, 5,9. GSK3β knockdown/inhibited cells lack Golgi-derived MTs.
A, Immunostaining of MTs (YL1/2 antibody) (left) reveals Golgi-derived (green arrow) and centrosomal (red arrow) MT arrays in NT CTL RPE1 cells. Right, merge with Golgi (GM130, green) staining. GSK3β knockdown (**B**) cells and LiCl treated cells (**C**) exhibit a prominent radial centrosomal MT array (red arrow), while lacking a Golgi derived MT array.

Discussion and Future Directions

Taking all previous data into consideration, we propose a model (Fig 5.10) whereby GSK3β promotes fast exchange of CLASPs at GCC185 anchoring sites. This fast exchange allows redistribution and coating of MT seeds that ultimately leads to Golgi-derived MT formation. Inhibition of GSK3β by lithium chloride treatment results in slow CLASP turnover rates (Fig. 5.6 C) at the Golgi and results in loss of Gogli-derived MTs (Fig 5.8 B, Fig 5.9 C)), which is consistent with what we see in GSK3β knockdown cells (Fig.5.9 B). These results are also consistent with the decrease in MT intensity near the cell center previously observed in GSK3β knockdown cells (Fumoto et al., 2006). Future experiments will includle FRAP analysis and EB3 tracking in GSK3β knockdown cells.

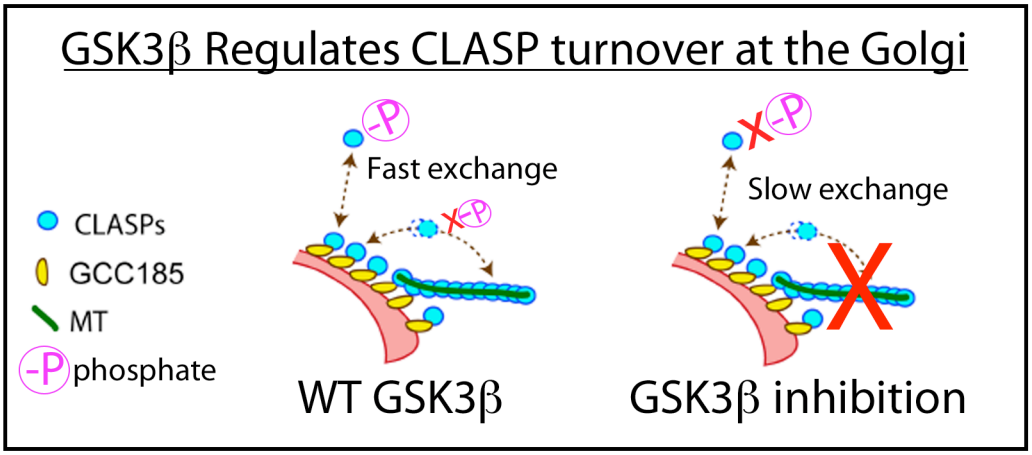

Fig. 5.10. Model of GSK3β regulating MT formation at the Golgi via CLASP turnover.

Due to the fact that GSK3β phosphorylation of CLASPs inhibits MT binding (Wittmann and Waterman-Storer 2005; Kumar et al., 2009), in order for this model to hold true, CLASPs in the presence of endogenous GSK3β must be rapidly dephosphorylated upon dissociation from the Golgi in order to coat and stabilize MT seeds. This is plausible due to the fact that upon expression of a constituitively active form of GSK3β in cells, we see prominent Golgi localization. Therefore, the Golgi could be serving as a site of CLASP phosphorylation.

Since Golgi-derived MTs are coated with CLASPs (Fig 5.1) (Efimov et al., 2007) and we know that MT coating of CLASPs is regulated GSK3β phosphorylation (Akhmanova et al., 2001; Wittmann and Waterman-Storer 2005; Kumar et al., 2009), we initially expected to see an increase in the amount of Golgi-derived MT formation upon GSK3β inhibition. However, this was not the case. Instead, we found that when CLASPs are dephosphorylated (either by GSK3β inhibition or expression of non-phosphorylatable CLASP 9S/A) that the turnover rate at the Golgi is approximately 5 times slower than CLASPs in WT cells.

Based upon FRAP analysis, we expect that dephosphorylated CLASPs have a higher binding affinity for GCC185 and this may be the reason that they are not capable of rapidly exchanging at the Golgi membrane. To test this hypothesis, we will perform co-immunoprecipitation experiments in HEK 293T

cells to evaluate the binding affinity of CLASP and GCC185 under the following conditions: GFP-WT CLASP2 expression (with and without lithium chloride treatment), GFP-CLASP 9S/A expression (with and without lithium chloride treatment), and GSK3β knockdown cells. We will IP with anti-GFP antibodies to pull out our CLASP constructs and then immunoblot against GCC185 in order to determine if certain conditions produce stronger/weaker CLASP/GCC185 binding. We expect that under conditions of CLASP dephosphorylation that we will IP more GCC185 protein which would correlate with our FRAP results.

The results presented in this chapter will be combined with on-going experiments and submitted for publication upon completion.

Methods

Cells

Immortalized human retinal pigment epithelial cells hTert-RPE1 (Clontech) were maintained in DMEM/F12 with 10% fetal bovine serum (FBS). Cells were grown in 5% CO_2 at 37ºC. Cells were plated on fibronectin-coated glass coverslips 24 hours before experiments.

Treatments

For MT depolymerization and Golgi dispersal, nocodazole (2.5µg/ml) was added to culture media for 2 hours. For nocodazole washout experiments, cells were rinsed five times with ice cold medium to remove nocodazole and then placed in a dish with warm (37°C) medium for 45 seconds to allow MT regrowth.

For GSK3β inhibition, 100mM of lithium chloride was added to culture medium for at least 4 hours prior to experiments.

siRNA and Expression Constructs

Mixed siRNA oligos against the 3'UTR region of CLASP1 and CLASP2 were custom designed (Sigma) and transfected using HiPerFect (Qiagen) according to the manufacturer's protocol. CLASP1 siRNA targeted sequence 5'-CUUUAUCUCCUACUAGUUA-3'; CLASP2 siRNA targeted sequence 5'-CUGGGCGGCUCUCGGCGAA-3'. Experiments were conducted 72 hours post-transfection as at this time minimal protein levels were detected. Nontargeting siRNA (Dharmacon) was used for controls. Pre-designed siRNA oligos (Sigma) against GSK3β were also transfected with HiPerFect (Quiagen) and experiments were conducted 48 hours post-transfection. GSK3β siRNA targeted sequence 5'-GGACUAUGUUCCGGAAACA-3'. Anti-GCC185 siRNA oligos (corresponding to nucleotides 767-784 in KIAA0336 cDNA) were designed by Ambion and experiments were conducted 48 hours post-transfection. EGFP-EB3 (gift from A. Akhmanova, Rotterdam, The Netherlands) was used for MT tip tracking. tdTomato-GCC185 was used for Golgi visualization. GFP-CLASP2 and GFP-CLASP 9S/A were provided by Torsten Wittmann (Kumar et al., 2009).

Antibodies and Immunofluorescence Details

Rabbit polyclonal antibodies against CLASP2 VU-83 are described in Efimov et al. (Efimov et al., 2007). Rabbit polyclonal antibodies against CLASP1

were provided by Dr. F. Severin (Dresden). A mouse polyclonal antibody against Actin (NeoMarkers) was used. A rabbit monoclonal antibody against GSK3β (27C10) (Cell Signaling) was used. For Golgi compartment identification, a mouse monoclonal antibody against GM130 (Transduction Laboratories) and a guinea pig polyclonal antibody against GCC185 VU-140) (Chapter II of this thesis and (Efimov et al., 2007)) were used. Mouse monoclonal antibodies against EB1 were from Transduction Laboratories. MTs were stained with a rat monoclonal YL1/2 antibody (Abcam). Cells were fixed in cold methanol (10' at -20°C) for CLASPs stainings. For MT staining cells were fixed (15' at room temp.) in 2% paraformaldehyde, 0.1% Glutaraldehyde, 0.3% triton in cytoskeleton buffer (10 mM MES, 150 mM NaCL, 5 mM EGTA, 5 mM glucose, and 5 mM $MgCL_2$, pH 6.1). For EB1 stainings, cells were fixed in cold methanol (5' at -20°C) then immediately placed in 2% PFA with 0.1% triton (5' at RT). Pacific Blue goat anti-mouse IgG, Alexa488 and Alexa568-conjugated highly cross-absorbed goat anti-mouse IgG antibodies, Alexa568-conjugated goat anti-rat IgG antibodies, and Alexa488 and Alexa568- conjugated highly cross-absorbed goat anti-guinea pig IgG (Invitrogen) antibodies were used as secondary antibodies.

MT pixel intensity quantification and 3-dimensional reconstruction

For Figure 1, confocal z-stacks were taken at 0.2um intervals on a Quorum WaveFX spinning disk confocal attached to a Nikon Eclipse Ti with a PlanApo 60x TIRF objective (NA 1.49). Triple color images were acquired by 406 nm, 491 nm, and 561 nm laser lines and a Hamatsu ImageEM-CCD camera

driven by MetaMorph software. Line scans with a 2 pixel width were performed on a sum projection of three 0.2um slices using ImageJ software. Before analysis, the Straighten Curved Objects plugin was used in order to get a straight line for analysis. 3-dimensional reconstructions were obtained by the VolumeView plugin in ImageJ.

CLASP and GCC185 Quantification at the Golgi

RPE1 cells were stained with antibodies against GM130, GCC185, and CLASP. Wide-field fluorescence imaging was performed using a Nikon 80i microscope with a CFI APO 60x oil lens, NA 1.4, and a CoolSnap ES CCD camera (Photometrics). All images were obtained using the same filter settings and exposure times on a linear acquisition scale. GM130 was used to highlight the Golgi area and respective pixel intensities of GCC185 and CLASPs were measured in the same area using ImageJ software.

Fluorescence Recovery after Photobleaching

FRAP on RPE1 cells expressing td-Tomato GCC185 and either GFP-WT CLASP2 or GFP-CLASP 9S/A was carried out on a Quorum WaveFX spinning disk confocal system equipped with a mosaic digital illumination system (Photonic Instruments) attached to a Nikon Eclipse Ti with a PlanApo 60x TIRF objective (NA 1.49). A 405 nm laser line was used for photobleaching. For green and red imaging, samples were excited with 491 nm and 561 nm laser lines respectively. Images were simultaneously obtained using MetaMorph

software and a Hamatsu ImageEM-CCD dual camera setup. The bleached region of the Golgi was pulsed for 2 seconds with the 405 nm laser and images were acquired at 1 second intervals for a 2 minute time span.

MT plus end tracking

For plus end tracking, time lapse recordings of RPE1 cells expressing fluorescently labeled MT tip marker EB3 and Golgi marker td-Tomato GCC185 were recorded at 5 second intervals (3 confocal slices at 0.5um intervals) over a period of two minutes.

MT Network Images

Confocal z-stacks were taken by a Yokogawa QLC-100/CSU-10 spinning disk head (Visitec assembled by Vashaw) attached to a Nikon TE2000E microscope using a CFI PLAN APO VC 100x oil lens, NA 1.4, and a back illuminated EM-CCD camera Cascade 512B (Photometrics) driven by IPLab software (Scanalytics). A krypton-argon laser (75 mW 488/568; Melles Griot) with AOTF was used for two-color excitation. Custom double dichroic mirror and filters (Chroma) in a filter wheel (Ludl) were used in the emission light path. Z steps (0.2um) were driven by a Nikon built-in Z motor. Images presented above are a maximal projection of 6 z-slices.

CHAPTER VI

CONCULSIONS AND FUTURE DIRECTIONS

Conclusions

The studies presented here contribute to a better mechanistic understanding of how the Golgi-derived MT array impacts the process of cell motility. These findings shed new light on how cells establish and regulate an asymmetric MT array that is required for directionally persistent migration. Biologically, this is extremely important due to the fact that cell motility is essential for processes such as embryonic development, wound healing, and cancer invasion and metastasis (Magdalena et al., 2003; Harris and Peifer 2007; Prager-Khoutorsky et al., 2007). Not only do we provide a unique functional characterization of Golgi-derived MTs, we also provide insight to the regulatory mechanism underlying formation of this distinct MT array.

Chapter II highlights my contribution to our publication that identified the Golgi as a MTOC (Efimov et al., 2007). Designing and testing antibodies against GCC185 (VU-140) played a critical role in completing this manuscript as well as providing a valuable tool for subsequent studies. Further, live-cell nocodazole washout experiments confirmed that Golgi-derived MTs are unique from centrosomal MTs in the fact that they are specifically coated with CLASPs during their initial growth phase. This unique property of Golgi-derived MTs sets the

stage for our studies in Chapter V regarding regulation of MT formation at the Golgi.

Chapter III addresses mechanisms by which cells establish MT network asymmetry. Here, we discuss four general principles by which symmetry of the radial centrosomal array can be broken. First, asymmetry can be achieved by differential modulation of MT dynamics. If this case, MTs can be preferentially stabilized at one side of the cell (e.g. the front) and destroyed at the other side (e.g. the cell rear). Second, existing MTs may be relocated within the cell. This can occur by movement of MTs within the array via severing and bending or even detachment of MTs from the array. Third, adding a non-centrosomal MT nucleation site can contribute to MT network asymmetry. We have shown that the Golgi is capable of serving as an additional MTOC and that MTs nucleated at this organelle are predominately oriented toward the cell front. Fourth, repositioning of a symmetric nucleation site to one side of the cell can lead to MT network asymmetry. In many motile cells, the centrosome is located in front of the nucleus and this positioning is thought to be very important for cellular and MT network polarization. Different combinations of the principles described above lead to the establishment of MT asymmetry in various types of motile cells. In particular, we emphasize the contribution of the Golgi-derived MT array to the asymmetry of the MT network. If the Golgi-derived MT array is eliminated (via depletion of CLASPs) or displaced (via depletion of GCC185) the ability for motile cells to form an asymmetric MT array is significantly impaired.

Chapter IV begins the detailed investigation of Golgi-derived MT function in motile cells. Here, we describe the roles that Golgi-derived MTs play in Golgi organization as well as polarized trafficking. In terms of Golgi organization, Golgi-derived MTs play a critical role in assembling a continuous Golgi ribbon. This is an extremely important function because each time a cell divides, it must properly assemble its fragmented Golgi into a “ribbon-like” network. In cells lacking Golgi-derived MTs, the Golgi is disorganized and highly fragmented. Not only does the Golgi in cells lacking Golgi-derived MTs exhibit structural defects, functional defects are also present. Examining post-Golgi trafficking, in control cells we found that trafficking was polarized toward the edge of directionally persistent migrating cells. In contrast, cells lacking Golgi-derived MTs exhibited random trafficking patterns that correlated with the inability of these cells to maintain directionally persistent migration patterns. Overall trafficking to the plasma membrane was not inhibited in cells lacking Golgi-derived MTs, however, the polarity of post-Golgi trafficking was specifically impacted. Based upon these studies we draw a model whereby CLASP-dependent MTs polarize post-Golgi trafficking by two mechanisms. First, Golgi-derived MTs organize an asymmetric Golgi ribbon oriented toward the leading edge of motile cells. Second, Golgi-derived MTs create MT array asymmetry by providing a direct link between the Golgi and the cell front. Since post-Golgi vesicle tracks in control cells directly correspond to sites of active actin polymerization at the cell front, we propose that Golgi-derived MTs facilitate directional migration via delivery of important signaling factors to the leading edge of migrating cells.

In Chapter V, I explore regulation of the CLASP-dependent MT array at the Golgi. This work stems from our observation that Golgi-derived MTs are specifically coated with CLASPs (Chapter II of this thesis, (Efimov et al., 2007)). Due to the fact that CLASP binding to MTs is regulated via phosphorylation by GSK3β, we hypothesized that GSK3β may regulate MT formation at the Golgi. Thus far, we have determined that GSK3β knockdown/inhibition does not regulate the Golgi-derived MT array by modulating the amount of CLASPs or GCC185 at the Golgi. However, utilizing FRAP analysis we have determined that WT CLASPs exchange rapidly at GCC185 anchoring sites whereas dephosphorylated CLASPs (lithium chloride treated/GSK3β siRNA treated cells, or CLASP 9S/A expressing cells) exchange approximately 5 times slower. Further, live-cell EB3 tracking experiments confirm that MTs are no longer formed at the Golgi upon full CLASP dephosphorylation. Live-cell experiments are consistent with MT patterns observed by immunostainings. WT cells show both Golgi-derived and centrosomal MT arrays, whereas the Golgi-derived MT array is absent from GSK3β knockdown/inhibited cells. Based upon these results, we propose a model where fast exchange of CLASP molecules at the Golgi results in coating and formation of Golgi-derived MTs. Slow CLASP exchange resulting from GSK3β inhibition results in lack of MT formation at the Golgi. Studies are ongoing to determine if the binding affinity of CLASP/GCC185 is modulated by GSK3β. FRAP results indicate that dephosphorylated CLASPs turnover slower at GCC185 anchoring sites, therefore co-immunoprecipitation experiments will be performed to further examine the binding affinity of these

proteins. If CLASPs cannot rapidly exchange at the Golgi, they will not be available to coat and stabilize MT seeds that lead to Golgi-derived MT formation.

In sum, these studies provide a detailed analysis of the function and regulation of the Golgi-derived MT array. Functionally, we have determined that Golgi-derived MTs are critical for proper Golgi assembly/organization and polarized post-Golgi trafficking. Both of these functions contribute to cellular polarization and development of an asymmetric MT array that is required for cell migration. In terms of regulation, we have found that phosphorylation of CLASPs by GSK3β plays an important role in CLASP turnover at GCC185 anchoring sites and subsequent MT nucleation at the Golgi.

Future Directions

Determine CLASP and GCC185 interaction domains

Revealing the mechanism regulating CLASP recruitment to the Golgi is critical for understanding how MT formation at the Golgi is regulated. We have found that GCC185 is required for CLASP localization to the Golgi (Efimov et al., 2007), therefore, determining the protein-protein interaction domains may provide useful insight as to how the amount of CLASPs at the Golgi is regulated. To date, we have determined that the C-terminus of CLASP2 that was previously found to localize to the Golgi (Mimori-Kiyosue et al., 2005) binds GCC185 (Fig. 6.1). Glutathione beads coated with GST-CLASP2N (AA 56-580) and GST-CLASP2C (AA 994-1296) terminal domains (expressed in E. *coli*) were incubated

with RPE1 cell lysate and tested for the presence of GCC185 by western blot. GCC185 was associated with the C-terminal but not N-terminal CLASP2-coated beads (Fig. 6.1). Further, in collaboration with Dr. Ikuko Hayashi (Yokohama City University, Japan) we have found that a specific region (AA 342-441) in the second coiled-coil (CC) domain of GCC185 (AA 294-650) interacts with CLASP2 by yeast-two hybrid analysis. When we expressed this portion of GCC185 in cells, it acted as a dominate-negative and removed CLASPs from the Golgi but not from MT tips. However, we still need to determine all the details of this interaction: Is this interaction direct? Are other co-factors required for this interaction?

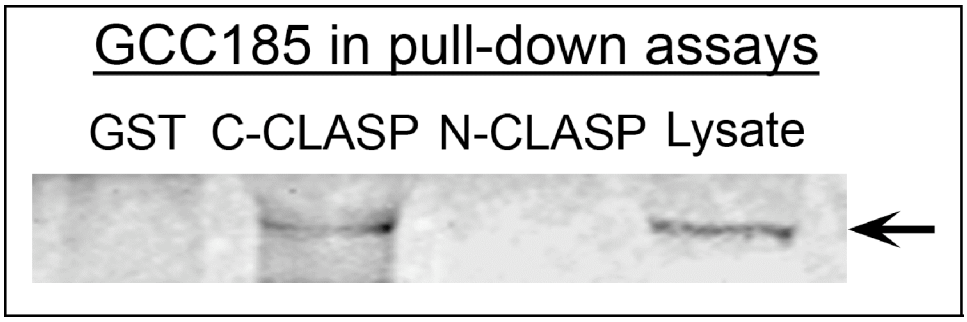

Fig. 6.1. GCC185 binds GST-CLASP2 C-terminus but not CLASP2 N-terminus or GST only-coated beads

Determine the precise location of MT outgrowth from Golgi mini-stacks

Our data indicate that Golgi-derived MTs cooperate with centrosomal MTs to assemble and organize a continuous Golgi ribbon (Miller et al., 2009). However, mechanistic details of how Golgi-derived MTs influence proper Golgi integrity and positioning remain unclear. Critical to understanding this process is determining how positioning of essential molecular players within a Golgi stack regulate geometry of MT outgrowth. Based upon our studies (Efimov et al., 2007), Golgi-derived MT formation occurs at the *trans*-Golgi network where CLASPs and GCC185 are localized. However, a recent publication by Rivero et al. (Rivero et al., 2009) states that MT nucleation occurs at the *cis*-Golgi and requires *cis*-Golgi proteins AKAP450 and GM130. In order to determine the precise location of MT formation at the Golgi, correlative light and electron microscopy will be utilized. To date, we have used this approach to localize *cis* and *trans* Golgi proteins to mini-stacks in nocodazole. This approach reveals the structure of GCC185 and GM130 containing membranes (Fig. 6.2). GM130-rich membranes are more compact than GCC185-rich membranes and these characteristics are consistent with previous electron microscopy characterizations of *cis/trans* Golgi membranes. This approach will be combined with nocodazole washout experiments to determine the precise location of MT outgrowth from Golgi mini-stacks. These nocodazole washout experiments may be performed by either 2-color live-cell imaging to image one Golgi compartment and MTs (Fig. 6.3) or by 3-color imaging with *cis* and *trans*-Golgi markers as well as a MT-tip marker (Fig 6.4). Upon nocodazole washout, live confocal z-sections

will be taken to record the initial growth of MTs from Golgi mini-stacks. Cells will be immediately fixed and processed for electron microscopy analysis and correlation will be performed as in Fig. 6.2.

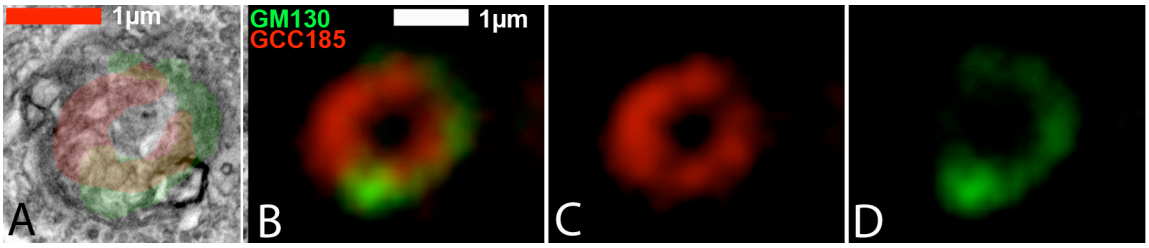

Fig. 6.2. Correlative light and electron microscopy localization of Golgi proteins. **A,** EM image overlaid with false-colors corresponding to GM130 (green) and GCC185 (red) localizations. **B,C,D,** fluorescent images showing mini-stack localizations of *trans*-Golgi protein GCC185 (red) and *cis*-Golgi protein GM130 (green) in nocodazole.

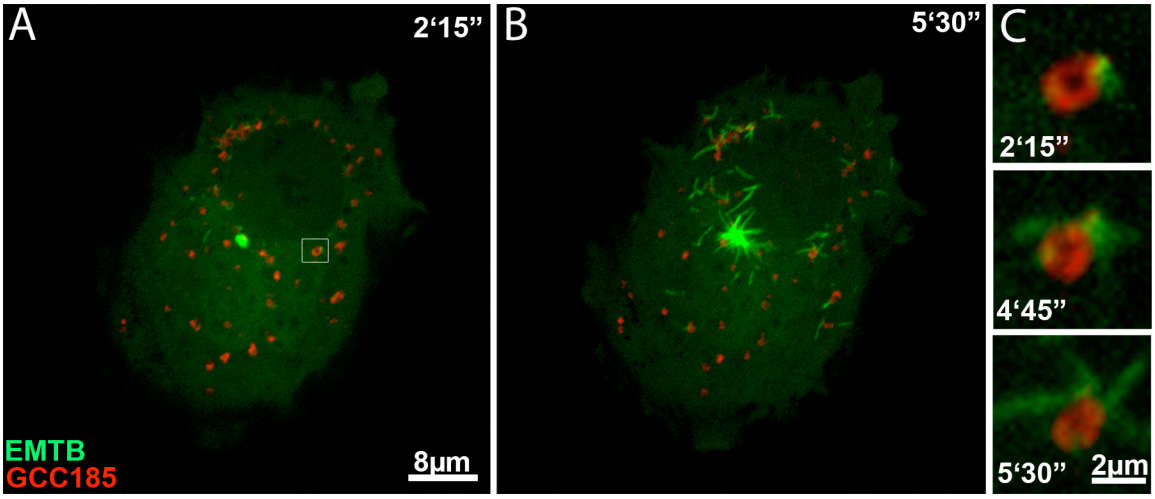

Fig. 6.3. Two-color live imaging of MT outgrowth from a Golgi mini-stack after nocodazole washout (time after washout shown). **A, B,** RPE1 cell transfected with td-Tomato GCC185 (red) to mark the Golgi and EMTB (green) to mark MTs upon nocodazole washout. **C,** Inset from (**A**) highlighting MT growth (green) from a GCC185-rich (red) region of an individual Golgi mini-stack.

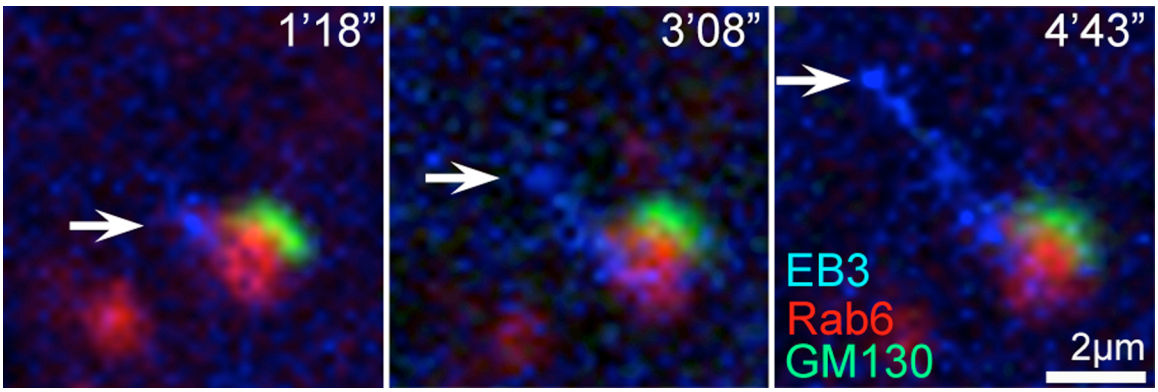

Fig. 6.4. Three-color live imaging of MT outgrowth from a Golgi mini-stack after nocodazole washout (time after washout shown). RPE1 cell transfected with CFP-EB3 (blue), mCherry-Rab6 (red), GFP-GM130 (green). MT tip, arrow. MT forms at the TGN (Rab6-rich) side of the Golgi stack.

Determine if Golgi mini-stacks fuse along Golgi-derived MTs

Our data indicate that Golgi-derived MTs play a critical role in Golgi assembly by promoting mini-stack clustering in the cell periphery as well as maintaining a continuous Golgi ribbon (Miller et al., 2009). However, it is not clear whether mini-stack fusion occurs along Golgi-derived MTs. Since the Golgi is highly fragmented in cells lacking Golgi-derived MTs, we hypothesize that Golgi-derived MTs serve as surface catalysts upon which mini-stacks fuse. To test if Golgi-derived MTs play a role in mini-stack fusion in the cell periphery, nocodazole washout experiments will be performed in cells expressing various photoswitchable (EOS-tagged (McKinney et al., 2009)) Golgi markers. I have successfully created a photoswitchable GCC185 construct (tdEOS-GCC185) and we have available tdEos-GalT. These markers mark the mid/trans (GalT) and *trans*-Golgi (GCC185). We still need to create a *cis*-Golgi construct (e.g. tdEOS-

GM130) if we want the ability to compare the fusion of different Golgi compartments. Cells expressing these constructs will be treated with nocodazole to depolymerize all MTs and disperse the Golgi. Then a selected region of the cell will be illuminated with a pulse of UV/blue light, converting a population of mini-stacks from green to red and resulting in a mixed population of fluorescent mini-stacks. Nocodazole will then be washed out to allow MT repolymerization, and the process of Golgi assembly will be recorded by live cell imaging. Mini-stack clustering in the cell periphery driven by Golgi-derived MTs (G-stage of Golgi assembly) usually occurs within 20 minutes of nocodazole removal, therefore fusion events will be monitored within this timeframe (Miller et al., 2009). Following individual mini-stacks will reveal if GFP and RFP signals merge in the cell periphery indicating that a fusion event has occurred. Utilizing constructs targeted to different domains within the mini-stack, the same washout and photoswitching experiments will reveal if Golgi-derived MTs facilitate fusion of all or certain Golgi compartments.

REFERENCES

Akhmanova, A. and C. C. Hoogenraad (2005). "Microtubule plus-end-tracking proteins: mechanisms and functions." Curr Opin Cell Biol **17**(1): 47-54.

Akhmanova, A., C. C. Hoogenraad, K. Drabek, T. Stepanova, B. Dortland, T. Verkerk, W. Vermeulen, B. M. Burgering, C. I. De Zeeuw, F. Grosveld, et al. (2001). "Clasps are CLIP-115 and -170 associating proteins involved in the regional regulation of microtubule dynamics in motile fibroblasts." Cell **104**(6): 923-35.

Allan, V. J., H. M. Thompson and M. A. McNiven (2002). "Motoring around the Golgi." Nat Cell Biol **4**(10): E236-42.

Amos, L. A. and D. Schlieper (2005). "Microtubules and maps." Adv Protein Chem **71**: 257-98.

Arimura, N. and K. Kaibuchi (2007). "Neuronal polarity: from extracellular signals to intracellular mechanisms." Nat Rev Neurosci **8**(3): 194-205.

Baas, P. W. (1998). "The role of motor proteins in establishing the microtubule arrays of axons and dendrites." J Chem Neuroanat **14**(3-4): 175-80.

Baas, P. W., C. Vidya Nadar and K. A. Myers (2006). "Axonal transport of microtubules: the long and short of it." Traffic **7**(5): 490-8.

Barr, F. A. (1999). "A novel Rab6-interacting domain defines a family of Golgi-targeted coiled-coil proteins." Curr Biol **9**(7): 381-4.

Barr, F. A. and J. Egerer (2005). "Golgi positioning: are we looking at the right MAP?" J Cell Biol **168**(7): 993-8.

Bartolini, F. and G. G. Gundersen (2006). "Generation of noncentrosomal microtubule arrays." J Cell Sci **119**(Pt 20): 4155-63.

Bergen, L. G., R. Kuriyama and G. G. Borisy (1980). "Polarity of microtubules nucleated by centrosomes and chromosomes of Chinese hamster ovary cells in vitro." J Cell Biol **84**(1): 151-9.

Bisel, B., Y. Wang, J. H. Wei, Y. Xiang, D. Tang, M. Miron-Mendoza, S. Yoshimura, N. Nakamura and J. Seemann (2008). "ERK regulates Golgi and centrosome orientation towards the leading edge through GRASP65." J Cell Biol **182**(5): 837-43.

Bobinnec, Y., X. Morin and A. Debec (2006). "Shaggy/GSK-3beta kinase localizes to the centrosome and to specialized cytoskeletal structures in Drosophila." Cell Motil Cytoskeleton **63**(6): 313-20.

Bornens, M. (2008). "Organelle positioning and cell polarity." Nat Rev Mol Cell Biol **9**(11): 874-86.

Bretscher, A. (2005). "Microtubule tips redirect actin assembly." Dev Cell **8**(4): 458-9.

Bruun, A., K. Tornqvist and B. Ehinger (1986). "Neuropeptide Y (NPY) immunoreactive neurons in the retina of different species." Histochemistry **86**(2): 135-40.

Bugnard, E., K. J. Zaal and E. Ralston (2005). "Reorganization of microtubule nucleation during muscle differentiation." Cell Motil Cytoskeleton **60**(1): 1-13.

Bulinski, J. C., J. E. Richards and G. Piperno (1988). "Posttranslational modifications of alpha tubulin: detyrosination and acetylation differentiate populations of interphase microtubules in cultured cells." J Cell Biol **106**(4): 1213-20.

Burakov, A., E. Nadezhdina, B. Slepchenko and V. Rodionov (2003). "Centrosome positioning in interphase cells." J Cell Biol **162**(6): 963-9.

Burguete, A. S., T. D. Fenn, A. T. Brunger and S. R. Pfeffer (2008). "Rab and Arl GTPase family members cooperate in the localization of the golgin GCC185." Cell **132**(2): 286-98.

Burkhardt, J. K. (1998). "The role of microtubule-based motor proteins in maintaining the structure and function of the Golgi complex." Biochim Biophys Acta **1404**(1-2): 113-26.

Burkhardt, J. K., C. J. Echeverri, T. Nilsson and R. B. Vallee (1997). "Overexpression of the dynamitin (p50) subunit of the dynactin complex disrupts dynein-dependent maintenance of membrane organelle distribution." J Cell Biol **139**(2): 469-84.

Burnette, D. T., L. Ji, A. W. Schaefer, N. A. Medeiros, G. Danuser and P. Forscher (2008). "Myosin II activity facilitates microtubule bundling in the neuronal growth cone neck." Dev Cell **15**(1): 163-9.

Caswell, P. T. and J. C. Norman (2006). "Integrin trafficking and the control of cell migration." Traffic **7**(1): 14-21.

Caviston, J. P. and E. L. Holzbaur (2006). "Microtubule motors at the intersection of trafficking and transport." Trends Cell Biol **16**(10): 530-7.

Chabin-Brion, K., J. Marceiller, F. Perez, C. Settegrana, A. Drechou, G. Durand and C. Pous (2001). "The Golgi complex is a microtubule-organizing organelle." Mol Biol Cell **12**(7): 2047-60.

Cole, N. B., N. Sciaky, A. Marotta, J. Song and J. Lippincott-Schwartz (1996). "Golgi dispersal during microtubule disruption: regeneration of Golgi stacks at peripheral endoplasmic reticulum exit sites." Mol Biol Cell **7**(4): 631-50.

Collin, L., K. Schlessinger and A. Hall (2008). "APC nuclear membrane association and microtubule polarity." Biol Cell **100**(4): 243-52.

Condeelis, J., R. H. Singer and J. E. Segall (2005). "The great escape: when cancer cells hijack the genes for chemotaxis and motility." Annu Rev Cell Dev Biol **21**: 695-718.

Cullen, C. F., P. Deak, D. M. Glover and H. Ohkura (1999). "mini spindles: A gene encoding a conserved microtubule-associated protein required for the integrity of the mitotic spindle in Drosophila." J Cell Biol **146**(5): 1005-18.

Cytrynbaum, E. N., V. Rodionov and A. Mogilner (2004). "Computational model of dynein-dependent self-organization of microtubule asters." J Cell Sci **117**(Pt 8): 1381-97.

Daly, R. J. (2004). "Cortactin signalling and dynamic actin networks." Biochem J **382**(Pt 1): 13-25.

de Anda, F. C., G. Pollarolo, J. S. Da Silva, P. G. Camoletto, F. Feiguin and C. G. Dotti (2005). "Centrosome localization determines neuronal polarity." Nature **436**(7051): 704-8.

Derby, M. C., Z. Z. Lieu, D. Brown, J. L. Stow, B. Goud and P. A. Gleeson (2007). "The trans-Golgi network Golgin, GCC185, is required for endosome-to-Golgi transport and maintenance of Golgi structure." Traffic **8**(6): 758-73.

Derby, M. C., C. van Vliet, D. Brown, M. R. Luke, L. Lu, W. Hong, J. L. Stow and P. A. Gleeson (2004). "Mammalian GRIP domain proteins differ in their membrane binding properties and are recruited to distinct domains of the TGN." J Cell Sci **117**(Pt 24): 5865-74.

Detrich, H. W., 3rd (1997). "Microtubule assembly in cold-adapted organisms: functional properties and structural adaptations of tubulins from antarctic fishes." Comp Biochem Physiol A Physiol **118**(3): 501-13.

Drabek, K., M. van Ham, T. Stepanova, K. Draegestein, R. van Horssen, C. L. Sayas, A. Akhmanova, T. Ten Hagen, R. Smits, R. Fodde, et al. (2006). "Role of CLASP2 in microtubule stabilization and the regulation of persistent motility." Curr Biol **16**(22): 2259-64.

Dunn, S., E. E. Morrison, T. B. Liverpool, C. Molina-Paris, R. A. Cross, M. C. Alonso and M. Peckham (2008). "Differential trafficking of Kif5c on tyrosinated and detyrosinated microtubules in live cells." J Cell Sci **121**(Pt 7): 1085-95.

Eddy, R. J., L. M. Pierini and F. R. Maxfield (2002). "Microtubule asymmetry during neutrophil polarization and migration." Mol Biol Cell **13**(12): 4470-83.

Efimov, A., A. Kharitonov, N. Efimova, J. Loncarek, P. M. Miller, N. Andreyeva, P. Gleeson, N. Galjart, A. R. Maia, I. X. McLeod, et al. (2007). "Asymmetric CLASP-dependent nucleation of noncentrosomal microtubules at the trans-Golgi network." Dev Cell **12**(6): 917-30.

Efimov, A., N. Schiefermeier, I. Grigoriev, R. Ohi, M. C. Brown, C. E. Turner, J. V. Small and I. Kaverina (2008). "Paxillin-dependent stimulation of microtubule catastrophes at focal adhesion sites." J Cell Sci **121**(Pt 2): 196-204.

Etienne-Manneville, S. (2004). "Actin and microtubules in cell motility: which one is in control?" Traffic **5**(7): 470-7.

Etienne-Manneville, S. and A. Hall (2003). "Cdc42 regulates GSK-3beta and adenomatous polyposis coli to control cell polarity." Nature **421**(6924): 753-6.

Ezratty, E. J., M. A. Partridge and G. G. Gundersen (2005). "Microtubule-induced focal adhesion disassembly is mediated by dynamin and focal adhesion kinase." Nat Cell Biol **7**(6): 581-90.

Faire, K., C. M. Waterman-Storer, D. Gruber, D. Masson, E. D. Salmon and J. C. Bulinski (1999). "E-MAP-115 (ensconsin) associates dynamically with microtubules in vivo and is not a physiological modulator of microtubule dynamics." J Cell Sci **112 (Pt 23)**: 4243-55.

Feinstein, T. N. and A. D. Linstedt (2008). "GRASP55 regulates Golgi ribbon formation." Mol Biol Cell **19**(7): 2696-707.

Fukata, M., T. Watanabe, J. Noritake, M. Nakagawa, M. Yamaga, S. Kuroda, Y. Matsuura, A. Iwamatsu, F. Perez and K. Kaibuchi (2002). "Rac1 and Cdc42 capture microtubules through IQGAP1 and CLIP-170." Cell **109**(7): 873-85.

Fumoto, K., C. C. Hoogenraad and A. Kikuchi (2006). "GSK-3beta-regulated interaction of BICD with dynein is involved in microtubule anchorage at centrosome." EMBO J **25**(24): 5670-82.

Galjart, N. (2005). "CLIPs and CLASPs and cellular dynamics." Nat Rev Mol Cell Biol **6**(6): 487-98.

Geiger, B. and A. Bershadsky (2002). "Exploring the neighborhood: adhesion-coupled cell mechanosensors." Cell **110**(2): 139-42.

Goldstein, L. S. and Z. Yang (2000). "Microtubule-based transport systems in neurons: the roles of kinesins and dyneins." Annu Rev Neurosci **23**: 39-71.

Gomes, E. R., S. Jani and G. G. Gundersen (2005). "Nuclear movement regulated by Cdc42, MRCK, myosin, and actin flow establishes MTOC polarization in migrating cells." Cell **121**(3): 451-63.

Gonczy, P., C. Echeverri, K. Oegema, A. Coulson, S. J. Jones, R. R. Copley, J. Duperon, J. Oegema, M. Brehm, E. Cassin, et al. (2000). "Functional genomic analysis of cell division in C. elegans using RNAi of genes on chromosome III." Nature **408**(6810): 331-6.

Graham, T. R. (2004). "Membrane targeting: getting Arl to the Golgi." Curr Biol **14**(12): R483-5.

Grallert, A., C. Beuter, R. A. Craven, S. Bagley, D. Wilks, U. Fleig and I. M. Hagan (2006). "S. pombe CLASP needs dynein, not EB1 or CLIP170, to induce microtubule instability and slows polymerization rates at cell tips in a dynein-dependent manner." Genes Dev **20**(17): 2421-36.

Griffiths, G. and K. Simons (1986). "The trans Golgi network: sorting at the exit site of the Golgi complex." Science **234**(4775): 438-43.

Gundersen, G. G. and J. C. Bulinski (1988). "Selective stabilization of microtubules oriented toward the direction of cell migration." Proc Natl Acad Sci U S A **85**(16): 5946-50.

Gundersen, G. G., E. R. Gomes and Y. Wen (2004). "Cortical control of microtubule stability and polarization." Curr Opin Cell Biol **16**(1): 106-12.

Gundersen, G. G., M. H. Kalnoski and J. C. Bulinski (1984). "Distinct populations of microtubules: tyrosinated and nontyrosinated alpha tubulin are distributed differently in vivo." Cell **38**(3): 779-89.

Hannak, E. and R. Heald (2006). "Xorbit/CLASP links dynamic microtubules to chromosomes in the Xenopus meiotic spindle." J Cell Biol **172**(1): 19-25.

Harris, T. J. and M. Peifer (2007). "aPKC controls microtubule organization to balance adherens junction symmetry and planar polarity during development." Dev Cell **12**(5): 727-38.

Hasaka, T. P., K. A. Myers and P. W. Baas (2004). "Role of actin filaments in the axonal transport of microtubules." J Neurosci **24**(50): 11291-301.

Hayes, G. L., F. C. Brown, A. K. Haas, R. M. Nottingham, F. A. Barr and S. R. Pfeffer (2009). "Multiple Rab GTPase binding sites in GCC185 suggest a model for vesicle tethering at the trans-Golgi." Mol Biol Cell **20**(1): 209-17.

Hirokawa, N. (1998). "Kinesin and dynein superfamily proteins and the mechanism of organelle transport." Science **279**(5350): 519-26.

Hirschberg, K., C. M. Miller, J. Ellenberg, J. F. Presley, E. D. Siggia, R. D. Phair and J. Lippincott-Schwartz (1998). "Kinetic analysis of secretory protein traffic and characterization of golgi to plasma membrane transport intermediates in living cells." J Cell Biol **143**(6): 1485-503.

Holy, T. E., M. Dogterom, B. Yurke and S. Leibler (1997). "Assembly and positioning of microtubule asters in microfabricated chambers." Proc Natl Acad Sci U S A **94**(12): 6228-31.

Hong, F. D., J. Chen, S. Donovan, N. Schneider and P. D. Nisen (1999). "Taxol, vincristine or nocodazole induces lethality in G1-checkpoint-defective human astrocytoma U373MG cells by triggering hyperploid progression." Carcinogenesis **20**(7): 1161-8.

Hoppeler-Lebel, A., C. Celati, G. Bellett, M. M. Mogensen, L. Klein-Hitpass, M. Bornens and A. M. Tassin (2007). "Centrosomal CAP350 protein stabilises microtubules associated with the Golgi complex." J Cell Sci **120**(Pt 18): 3299-308.

Houghton, F. J., P. L. Chew, S. Lodeho, B. Goud and P. A. Gleeson (2009). "The localization of the Golgin GCC185 is independent of Rab6A/A' and Arl1." Cell **138**(4): 787-94.

Howng, S. L., H. C. Hsu, T. S. Cheng, Y. L. Lee, L. K. Chang, P. J. Lu and Y. R. Hong (2004). "A novel ninein-interaction protein, CGI-99, blocks ninein phosphorylation by GSK3beta and is highly expressed in brain tumors." FEBS Lett **566**(1-3): 162-8.

Hulspas, R., A. B. Houtsmuller, J. G. Bauman and N. Nanninga (1994). "The centrosome moves out of a nuclear indentation in human lymphocytes upon activation." Exp Cell Res **215**(1): 28-32.

Inoue, Y. H., M. do Carmo Avides, M. Shiraki, P. Deak, M. Yamaguchi, Y. Nishimoto, A. Matsukage and D. M. Glover (2000). "Orbit, a novel microtubule-associated protein essential for mitosis in Drosophila melanogaster." J Cell Biol **149**(1): 153-66.

Karsenti, E., J. Newport, R. Hubble and M. Kirschner (1984). "Interconversion of metaphase and interphase microtubule arrays, as studied by the injection of centrosomes and nuclei into Xenopus eggs." J Cell Biol **98**(5): 1730-45.

Kaverina, I., O. Krylyshkina and J. V. Small (1999). "Microtubule targeting of substrate contacts promotes their relaxation and dissociation." J Cell Biol **146**(5): 1033-44.

Kaverina, I., O. Krylyshkina and J. V. Small (2002). "Regulation of substrate adhesion dynamics during cell motility." Int J Biochem Cell Biol **34**(7): 746-61.

Kaverina, I., K. Rottner and J. V. Small (1998). "Targeting, capture, and stabilization of microtubules at early focal adhesions." J Cell Biol **142**(1): 181-90.

Keating, T. J., J. G. Peloquin, V. I. Rodionov, D. Momcilovic and G. G. Borisy (1997). "Microtubule release from the centrosome." Proc Natl Acad Sci U S A **94**(10): 5078-83.

Kirschner, M. and T. Mitchison (1986). "Beyond self-assembly: from microtubules to morphogenesis." Cell **45**(3): 329-42.

Kirschner, M. W. and T. Mitchison (1986). "Microtubule dynamics." Nature **324**(6098): 621.

Kjer-Nielsen, L., R. D. Teasdale, C. van Vliet and P. A. Gleeson (1999). "A novel Golgi-localisation domain shared by a class of coiled-coil peripheral membrane proteins." Curr Biol **9**(7): 385-8.

Klein, P. S. and D. A. Melton (1996). "A molecular mechanism for the effect of lithium on development." Proc Natl Acad Sci U S A **93**(16): 8455-9.

Komarova, Y. A., A. S. Akhmanova, S. Kojima, N. Galjart and G. G. Borisy (2002). "Cytoplasmic linker proteins promote microtubule rescue in vivo." J Cell Biol **159**(4): 589-99.

Komarova, Y. A., I. A. Vorobjev and G. G. Borisy (2002). "Life cycle of MTs: persistent growth in the cell interior, asymmetric transition frequencies and effects of the cell boundary." J Cell Sci **115**(Pt 17): 3527-39.

Konishi, Y. and M. Setou (2009). "Tubulin tyrosination navigates the kinesin-1 motor domain to axons." Nat Neurosci **12**(5): 559-67.

Krendel, M., F. T. Zenke and G. M. Bokoch (2002). "Nucleotide exchange factor GEF-H1 mediates cross-talk between microtubules and the actin cytoskeleton." Nat Cell Biol **4**(4): 294-301.

Kriebel, P. W., V. A. Barr, E. C. Rericha, G. Zhang and C. A. Parent (2008). "Collective cell migration requires vesicular trafficking for chemoattractant delivery at the trailing edge." J Cell Biol **183**(5): 949-61.

Kumar, P., K. S. Lyle, S. Gierke, A. Matov, G. Danuser and T. Wittmann (2009). "GSK3beta phosphorylation modulates CLASP-microtubule association and lamella microtubule attachment." J Cell Biol **184**(6): 895-908.

Kwan, K. M. and M. W. Kirschner (2005). "A microtubule-binding Rho-GEF controls cell morphology during convergent extension of Xenopus laevis." Development **132**(20): 4599-610.

Ladinsky, M. S., C. C. Wu, S. McIntosh, J. R. McIntosh and K. E. Howell (2002). "Structure of the Golgi and distribution of reporter molecules at 20 degrees C reveals the complexity of the exit compartments." Mol Biol Cell **13**(8): 2810-25.

Lansbergen, G., I. Grigoriev, Y. Mimori-Kiyosue, T. Ohtsuka, S. Higa, I. Kitajima, J. Demmers, N. Galjart, A. B. Houtsmuller, F. Grosveld, et al. (2006). "CLASPs attach microtubule plus ends to the cell cortex through a complex with LL5beta." Dev Cell **11**(1): 21-32.

Larocca, M. C., M. Jin and J. R. Goldenring (2006). "AKAP350 modulates microtubule dynamics." Eur J Cell Biol **85**(7): 611-9.

Lemos, C. L., P. Sampaio, H. Maiato, M. Costa, L. V. Omel'yanchuk, V. Liberal and C. E. Sunkel (2000). "Mast, a conserved microtubule-associated protein required for bipolar mitotic spindle organization." Embo J **19**(14): 3668-82.

Linstedt, A. D. (2004). "Positioning the Golgi apparatus." Cell **118**(3): 271-2.

Lippincott-Schwartz, J., N. Cole and J. Presley (1998). "Unravelling Golgi membrane traffic with green fluorescent protein chimeras." Trends Cell Biol **8**(1): 16-20.

Liu, Z., Q. P. Vong and Y. Zheng (2007). "CLASPing microtubules at the trans-Golgi network." Dev Cell **12**(6): 839-40.

Luders, J. and T. Stearns (2007). "Microtubule-organizing centres: a re-evaluation." Nat Rev Mol Cell Biol **8**(2): 161-7.

Luke, M. R., L. Kjer-Nielsen, D. L. Brown, J. L. Stow and P. A. Gleeson (2003). "GRIP domain-mediated targeting of two new coiled-coil proteins, GCC88 and GCC185, to subcompartments of the trans-Golgi network." J Biol Chem **278**(6): 4216-26.

Magdalena, J., T. H. Millard, S. Etienne-Manneville, S. Launay, H. K. Warwick and L. M. Machesky (2003). "Involvement of the Arp2/3 complex and Scar2 in Golgi polarity in scratch wound models." Mol Biol Cell **14**(2): 670-84.

Maiato, H., E. A. Fairley, C. L. Rieder, J. R. Swedlow, C. E. Sunkel and W. C. Earnshaw (2003). "Human CLASP1 is an outer kinetochore component that regulates spindle microtubule dynamics." Cell **113**(7): 891-904.

Maiato, H., A. Khodjakov and C. L. Rieder (2005). "Drosophila CLASP is required for the incorporation of microtubule subunits into fluxing kinetochore fibres." Nat Cell Biol **7**(1): 42-7.

Maiato, H., C. L. Rieder, W. C. Earnshaw and C. E. Sunkel (2003). "How do kinetochores CLASP dynamic microtubules?" Cell Cycle **2**(6): 511-4.

Maiato, H., P. Sampaio, C. L. Lemos, J. Findlay, M. Carmena, W. C. Earnshaw and C. E. Sunkel (2002). "MAST/Orbit has a role in microtubule-kinetochore

attachment and is essential for chromosome alignment and maintenance of spindle bipolarity." J Cell Biol **157**(5): 749-60.

Malikov, V., A. Kashina and V. Rodionov (2004). "Cytoplasmic dynein nucleates microtubules to organize them into radial arrays in vivo." Mol Biol Cell **15**(6): 2742-9.

Malone, C. J., L. Misner, N. Le Bot, M. C. Tsai, J. M. Campbell, J. Ahringer and J. G. White (2003). "The C. elegans hook protein, ZYG-12, mediates the essential attachment between the centrosome and nucleus." Cell **115**(7): 825-36.

Marra, P., L. Salvatore, A. Mironov, Jr., A. Di Campli, G. Di Tullio, A. Trucco, G. Beznoussenko, A. Mironov and M. A. De Matteis (2007). "The biogenesis of the Golgi ribbon: the roles of membrane input from the ER and of GM130." Mol Biol Cell **18**(5): 1595-608.

Matthews, L. R., P. Carter, D. Thierry-Mieg and K. Kemphues (1998). "ZYG-9, a Caenorhabditis elegans protein required for microtubule organization and function, is a component of meiotic and mitotic spindle poles." J Cell Biol **141**(5): 1159-68.

McKinney, S. A., C. S. Murphy, K. L. Hazelwood, M. W. Davidson and L. L. Looger (2009). "A bright and photostable photoconvertible fluorescent protein." Nat Methods **6**(2): 131-3.

Mellman, I. and K. Simons (1992). "The Golgi complex: in vitro veritas?" Cell **68**(5): 829-40.

Mellor, H. (2004). "Cell motility: Golgi signalling shapes up to ship out." Curr Biol **14**(11): R434-5.

Miller, M. W., M. R. Caracciolo, W. K. Berlin and J. A. Hanover (1999). "Phosphorylation and glycosylation of nucleoporins." Arch Biochem Biophys **367**(1): 51-60.

Miller, P. M., A. W. Folkmann, A. R. Maia, N. Efimova, A. Efimov and I. Kaverina (2009). "Golgi-derived CLASP-dependent microtubules control Golgi organization and polarized trafficking in motile cells." Nat Cell Biol **11**(9): 1069-80.

Mimori-Kiyosue, Y., I. Grigoriev, G. Lansbergen, H. Sasaki, C. Matsui, F. Severin, N. Galjart, F. Grosveld, I. Vorobjev, S. Tsukita, et al. (2005). "CLASP1 and CLASP2 bind to EB1 and regulate microtubule plus-end dynamics at the cell cortex." J Cell Biol **168**(1): 141-53.

Moritz, M., M. B. Braunfeld, V. Guenebaut, J. Heuser and D. A. Agard (2000). "Structure of the gamma-tubulin ring complex: a template for microtubule nucleation." Nat Cell Biol **2**(6): 365-70.

Moritz, M., M. B. Braunfeld, J. W. Sedat, B. Alberts and D. A. Agard (1995). "Microtubule nucleation by gamma-tubulin-containing rings in the centrosome." Nature **378**(6557): 638-40.

Morrison, E. E., B. N. Wardleworth, J. M. Askham, A. F. Markham and D. M. Meredith (1998). "EB1, a protein which interacts with the APC tumour suppressor, is associated with the microtubule cytoskeleton throughout the cell cycle." Oncogene **17**(26): 3471-7.

Munro, S. (2005). "The Arf-like GTPase Arl1 and its role in membrane traffic." Biochem Soc Trans **33**(Pt 4): 601-5.

Munro, S. and B. J. Nichols (1999). "The GRIP domain - a novel Golgi-targeting domain found in several coiled-coil proteins." Curr Biol **9**(7): 377-80.

Musch, A. (2004). "Microtubule organization and function in epithelial cells." Traffic **5**(1): 1-9.

Myers, K. A. and P. W. Baas (2007). "Kinesin-5 regulates the growth of the axon by acting as a brake on its microtubule array." J Cell Biol **178**(6): 1081-91.

Nabi, I. R. (1999). "The polarization of the motile cell." J Cell Sci **112 (Pt 12)**: 1803-11.

Niethammer, P., P. Bastiaens and E. Karsenti (2004). "Stathmin-tubulin interaction gradients in motile and mitotic cells." Science **303**(5665): 1862-6.

Noritake, J., T. Watanabe, K. Sato, S. Wang and K. Kaibuchi (2005). "IQGAP1: a key regulator of adhesion and migration." J Cell Sci **118**(Pt 10): 2085-92.

O'Connell, C. B. and A. L. Khodjakov (2007). "Cooperative mechanisms of mitotic spindle formation." J Cell Sci **120**(Pt 10): 1717-22.

Oleynikov, Y. and R. H. Singer (1998). "RNA localization: different zipcodes, same postman?" Trends Cell Biol **8**(10): 381-3.

Oliferenko, S., I. Kaverina, J. V. Small and L. A. Huber (2000). "Hyaluronic acid (HA) binding to CD44 activates Rac1 and induces lamellipodia outgrowth." J Cell Biol **148**(6): 1159-64.

Patel, H., I. Konig, M. Tsujioka, M. C. Frame, K. I. Anderson and V. G. Brunton (2008). "The multi-FERM-domain-containing protein FrmA is required for turnover of paxillin-adhesion sites during cell migration of Dictyostelium." J Cell Sci **121**(Pt 8): 1159-64.

Piehl, M., U. S. Tulu, P. Wadsworth and L. Cassimeris (2004). "Centrosome maturation: measurement of microtubule nucleation throughout the cell cycle by using GFP-tagged EB1." Proc Natl Acad Sci U S A **101**(6): 1584-8.

Prager-Khoutorsky, M., I. Goncharov, A. Rabinkov, D. Mirelman, B. Geiger and A. D. Bershadsky (2007). "Allicin inhibits cell polarization, migration and division via its direct effect on microtubules." Cell Motil Cytoskeleton **64**(5): 321-37.

Prigozhina, N. L. and C. M. Waterman-Storer (2004). "Protein kinase D-mediated anterograde membrane trafficking is required for fibroblast motility." Curr Biol **14**(2): 88-98.

Puthenveedu, M. A., C. Bachert, S. Puri, F. Lanni and A. D. Linstedt (2006). "GM130 and GRASP65-dependent lateral cisternal fusion allows uniform Golgi-enzyme distribution." Nat Cell Biol **8**(3): 238-48.

Puthenveedu, M. A. and A. D. Linstedt (2005). "Subcompartmentalizing the Golgi apparatus." Curr Opin Cell Biol **17**(4): 369-75.

Quintyne, N. J. and T. A. Schroer (2002). "Distinct cell cycle-dependent roles for dynactin and dynein at centrosomes." J Cell Biol **159**(2): 245-54.

Raftopoulou, M. and A. Hall (2004). "Cell migration: Rho GTPases lead the way." Dev Biol **265**(1): 23-32.

Raynaud-Messina, B. and A. Merdes (2007). "Gamma-tubulin complexes and microtubule organization." Curr Opin Cell Biol **19**(1): 24-30.

Reed, N. A., D. Cai, T. L. Blasius, G. T. Jih, E. Meyhofer, J. Gaertig and K. J. Verhey (2006). "Microtubule acetylation promotes kinesin-1 binding and transport." Curr Biol **16**(21): 2166-72.

Rid, R., N. Schiefermeier, I. Grigoriev, J. V. Small and I. Kaverina (2005). "The last but not the least: the origin and significance of trailing adhesions in fibroblastic cells." Cell Motil Cytoskeleton **61**(3): 161-71.

Rios, R. M., A. Sanchis, A. M. Tassin, C. Fedriani and M. Bornens (2004). "GMAP-210 recruits gamma-tubulin complexes to cis-Golgi membranes and is required for Golgi ribbon formation." Cell **118**(3): 323-35.

Rivero, S., J. Cardenas, M. Bornens and R. M. Rios (2009). "Microtubule nucleation at the cis-side of the Golgi apparatus requires AKAP450 and GM130." Embo J **28**(8): 1016-28.

Robinson, J. T., E. J. Wojcik, M. A. Sanders, M. McGrail and T. S. Hays (1999). "Cytoplasmic dynein is required for the nuclear attachment and migration of centrosomes during mitosis in Drosophila." J Cell Biol **146**(3): 597-608.

Rodriguez, O. C., A. W. Schaefer, C. A. Mandato, P. Forscher, W. M. Bement and C. M. Waterman-Storer (2003). "Conserved microtubule-actin interactions in cell movement and morphogenesis." Nat Cell Biol **5**(7): 599-609.

Rogalski, A. A., J. E. Bergmann and S. J. Singer (1984). "Effect of microtubule assembly status on the intracellular processing and surface expression of an integral protein of the plasma membrane." J Cell Biol **99**(3): 1101-9.

Roghi, C. and V. J. Allan (1999). "Dynamic association of cytoplasmic dynein heavy chain 1a with the Golgi apparatus and intermediate compartment." J Cell Sci **112 (Pt 24)**: 4673-85.

Salaycik, K. J., C. J. Fagerstrom, K. Murthy, U. S. Tulu and P. Wadsworth (2005). "Quantification of microtubule nucleation, growth and dynamics in wound-edge cells." J Cell Sci **118**(Pt 18): 4113-22.

Schaefer, A. W., N. Kabir and P. Forscher (2002). "Filopodia and actin arcs guide the assembly and transport of two populations of microtubules with unique dynamic parameters in neuronal growth cones." J Cell Biol **158**(1): 139-52.

Schmit, A. C. (2002). "Acentrosomal microtubule nucleation in higher plants." Int Rev Cytol **220**: 257-89.

Schweizer, A., J. A. Fransen, T. Bachi, L. Ginsel and H. P. Hauri (1988). "Identification, by a monoclonal antibody, of a 53-kD protein associated with a tubulo-vesicular compartment at the cis-side of the Golgi apparatus." J Cell Biol **107**(5): 1643-53.

Sheetz, M. P. (1996). "Microtubule motor complexes moving membranous organelles." Cell Struct Funct **21**(5): 369-73.

Short, B., A. Haas and F. A. Barr (2005). "Golgins and GTPases, giving identity and structure to the Golgi apparatus." Biochim Biophys Acta **1744**(3): 383-95.

Shorter, J. and G. Warren (2002). "Golgi architecture and inheritance." Annu Rev Cell Dev Biol **18**: 379-420.

Siegrist, S. E. and C. Q. Doe (2007). "Microtubule-induced cortical cell polarity." Genes Dev **21**(5): 483-96.

Small, J. V., B. Geiger, I. Kaverina and A. Bershadsky (2002). "How do microtubules guide migrating cells?" Nat Rev Mol Cell Biol **3**(12): 957-64.

Small, J. V. and I. Kaverina (2003). "Microtubules meet substrate adhesions to arrange cell polarity." Curr Opin Cell Biol **15**(1): 40-7.

Small, J. V. and G. P. Resch (2005). "The comings and goings of actin: coupling protrusion and retraction in cell motility." Curr Opin Cell Biol **17**(5): 517-23.

Spiliotis, E. T., S. J. Hunt, Q. Hu, M. Kinoshita and W. J. Nelson (2008). "Epithelial polarity requires septin coupling of vesicle transport to polyglutamylated microtubules." J Cell Biol **180**(2): 295-303.

Storrie, B. and W. Yang (1998). "Dynamics of the interphase mammalian Golgi complex as revealed through drugs producing reversible Golgi disassembly." Biochim Biophys Acta **1404**(1-2): 127-37.

Tanaka, T., F. F. Serneo, C. Higgins, M. J. Gambello, A. Wynshaw-Boris and J. G. Gleeson (2004). "Lis1 and doublecortin function with dynein to mediate coupling of the nucleus to the centrosome in neuronal migration." J Cell Biol **165**(5): 709-21.

Tang, D., K. Mar, G. Warren and Y. Wang (2008). "Molecular mechanism of mitotic Golgi disassembly and reassembly revealed by a defined reconstitution assay." J Biol Chem **283**(10): 6085-94.

Taraska, J. W., D. Perrais, M. Ohara-Imaizumi, S. Nagamatsu and W. Almers (2003). "Secretory granules are recaptured largely intact after stimulated exocytosis in cultured endocrine cells." Proc Natl Acad Sci U S A **100**(4): 2070-5.

Thomas, J. H. and E. Wieschaus (2004). "src64 and tec29 are required for microfilament contraction during Drosophila cellularization." Development **131**(4): 863-71.

Thyberg, J. and S. Moskalewski (1985). "Microtubules and the organization of the Golgi complex." Exp Cell Res **159**(1): 1-16.

Thyberg, J. and S. Moskalewski (1993). "Relationship between the Golgi complex and microtubules enriched in detyrosinated or acetylated alpha-tubulin: studies on cells recovering from nocodazole and cells in the terminal phase of cytokinesis." Cell Tissue Res **273**(3): 457-66.

Thyberg, J. and S. Moskalewski (1999). "Role of microtubules in the organization of the Golgi complex." Exp Cell Res **246**(2): 263-79.

Vasiliev, J. M., I. M. Gelfand, L. V. Domnina, O. Y. Ivanova, S. G. Komm and L. V. Olshevskaja (1970). "Effect of colcemid on the locomotory behaviour of fibroblasts." J Embryol Exp Morphol **24**(3): 625-40.

Vaughan, K. T. (2005). "Microtubule plus ends, motors, and traffic of Golgi membranes." Biochim Biophys Acta **1744**(3): 316-24.

Wadsworth, P. (1999). "Regional regulation of microtubule dynamics in polarized, motile cells." Cell Motil Cytoskeleton **42**(1): 48-59.

Walczak, C. E. and R. Heald (2008). "Mechanisms of mitotic spindle assembly and function." Int Rev Cytol **265**: 111-58.

Wallin, M. and E. Stromberg (1995). "Cold-stable and cold-adapted microtubules." Int Rev Cytol **157**: 1-31.

Watanabe, T., J. Noritake and K. Kaibuchi (2005). "Roles of IQGAP1 in cell polarization and migration." Novartis Found Symp **269**: 92-101; discussion 101-5, 223-30.

Watanabe, T., J. Noritake, M. Kakeno, T. Matsui, T. Harada, S. Wang, N. Itoh, K. Sato, K. Matsuzawa, A. Iwamatsu, et al. (2009). "Phosphorylation of CLASP2 by GSK-3beta regulates its interaction with IQGAP1, EB1 and microtubules." J Cell Sci **122**(Pt 16): 2969-79.

Watanabe, T., S. Wang, J. Noritake, K. Sato, M. Fukata, M. Takefuji, M. Nakagawa, N. Izumi, T. Akiyama and K. Kaibuchi (2004). "Interaction with IQGAP1 links APC to Rac1, Cdc42, and actin filaments during cell polarization and migration." Dev Cell **7**(6): 871-83.

Waterman-Storer, C. M. and E. D. Salmon (1997). "Actomyosin-based retrograde flow of microtubules in the lamella of migrating epithelial cells influences microtubule dynamic instability and turnover and is associated with microtubule breakage and treadmilling." J Cell Biol **139**(2): 417-34.

Waterman-Storer, C. M., R. A. Worthylake, B. P. Liu, K. Burridge and E. D. Salmon (1999). "Microtubule growth activates Rac1 to promote lamellipodial protrusion in fibroblasts." Nat Cell Biol **1**(1): 45-50.

Wen, Y., C. H. Eng, J. Schmoranzer, N. Cabrera-Poch, E. J. Morris, M. Chen, B. J. Wallar, A. S. Alberts and G. G. Gundersen (2004). "EB1 and APC bind to mDia to stabilize microtubules downstream of Rho and promote cell migration." Nat Cell Biol **6**(9): 820-30.

Wiese, C. and Y. Zheng (2006). "Microtubule nucleation: gamma-tubulin and beyond." J Cell Sci **119**(Pt 20): 4143-53.

Wittmann, T., G. M. Bokoch and C. M. Waterman-Storer (2003). "Regulation of leading edge microtubule and actin dynamics downstream of Rac1." J Cell Biol **161**(5): 845-51.

Wittmann, T., G. M. Bokoch and C. M. Waterman-Storer (2004). "Regulation of microtubule destabilizing activity of Op18/stathmin downstream of Rac1." J Biol Chem **279**(7): 6196-203.

Wittmann, T. and C. M. Waterman-Storer (2005). "Spatial regulation of CLASP affinity for microtubules by Rac1 and GSK3beta in migrating epithelial cells." J Cell Biol **169**(6): 929-39.

Xu, J., F. Wang, A. Van Keymeulen, M. Rentel and H. R. Bourne (2005). "Neutrophil microtubules suppress polarity and enhance directional migration." Proc Natl Acad Sci U S A **102**(19): 6884-9.

Yadav, S., S. Puri and A. D. Linstedt (2009). "A primary role for Golgi positioning in directed secretion, cell polarity, and wound healing." Mol Biol Cell **20**(6): 1728-36.

Yvon, A. M. and P. Wadsworth (2000). "Region-specific microtubule transport in motile cells." J Cell Biol **151**(5): 1003-12.

Zekert, N. and R. Fischer (2009). "The Aspergillus nidulans kinesin-3 UncA motor moves vesicles along a subpopulation of microtubules." Mol Biol Cell **20**(2): 673-84.

Zenke, F. T., M. Krendel, C. DerMardirossian, C. C. King, B. P. Bohl and G. M. Bokoch (2004). "p21-activated kinase 1 phosphorylates and regulates 14-3-3 binding to GEF-H1, a microtubule-localized Rho exchange factor." J Biol Chem **279**(18): 18392-400.

Zhai, Y., P. J. Kronebusch, P. M. Simon and G. G. Borisy (1996). "Microtubule dynamics at the G2/M transition: abrupt breakdown of cytoplasmic microtubules at nuclear envelope breakdown and implications for spindle morphogenesis." J Cell Biol **135**(1): 201-14.